Thermodynamics of Aqueous Electrolyte Solutions - Application to Ion Exchange Systems

Christensen, Søren Gregers; Thomsen, Kaj

Publication date:
2005

Document Version
Publisher's PDF, also known as Version of record

Thermodynamics of Aqueous Electrolyte Solutions - Application to Ion Exchange Systems

Søren Gregers Christensen

2005

Ph.D. Thesis

DTU

TECHNICAL UNIVERSITY OF DENMARK
DEPARTMENT OF CHEMICAL ENGINEERING

Thermodynamics of Aqueous Electrolyte Solutions -
Application to Ion Exchange Systems

Søren Gregers Christensen

2004

ISBN 87-91435-24-2

Printed by Book Partner,
Nørhaven Digital,
Copenhagen, Denmark

Preface

This thesis is submitted as a partial fulfillment of the requirements for the Ph.D. degree at the Technical University of Denmark.

The work was carried out from August 2001 to September 2004 at the IVC-SEP, Department of Chemical Engineering, under the supervision of Dr. Kaj Thomsen. Several different people should be thanked for their positive contribution to my past three years.

First of all I would like to thank my supervisor Dr. Kaj Thomsen for the enormous help and support he has provided me during the study.

Next, an enormous thanks to Professor Jørgen Mollerup and Dr. Martin Breil at the IVC-SEP for helping me, whenever I came with a thermodynamic question.

Thanks are also given to Dr. Emmanuel Zaganiaris at Rohm & Haas, Chauny, France for letting me use their experimental facilities for my external stay, and to Areski Rezkallah, my good friend and colleague at Rohm & Haas, for his efforts in making my stay in France pleasant.

I would also like to thank Mr. Flemming Mathiesen at Kemira Denmark for coming up with the idea for this Ph.D. project and for the valuable discussions we have had during the study.

Finally, I owe my gratitude to my dear girlfriend Annemarie who always gave me motivation when my work seemed difficult. No words can express my thanks for the support and encouragement she has given me in the past years.

Copenhagen, September 2004

Søren Gregers Christensen

List of Contents

Summary

The thesis addresses the thermodynamics involved in describing the properties of aqueous solutions of electrolytes and of mixtures with ion exchanging materials. The work uses both existing and new approaches for the description of these properties and also presents new data for ion exchange isotherms and adsorption/swelling of several different ion exchange resins in aqueous electrolyte solutions.

Chapter 1 is a short introduction to the thesis and describes some of the motivation for why the work has been carried out.

Chapter 2 gives a short introduction to the area of aqueous electrolyte thermodynamics including the most important definitions for the understanding of the following chapters. The basic thermodynamic models based on the theory of Debye and Hückel are shortly introduced and examples of more comprehensive models are given.

Chapter 3 deals with the volumetric properties of aqueous electrolyte solutions. Different theoretical approaches for description of these properties are discussed. A modification of the Masson equation combined with Young's rule based on ion specific parameters is applied to volumetric data for different mixtures of salts. The model is easily applied to multicomponent mixtures, and it is shown that the relative errors of the predicted results in both ternary and quaternary systems are well within the experimental accuracy of the data.

In chapter 4 the phase behavior of aqueous electrolyte solutions is dealt with. The Extended UNIQUAC model is used for describing the vapor - liquid equilibria, solid - liquid equilibria and thermal properties of aqueous solutions of electrolytes in the presence of phosphoric and nitric acid. The model parameters are regressed on the basis of a large amount of experimental data and there is a good agreement between calculated and experimental data points.

Chapter 5 introduces the basic principles of ion exchange equilibria. The different phenomena connected with the equilibria between an ion exchanging material and aqueous solutions of electrolytes are presented. The different theoretical approaches to describing these types of equilibria are discussed.

Chapter 6 deals with modeling of ion exchange isotherms using a model treating the ion exchanger and counter-ions as a solid solution. The approach is very simple and gives only information about the selectivity of the ion exchanging material. New ion exchange isotherm data is presented for the H^+ - K^+ and H^+ - Ca^{++} systems. The approach is applied to both new data and data found in literature, and the results are reasonable accurate.

Chapter 7 presents new experimental data for the distribution of solvent and ions between an aqueous solution and several different ion exchange resins. The data is modeled using the Extended UNIQUAC model for describing the thermodynamic properties of the two aqueous phases combined with an elastic term taking the elastic properties of the resin structure into account. The model is able to produce good predictions, and the deviations between model results and experimental data are all within the experimental error.

Chapter 8 gives a general conclusion of the work completed in this thesis.

Resumé på dansk

Der mærkes i stigende grad en interesse fra industrien for termodynamiske værktøjer som kan bruges til beregning samt forudsigelse af de fysiske og kemiske egenskaber af vandige opløsninger af salte samt i blandinger med ionbyttende materialer. Disse typer systemer indgår i både den traditionelle kemiske industri, men også i høj grad inden for bioteknologien hvor mange oprensningsprocesser foregår i vandige opløsninger med en høj saltkoncentration. En af de store fordele ved udviklingen af præcise termodynamiske værktøjer er, at man ud fra relativt få eksperimentelle data kan opbygge en model til beskrivelse af hele det relevante område af parametre. Hermed kan det eksperimentelle arbejde reduceres betragteligt. Især ved beskrivelse af opløsninger med mange komponenter vil en relevant model medføre en betydelig reduktion i arbejdet med beskrivelse af de termodynamiske egenskaber af hele systemet.

Denne afhandling bruger både nye og eksisterende metoder til at beskrive de termodynamiske egenskaber af de nævnte systemer. De volumetriske egenskaber af de vandige elektrolytopløsninger bliver i afhandlingen beskrevet vha. en ny model baseret på en modifikation af Masson ligningen kombineret med Young's blandingsregel. Til beskrivelse af damp-væske ligevægte, faststof-væske ligevægte samt termiske egenskaber af blandingerne bliver The Extended UNIQUAC model brugt. Modellen bliver i afhandlingen udvidet til også at kunne beskrive ligevægte mellem saltopløsninger og polystyren ionbyttere med forskellig grad af krydsbinding. Arbejdet viser at man vha. de anvendte modeller kan forudsige både graden af ionbytning samt den totale absorptionen af ioner og vand i ionbytteren på baggrund af få datapunkter.

1. Introduction

A short introduction is given to the thesis and some of the motivation and application of the work addressed in the thesis are explained. The introduction is very general and a more thorough introduction to the different subjects and methods is given in the different chapters. In the back of the thesis a list of notation is given which could hopefully help the reader through the thesis.

Aqueous solutions of electrolytes play an important role in both laboratories and in many industries e.g. the mineral, oil and pharmaceutical industry. In nature electrolytes are substantial in both geothermal systems and in the biological processes of all living organisms. There is therefore an increasing interest for the creation of tools for accurate description of the properties of these types of solutions. During the last decade, great progress has therefore been made in the development of thermodynamic models for electrolyte solutions. Some of these works are more or less successful extensions of existing thermodynamic models like the NRTL, UNIQUAC, SRK and Wilson models, but new equations of states are also under development.

One of the industries where a growing interest is seen for the application of thermodynamic models for electrolytes is the fertilizer industry. One example of where the fertilizer industry lacks a precise tool, is in the calculation of densities. Having a precise model for the density of different electrolyte solutions would help in designing process tubes and pumps, but a precise model could also make use of on-line density measurements for determining the composition of a process stream. However, very few models exist for description of the volumetric properties of multicomponent electrolyte solutions. The majorities of the existing models are very complex, involves a high amount of parameters and can only in a few cases be applied to multicomponent systems. The first part of this thesis therefore deals with a simple relation for accurately description of these kinds of properties. The intention of the presented model is to accurately predict the volumetric properties of multicomponent electrolyte solutions from binary data with the fewest parameters possible.

Another example of where there is a need for improvement, is when calculating solid-liquid equilibria (SLE). With a tool for prediction of the solubilities of different salts it would for example be possible to predict at which temperature it would be optimal to run a crystallizer

for production of KNO_3. However, production of fertilizer salts like KH_2PO_4 and KNO_3 most often involves highly acidic solutions. At present time no parameters exist for description of the solubility of multicomponent electrolyte solutions in acidic environments. Therefore, the second part of the thesis deals with the description of these types of solutions. The Extended UNIQUAC model is a thermodynamic model developed at the IVC-SEP and has previously been applied with success to many different water/alcohol – salt systems. The purpose of the second part of this thesis is therefore to try to apply the Extended UNIQUAC model to the highly acidic solutions that appears in the production of KH_2PO_4 and KNO_3 salts.

Like in the area of electrolytes a growing interest has developed in the description of the thermodynamics of ion exchange systems. One of the reasons for this is that in many instances ion exchange technology can successfully substitute the large-scale industrial separation/concentration processes that do not satisfy modern ecological standards. Description of the equilibrium between multi ionic solutions and ion exchanging materials is essential for the development and optimization of ion exchange processes. However, the progress in improving the tools for describing these kinds of equilibria has not seen the same development as for the area of electrolyte solutions. Many new models are to a high extend empirical and are still based on the first approaches introduced in the early 50's.

In this thesis one of the ambitions is to apply the knowledge of aqueous electrolyte thermodynamics to ion exchange systems in hope of gaining a deeper understanding of how to approach the modeling of ion exchange equilibria. One area, where thermodynamic modeling could help in designing industrial processes, is in the description of ion exchange isotherms. The selectivity of one ion over another is very dependent on e.g. the concentration of the solution. However, when dealing with multicompont solutions, comprehensive experiments should be performed to investigate the entire range of concentrations. A model that could accurately predict multicomponent ion exchange selectivities from binary data would limit the amount of needed experiments enormously. In the latter part of this thesis the objective is to describe ion exchange isotherms. In this part mainly existing models are used, but by using the knowledge of aqueous electrolyte thermodynamics developed in the first part of the thesis, the ambition is to both simplify the approach and to make the modeling more consistent. In addition new experimental data is measured that could verify the capabilities of the proposed model.

Another important aspect of ion exchange equilibria is the absorption of solutes and solution in the ion exchange particles. This phenomenon is e.g. very important in the regeneration step of the ion exchange process. During regeneration a highly concentrated solution of salt is passed through the ion exchange column to convert the ion exchanger into the desired form. Subsequently the column is rinsed with pure water and it is desirable to use the smallest amount of water as possible. However, the amount of water used in the washout of the column is dependent on the absorption of salt in the ion exchange particles. The intention of the last part of the thesis is to address the absorption phenomenon. Only very few data exist in open literature describing this type of equilibria and the data that can be found is of varying quality. New procedures should therefore be developed for determining this type of equilibria and a suitable amount of data should be obtained for the development and testing of a thermodynamic model.

2. Thermodynamics of Electrolyte Solutions

A short introduction is given to the area of aqueous electrolyte thermodynamics including the most important definitions for the understanding of the following chapters. The basic thermodynamic models based on the theory of Debye and Hückel are shortly introduced and examples of more comprehensive models are given.

2.1 Introduction

The first modern theory for the thermodynamics of electrolyte solutions was proposed by Arrhenius[3]. He assumed that when an electrolyte is dissolved into water it dissociates into positive ions (cations) and negative ions (anions). If an electric force field is applied to the solution, the ions will move freely; the cations will move towards the anode and the anions towards the cathode. The degree of dissociation depends on the type of electrolyte and its concentration in the solvent. If an electrolyte fully dissociates into ions when brought in contact with a polar solvent, it is defined as a strong electrolyte contrary to a weak electrolyte that only partially dissociates.

Since the work of Arrhenius, the area of aqueous electrolyte thermodynamics has been a subject of great interest for many scientists. Lately, an even larger effort has been made to fully understand the thermodynamics of these systems due to their high importance in industrial relations. This chapter gives a basic overview of the most important theories of the thermodynamics of electrolyte solutions. The chapter mainly deals with the definitions needed for fully understanding the following chapters in the thesis. For a more detailed description of the area of aqueous electrolyte thermodynamics, the reader is referred to the PhD. thesis of Thomsen[1] and the textbook of Pitzer[2].

2.2 Thermodynamic functions

The basic thermodynamic functions of electrolyte solutions are slightly different from those of non-electrolyte solutions due to the presence of charged species. In the following, the basic thermodynamic functions of electrolyte solutions are listed.

The number of negatively charged ions and positively charged ions are always equal in a solution of electrolytes. This leads to the electro neutrality criteria:

$$\sum m_i z_i = 0 \qquad [2.1]$$

where m_i is the molality of ion i (mol/kg) and z_i is the charge of ion i.

The Gibbs free energy of a solution could be written in terms of the sum of the chemical potentials μ:

$$G = \sum_{i=1}^{N_{ionic}+N_w} n_i \mu_i = n_w \mu_w + \sum_{i=1}^{N_{ionic}} n_i \mu_i \qquad [2.2]$$

The deviation from the ideality of the chemical potential of water and the different ions could be described by the equations:

$$\mu_i = \mu_i^{\nabla} + RT \ln(m_i \gamma_i^{\nabla}) \qquad [2.3]$$

$$\mu_w = \mu_w^0 + RT \ln(x_w \gamma_w^0) \qquad [2.4]$$

Where γ_i^{∇} is the molal activity coefficient, μ_i^{∇} is the chemical potential of the ion, i , in the standard state based on the asymmetrical convention and the molality scale. μ_w^0 is the chemical potential of pure water and γ_w^0 is the rational, symmetrical activity coefficient of water.

2.2.1 Apparent Molal Relative Enthalpy

Measurements of the heat of dilution yield differences in the apparent molal relative enthalpy of the salt. Therefore this is a very convenient factor for the determination of the temperature dependency of the activity coefficients.

By differentiation of the activity coefficient of the ions with respect to temperature at a constant pressure and a constant composition, the following equation is obtained:

$$\left(\frac{\partial \ln \gamma_i^{\nabla}}{\partial T} \right)_{P,\underline{n}} = -\frac{L_{i,\underline{n}}}{RT^2} \qquad [2.5]$$

where $L_{i,\underline{n}}$ is the so-called relative molal enthalpy of the ion at the specified composition. A similar expression for the relative molal enthalpy of water could be found from differentiation of the water activity coefficient.

The apparent relative molal enthalpy $L_{\phi,\underline{n}}$ of a salt is found by summarizing the relative molal enthalpy of all species:

$$n_s L_{\phi,\underline{n}} = \sum_{i=1}^{N_{ions}+N_w} n_i L_{\phi,\underline{n}} \qquad [2.6]$$

2.2.2 Apparent Molal Heat Capacity:

The apparent molal heat capacity of a salt can be measured by e.g. microcalorimetric methods. It is defined in the following manner:

$$C_{p,\phi} = \left(\frac{\partial L_{\phi,\underline{n}}}{\partial T} \right)_{P,\underline{n}=n_{\text{solubility}}} + \sum_{i=1}^{N_{ions}} \nu_i C_{p,i}^{\nabla} \qquad [2.7]$$

The differentiation of $L_{\phi,\underline{n}}$ is taken at a constant composition that equals the solubility of the salt in water. $C_{p,i}^{\nabla}$ is the heat capacity of the ion at infinite dilution.

2.2.3 Apparent Molar Volume

The apparent molar volume could be measured directly from volume expansion experiments or be found from density data. The definition of this expression is:

$$\phi_V = \frac{V - n_w \bar{V}_w^0}{n_s} \qquad [2.8]$$

where $\bar{V}_w^0$ is the partial molar volume of pure water at the given temperature and pressure.

A more comprehensive description of the volumetric properties of aqueous electrolyte solutions is given in chapter 3.

2.2.4 Mean Activity Coefficient

The mean molal activity coefficient of an electrolyte solution is the geometrical mean of the activity coefficients in the solution:

$$n \ln \gamma_{\pm} = \sum_{i=1}^{N_{ions}} n_i \ln \gamma_i^{\nabla} \qquad [2.9]$$

where n is the total moles of ions. The sum applies for all ionic components.

2.2.5 Osmotic Coefficient

The water activity coefficient is close to unity in dilute aqueous electrolyte solutions. Therefore, in order to report the water activity without a considerable number of significant digits, the osmotic coefficient Φ is introduced:

$$\Phi = -\frac{n_w}{\sum_{i=1}^{N_{ions}} n_i} \ln(x_w \gamma_w^0) \qquad [2.10]$$

At infinite dilution the osmotic coefficient has a limiting value of unity.

2.3 Chemical Equilibrium

The thermodynamics of electrolyte solutions are further complicated by the fact that ionic reactions occur in the aqueous phase. Ions can react and be in one or more solid phases. Vast amounts of solid-liquid equilibrium data for many salts at varying temperatures exist in the literature. This section deals with how the solubility product is connected with other thermodynamic relations.

2.3.1 Solubility Product

The solubility product of a salt can be found from the standard chemical potential of all the different componets and the activity coefficients of the aqueous components. Consider a solid salt dissociating into n moles of water, χ cations and ζ anions with corresponding ionic charges z_C and z_A:

$$C_\chi A_\zeta nH_2O \leftrightarrow \chi C^{z_C} + \zeta A^{z_A} + nH_2O \qquad [2.11]$$

At equilibrium the chemical potential of the solid salt equals the sum of the chemical potentials of the constituents:

$$\mu_{C_\chi A_\zeta nH_2O} = \chi\mu_{C^{z_C}} + \zeta\mu_{A^{z_A}} + n\mu_{H_2O} \qquad [2.12]$$

The activity of the solid salt is equal to unity; hence the chemical potential is equal to the standard chemical potential.

$$\mu_{C_\chi A_\zeta nH_2O} = \mu^0_{C_\chi A_\zeta nH_2O} + RT\ln(a_{C_\chi A_\zeta nH_2O}) = \mu^0_{C_\chi A_\zeta nH_2O} \qquad [2.13]$$

The chemical potential of the water and ions is given by:

$$\mu_w = \mu^0_w + RT\ln(a_w) = \mu^0_w + RT\ln(x_w\gamma^0_w) \qquad [2.14]$$

$$\mu_i = \mu^\nabla_i + RT\ln(a_i) = \mu^\nabla_i + RT\ln(m_i\gamma^\nabla_i) \qquad [2.15]$$

The solubility product of the salt is defined as:

$$K_{C_\chi A_\zeta nH_2O} = \left(m_{C^{z_C}}\gamma^\nabla_{C^{z_C}}\right)^\chi \left(m_{C^{z_C}}\gamma^\nabla_{C^{z_C}}\right)^\zeta \left(x_w\gamma^0_w\right) \qquad [2.16]$$

Substituting equations [2.13]-[2.15] in equation [2.16] gives:

$$\chi\mu^\nabla_{C^{z_C}} + \zeta\mu^\nabla_{A^{z_A}} + n\mu^0_w - \mu^0_{C_\chi A_\zeta nH_2O} = -RT\ln K_{C_\chi A_\zeta nH_2O} \qquad [2.17]$$

Eq. [2.17] states that activity coefficients could be regressed from experimental solubility data, when values of the standard state chemical potential of the different components are known.

2.3.2 Temperature Dependence

When dealing with systems at temperatures that are different from the standard states, the temperature dependence of the solubility product needs to be taken into account. The following section shows how this is dealt with in practice.

At constant pressure the Gibbs free energy, G, is given by:

$$G \equiv U + PV - TS \qquad [2.18]$$

$$\left(\frac{\partial G}{\partial T}\right)_{P,\underline{n}} = -S = \frac{G-H}{T} \qquad [2.19]$$

This equation could be rewritten to:

$$\left(\frac{\partial}{\partial T}\left(\frac{G}{T}\right)\right)_{P,\underline{n}} = -\frac{H}{T^2} \qquad [2.20]$$

This is also known as the Gibbs-Helmholtz equation.

The solubility product could be expressed in terms of the standard Gibbs free energy:

$$\Delta G^0 = -RT \ln K \qquad [2.21]$$

Substituting this expression in the Gibbs-Helmholz equations:

$$\left(\frac{\partial \ln K}{\partial T}\right)_P = \frac{-\Delta H^0}{RT^2} \qquad [2.22]$$

Integration of this expression from the standard state temperature T^0 to the actual temperature T:

$$\ln K(T) = \ln K(T^0) + \int_{T^0}^{T} \frac{\Delta H^0}{RT^2} dT \qquad [2.23]$$

The temperature dependence of ΔH^0 at a constant pressure is given by:

$$\frac{d\Delta H^0}{dT} = \Delta C_p^0 \qquad [2.24]$$

Where ΔC_p^0 refers to the change in the heat capacity of the reaction [2.11].

Several different expressions have been proposed for describing the temperature dependency of the partial heat capacity of ionic species. Most of these expressions are simple polynomials while others are more complex equations based on theoretical considerations. Thomsen[1] has shown that the heat capacity of ions could be represented by a simple expression which will be used in this thesis:

$$C_{p,i}^{0} = a_i + b_i T + \frac{c_i}{T - T^{\Theta}} \qquad [2.25]$$

Where T^{Θ} is a reference temperature of 200K. The *a*, *b* and *c* parameters of the expression are usually found from a data reduction of experimental data.

The change in the heat capacity for reaction [2.11] could therefore be given by:

$$\Delta C_p^0 = \Delta a + \Delta b T + \frac{\Delta c}{T - T^{\Theta}} \qquad [2.26]$$

Insertion of this expression in eq. [2.24] followed by an integration gives an equation of the change in the enthalpy for reaction [2.11] at a given temperature:

$$\Delta H^0(T) = \Delta a (T - T^0) + 0.5\Delta b (T^2 - (T^0)^2) + \Delta c \ln \frac{T - T^{\Theta}}{T^0 - T^{\Theta}} \qquad [2.27]$$

Using the above equation, an analytical expression for the solubility product at a given temperature could be found:

$$\begin{aligned} R \ln K(T) = R \ln K\left(T^0\right) - \Delta H\left(T^0\right)\left(\frac{1}{T} - \frac{1}{T^0}\right) + \Delta a \left(\ln \frac{T}{T^0} + \frac{T^0}{T} - 1\right) + \\ 0.5\Delta b \left(\frac{\left(T - T^0\right)^2}{T}\right) + \frac{\Delta c}{T^{\Theta}}\left(\frac{T - T^{\Theta}}{T^0} - T^{\Theta}\left(\frac{1}{T} - \frac{1}{T^0}\right)\ln\left(T^0 - T^{\Theta}\right)\right) \end{aligned} \qquad [2.28]$$

2.4 Modeling of Aqueous Electrolyte Solutions

The forces leading to non-ideality in electrolyte solutions are somewhat different from those in non-electrolyte solutions. The physical, thermodynamic and transport properties of aqueous electrolyte solutions depend on the forces acting between the various species. In these solutions there are basically two different species; dissociated ions and molecules. Hence, there are three different forces in the system; molecule-molecule, ion-ion and molecule-ion interactions.

The short range forces between molecules have been studied in great detail for non-electrolyte solutions and several different models, e.g. based on the local composition concept, have been applied to these kinds of systems. The interactions between ions and molecules are dominated

by electrostatic forces between permanent dipoles and ions. These forces are also short range by nature. The ion-ion interactions are dominated by electrostatic forces which are much larger in range than the previous forces mentioned. Therefore, these types of interactions are dominant in dilute electrolyte solutions while the short range interactions give the major contribution at higher concentrations.

2.4.1 The Debye-Hückel Limiting Law

Due to the fact of the long range ion-ion interaction forces, electrolytic systems can deviate from ideality at even very low concentrations. Debye and Hückel were the first scientists to describe the non-ideal behavior caused by the electrostatic forces in low concentration electrolyte systems. According to the Debye-Hückel limiting law, the Gibbs excess energy of an extremely dilute solution of electrolytes could be described by the equation:

$$\frac{ng^E}{RT} = -\frac{4}{3} n_w M_w A_{DH} I_m^{3/2} \qquad [2.29]$$

M_w is the molecular weight of water. I_m is the ionic strength based on the molality scale and A_{DH} is the Debye-Hückel constant given by the expression:

$$A_{DH} = \frac{F^3}{4\pi N_A} \sqrt{\frac{\rho_w}{2(\varepsilon_0 \varepsilon_r RT)}} \qquad [2.30]$$

where F is the Faraday constant, N_A is Avogadros number, R is the gas constant and T is the absolute temperature in kelvin. ε_r is the relative permittivity of water, ε_0 is the vacuum permittivity and ρ_w is the density of water.

An expression of the activity coefficient of the ion i is found by taking the molar derivative of eq. [2.29]:

$$\ln \gamma_i^{\nabla} = -A_{DH} z_i^2 \sqrt{I_m} \qquad [2.31]$$

In the original expression of Debye and Hückel, a factor a was introduced to describe the ionic atmosphere potential in order to be able to account for the distance of the closest approach. This resulted in what today is known as the extended Debye-Hückel expression which describes the Gibbs excess energy in the following manner:

$$\frac{ng^E}{RT} = -4n_w M_w \frac{A_{DH}}{b^3}\left[\ln(1+b\sqrt{I_m}) - b\sqrt{I_m} + \frac{b^2\sqrt{I_m}}{2}\right] \qquad [2.32]$$

Where the term b is given by:

$$b = a\sqrt{\frac{2\rho_w F^2}{\varepsilon_0 \varepsilon_r RT}} \qquad [2.33]$$

An expression of the activity coefficients could be derived from eq. [2.32]:

$$\ln \gamma_i^{\nabla} = -A_{DH}\frac{z_i^2\sqrt{I_m}}{1+b\sqrt{I_m}} \qquad [2.34]$$

The mean activity coefficient of NaCl has been calculated using eq. [2.31] and [2.34] with an *a*-parameter of 4.0Å. The results are compared with experimental data in figure 2.1. The figure shows that the limiting law of Debye-Hückel only predicts the properties in very dilute solutions. The extended model represents the data at higher concentrations. However, the extended model has the drawback that the parameter for the distance of the closest approach, *a*, should be estimated from experimental data.

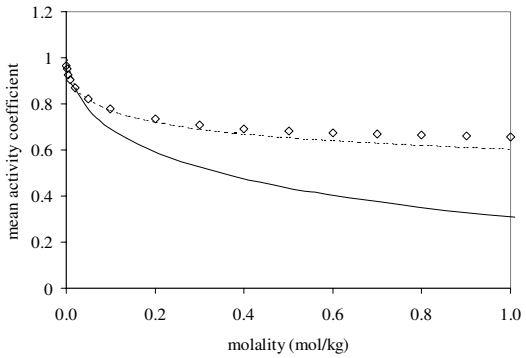

Figure 2.1. The mean activity coefficient of NaCl as function of molality. (◇) exp. datapoints[5]. (–) calculated by eq. (2.31), (--) calculated by eq. (2.34).

2.4.2 Application of G^E Models to Electrolyte Solutions

As seen in the previous section, the Debye-Hückel theory for aqueous electrolyte solutions could only be applied successfully to systems with a low solute concentration. This limitation of the Debye-Hückel theory arises mainly from the assumptions used when solving the Poisson-Boltzmann equation.

Quite a few improvements of the Debye-Hückel expression have been proposed. The first comprehensive work was presented by Pitzer[6,7] in 1973. He developed a model based on an expansion of the Debye-Hückel theory, but including terms for the short-range interactions. This model has subsequently been applied with success in describing the thermodynamics of many different electrolyte solutions and the model is still widely accepted in the academic world.

Another successful approach to the description of aqueous electrolyte thermodynamics is the extension of traditional G^E models. The local composition concept has been used by several researchers for developing models of short range forces between molecules. Lately, quite a few of these models have been extended to electrolyte solutions by adding electrostatic terms to the original equations. The most successful of these extensions are the Wilson model[8,9], the NRTL model[10] and the UNIQUAC model[1,11].

In this thesis aqueous phase thermodynamics is described using the Extended UNIQUAC model because the model has proven to give good predictions in multicomponent systems and has previously successfully been applied to a variety of different electrolyte systems[1,11]. An example of the calculation of the mean activity coefficient for solutions of NaCl using the Extended UNIQUAC model is shown in figure 2.2. The figure shows that the Debye-Hückel term as expected describes the mean activity coefficient satisfactory up to app. 0.5 molal. At higher concentrations the short-range forces are most dominant, and the UNIQUAC short range configurational terms correct for the shortcomings of the electrostatic term. The Extended UNIQUAC model is described in more detail in chapter 4 where the model has been applied to a large amount of aqueous salt/acid solutions.

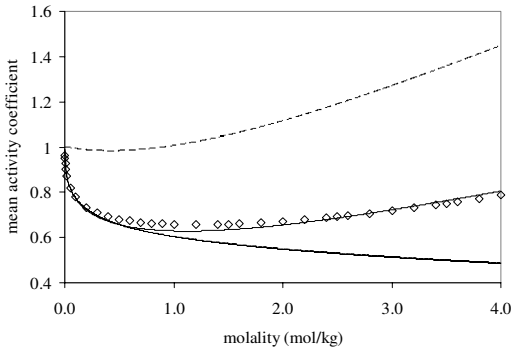

Figure 2.2. The mean activity coefficient of NaCl as a function of molality.

(◇) exp. datapoints[5]. (–) Extended UNIQUAC model. (– –) Contribution from residual and combinatorial term (···) contribution from Debye-Hückel term. Model and parameters has been used as given by Thomsen[1].

2.5 Conclusion

The most important definitions when dealing with aqueous electrolyte thermodynamics have been presented in this chapter. Furthermore, a short introduction has been given to the aspects of modeling the properties of these kinds of solutions. In the following chapters a more detailed description is given of different models and methods for describing the volumetric properties and the phase behavior of electrolyte solutions.

2.6 References

(1) Thomsen, K. Aqueous Electrolytes: Model Parameters and Process Simulation. Ph.D. Thesis. Technical University of Denmark. **1997**.

(2) Pitzer, K.S. Activity Coefficients in Electrolyte Solutions. 2nd Edition. CRC Press, Boston, **1991**.

(3) Arrhenius, S.A. *Z. Phys. Chem.* **1887**, 1, 285.

(4) Debye, P.; Hückel, E. Zur Theorie der Elektrolyte I/II. *Phys. Z.* **1923**, 24, 185.

(5) Clarke E.C.W.; Glew, D.N. Evaluation of the thermodynamic functions for aqueous sodium chloride from equilibrium and calorimetric measurements. J. Phys. Chem. Ref. Data. **1985**, 14, 489.

(6) Pitzer, K.S. Thermodynamics of Electrolytes. I. Theoretical Basis and General Equations. *J. Phys. Chem.* **1973**, 77, 268.

(7) Pitzer, K.S.; Mayorga, G. Thermodynamics of Electrolytes. II. Activity and Osmotic Coefficients for Strong Electrolytes with One or Both Ions Univalent. *J. Phys. Chem.* **1973**, 77, 2300.

(8) Zhao, E.; Yu, M.; Sauve, R.E.; Khoshkbarchi, M.K. Extension of the Wilson model to electrolyte solutions. *Fluid Phase Equilibria.* **2000,** 173, 161

(9) Xu, X.; Macedo, E.A. New Modified Wilson Model for Electrolyte Solutions. *Ind. & Eng. Chem. Res*. **2003**, 42, 5702.

(10) Jaretun, A.; Aly, G. New local composition model for electrolyte solutions: single solvent, single electrolyte systems. *Fluid Phase Equilibria*. **1999**. 163, 175.

(11) Thomsen, K.; Rasmussen, P.; Gani, R. Correlation and prediction of thermal properties and phase behavior for a class of aqueous electrolyte systems. *Chem. Eng. Sci.* **1996**, 51, 3675.

3. Volumetric Properties of Electrolyte Solutions

This chapter is a rewriting of the article *"Representation of volumetric data of electrolyte solutions at varying concentrations and temperatures"* co-authored with Kaj Thomsen and submitted to Industrial and Engineering Chemical Research.

A modification of the Masson equation combined with Young's rule based on ion specific parameters has been applied to volumetric data for mixtures of (H^+, Na^+, K^+, NH_4^+, Ca^{++}, Mg^{++}) (Cl^-,NO_3^-,SO_4^{--}). The parameters have been regressed from data in the temperature range 0 – 100°C and concentration range 0 – 11.8 mol/kg, but are shown to be valid up to saturation. The model only requires 5 parameters per ion in the entire range of concentration and temperature. The model is easily applied to multicomponent mixtures, and it is shown that the relative errors of the predicted results in both ternary and quaternary systems are well within the experimental accuracy of the data.

3.1 Introduction

The density and volumes of aqueous solutions of inorganic electrolytes are important properties in the field of chemical engineering. During the past two centuries volumetric properties have been measured for a large amount of salt-water systems in varying concentrations and temperatures. The large volume of data can be found in both periodical literature and in different monographs.

Many different approaches have been proposed for correlating these properties. Most of these works have been empirical and applied to only a few systems[1,2]. One of the most comprehensive works is the one of Söhnel and Novotny[3]. They have correlated densities of many different salts with polynomials of different degree. However, their work is only applicable to binary and ternary systems. Lately more complex models, e.g. models based on the Pitzer model, have been applied to volumetric data in a more systematic manner[4,5]. However, the drawbacks of most of these approaches are that they involve a large amount of parameters which often are on a salt basis and therefore not necessarily internally consistent and not applicable to multicomponent systems.

In this work, the apparent molal volumes for each species are collated using a variation of the Masson[1] rule based on ionic contributions. This implies that the apparent molal volumes for

mixtures of (H^+, Na^+, K^+, NH_4^+, Ca^{++}, Mg^{++}) (Cl^-, NO_3^-, SO_4^{--}) with reasonable accuracy can be modeled in a wide range of concentrations and temperatures using only 40 new parameters. The advantage of the introduced method is that reliable parameters can be found, even though data for all the implicated salt-water systems are not available in literature. Furthermore, due to the fact that the method uses ion specific parameters, it can easily be applied to multicomponent systems.

3.2 Theory

In chapter 2 the most basic equations for the thermodynamics of electrolyte systems were given. This section gives a more comprehensive description of the thermodynamic relations of the volumetric properties of electrolyte solutions.

3.2.1 Basic Equations

The volume, V, of a solution can be expressed in terms of the Gibbs energy of the system:

$$V = \left(\frac{\partial G}{\partial P} \right)_{T,n} \qquad [3.1]$$

If we consider a solution of water and ions, the Gibbs energy of the electrolyte solution can be described by the relation:

$$G = n_w \mu_w + \sum_{i=1}^{N_{ions}} n_i \mu_i \qquad [2.2]$$

The volume is then given by:

$$V = \frac{\partial}{\partial P} \left(n_w \mu_w + \sum_{i=1}^{N_{ions}} n_i \mu_i \right)_{T,\underline{n}} \qquad [3.2]$$

The chemical potential of ions and water can be expressed by the following equations:

$$\mu_i = \mu_i^{\nabla} + RT \ln(m_i) + RT \ln(\gamma_i^{\nabla}) \qquad [3.3]$$

$$\mu_w = \mu_w^0 + RT \ln(x_w) + RT \ln(\gamma_w^0) \qquad [3.4]$$

Where γ_i^{∇} is the molal activity coefficient, μ_i^{∇} is the chemical potential of the ion *i*, in the standard state based on the molality scale. μ_w^0 is the chemical potential of pure water and γ_w^0 is the rational, symmetrical activity coefficient of water.

Inserting the equations [3.3-3.4] in [3.2] gives following results:

$$V = \frac{\partial}{\partial P}\left(n_w\left(\mu_w^0 + RT\ln(x_w) + RT\ln(\gamma_w^0)\right) + \sum n_i\left(\mu_i^{\nabla} + RT\ln(m_i) + RT\ln(\gamma_i^{\nabla})\right)\right)_{T,\bar{n}}$$

$$V = \frac{\partial}{\partial P}\left(n_w\mu_w^0 + \sum n_i\mu_i^{\nabla}\right)_{T,\bar{n}} + \frac{\partial}{\partial P}\left(n_w RT\ln(\gamma_w^0) + \sum n_i RT\ln(\gamma_i^{\nabla})\right)_{T,\bar{n}} \qquad [3.5]$$

$$V = n_w\bar{v}_w^0 + \sum_{i=1}^{N_{ionic}} n_i\bar{v}_i^{\nabla} + \left(\frac{\partial G^E}{\partial P}\right)_{T,\bar{n}} = n_w\bar{v}_w^0 + \sum_{i=1}^{N_{ionic}} n_i\bar{v}_i^{\nabla} + nv^E \qquad [3.6]$$

where $\bar{v}_i^{\nabla}$ is the standard state molal volume of ion *i*, $\bar{v}_w^0$ is the standard state volume of water and nv^E is the excess volume of the solution.

The partial molal volume of a component *i* is defined as:

$$\bar{v}_i = \left(\frac{\partial V}{\partial n_i}\right)_{T,P,n_j,\, j\neq i} \qquad [3.7]$$

The partial molal volume concept could also be rewritten in the form:

$$V = \sum_{i=1}^{N_{comp}} n_i\bar{v}_i$$

For a solution of electrolytes this expression can be written as:

$$V = \sum_{i=1}^{N_{ionic}} n_i\bar{v}_i + n_w\bar{v}_w \qquad [3.8]$$

For n_s mol of a salt, the apparent molal volume is defined as:

$$\phi_{V,s} = \frac{(V - n_w\bar{v}_w^0)}{n_s} \qquad [3.9]$$

Equation [3.9] shows that the apparent molal volume is only a function of the volume of pure water, the concentrations of ions and the volume of the solution. From this it can be concluded that the apparent molal volume is equal to the actual volume expansion when adding an amount of salt to a solution of pure water. This definition is therefore very convenient when describing experimental data.

It is generally assumed that the molal volumes for the ions are additive. Hence eq. [3.8] can be written for multicomponent electrolyte solutions in the form:

$$V = \sum_{i=1}^{N_{ions}} n_i \phi_{V,i} + n_w \overline{v}_w^0 \qquad [3.10]$$

Comparing equation [3.6] with [3.10] it can easily be seen that following expression applies:

$$\sum_{i=1}^{N_{ions}} n_i \phi_{V,i} = \sum_{i=1}^{N_{ions}} n_i \overline{v}_i^{\nabla} + nv^E \qquad [3.11]$$

3.2.2 Volumetric Calculations Using Gibbs Excess Models

Equations [3.1-13.11] show that the volume of an electrolyte solution can be found if a suitable expression for the Gibbs excess energy exists. Several works have applied Gibbs excess energy expressions to the calculation of volumetric properties of electrolyte solutions. One of the first examples is the work of Redlich and Rosenfield[6]. They showed in 1931 that the so-called limiting law of Debye-Hückel can be used to predict the apparent molal volume for a few simple electrolytes in dilute solutions.

As explained in chapter 2, according to the limiting law of Debye and Hückel the Gibbs excess energy of a very dilute electrolyte solution can be described by the expression:

$$\frac{ng^E}{RT} = -\frac{4}{3} n_w M_w A_{DH} I_m^{3/2} \qquad [2.29]$$

The excess volume of the solution is then given by (see appendix A):

$$nv^E = \left(\frac{\partial ng^E}{\partial P}\right)_{T,\underline{n}} = \frac{2}{3} RTn_w M_w A_{DH} \left(\frac{3}{\varepsilon_r}\frac{\partial \varepsilon_r}{\partial P} - \frac{1}{\rho_w}\frac{\partial \rho_w}{\partial P}\right)_{T,\underline{n}} I_m^{3/2} = \alpha I_m^{3/2} \qquad [3.12]$$

M_w is the molecular mass of water, ε_r is the relative permittivity of water. I_m is the ionic strength based on the molality scale and A_{DH} is the Debye-Hückel constant given by the expression:

$$A_{DH} = \frac{F^3}{4\pi N_A}\sqrt{\frac{\rho_w}{2(\varepsilon_0\varepsilon_r RT)^3}} \qquad [2.30]$$

where F is the Faraday constant, ρ_w is the density of water, ε_0 is the vacuum permittivity, N_A is Avogadros number, R is the gas constant and T is the temperature in Kelvin.

Eq. [3.12] corresponds to the expression presented by Redlich and Rosenfield in 1931. Applying eq. [3.12] to a 1:1 salt in 1 kg of water then the apparent molal volume is given by the expression:

$$\phi_{V,S} = v_S^{\nabla} + \alpha\sqrt{m_S} \qquad [3.13]$$

Where $v_S^{\nabla} = \sum_{i=1}^{N_{ions}} n_i \overline{V}_i^{\nabla}$, that is, the theoretical volume of the dissolved salt at infinite dilution.

Using eq. [3.13] the apparent molal volume for a 1:1 electrolyte has been calculated at 25°C and is compared to experimental data in figure 3.1. For the calculation of the density and dielectric constant of water the NIST/ASME[7] steam properties have been used.

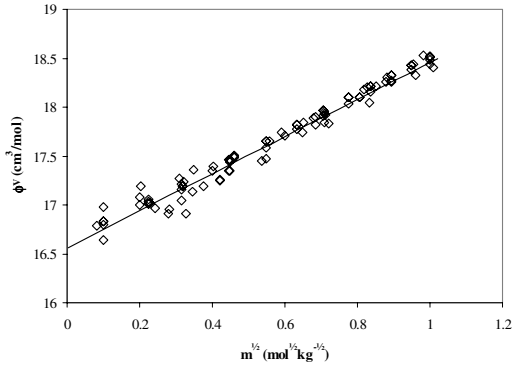

Figure 3.1. The apparent molal volume of NaCl at 25°C as function of the square

root of molality for dilute solutions.
(◇) exp. datapoints. (–) calculated by eq. [3.13].

The figure shows excellent agreement between the predicted and the experimental values. However, the variance of the apparent molal volume with the molality is not equal for all 1:1 electrolytes and can therefore not be predicted using eq. [3.12]. Additionally, the temperature variation of eq. [3.12] does not follow the general trend of experimental data. In figure 3.2 the coefficient α has been calculated at different temperatures using eq. [3.12] and is compared with values regressed from volumetric data for solutions of NaCl. The figure shows that the coefficient α actually is equal to the experimental value at 25° for NaCl. Therefore, the prediction in figure 3.1 is acceptable. However, at any other temperature the predictions would be far from the experimental values.

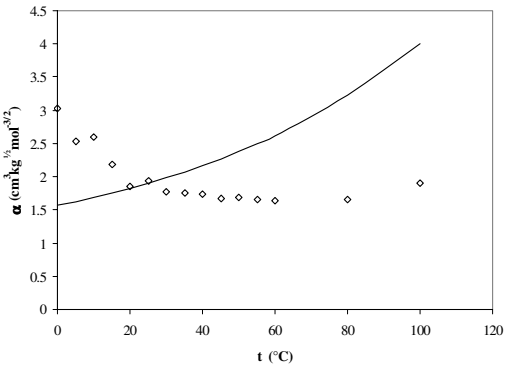

Figure 3.2. The α factor of eq. [3.12] for NaCl as function of square root of molality at different temperatures.
(◇) regressed from exp. datapoints. (–) calculated by eq. [3.12].

In the so-called extended Debye-Hückel expression the factor *a* is introduced to account for the average distance of closest approach. In this expression the Gibbs excess energy is described as:

$$\frac{ng^E}{RT} = -4n_w M_w \frac{A_{DH}}{b^3}\left[\ln(1+b\sqrt{I_m}) - b\sqrt{I_m} + \frac{b^2 I_m}{2}\right] \qquad [2.32]$$

Where the term b is given by:

$$b = a\sqrt{\frac{2\rho_w F^2}{\varepsilon_0 \varepsilon_r RT}} \qquad [2.33]$$

By differentiation of eq. [2.32] with regard to pressure, the following expression for the excess volume is obtained (see appendix B):

$$nv^E = \frac{\partial ng^E}{\partial P} = -2RTn_w M_w A_{DH} \cdot \left[\begin{array}{l} \omega\left(\frac{\sqrt{I_m}}{b^2(1+b\sqrt{I_m})} - \frac{3\ln(1+b\sqrt{I_m})}{b^3} + \frac{2\sqrt{I_m}}{b^2} - \frac{I_m}{2b} \right) \\ +\beta\left(\frac{\ln(1+b\sqrt{I_m})}{b^3} - \frac{\sqrt{I_m}}{b^2} + \frac{I_m}{2b} \right) \end{array} \right] \qquad [3.14]$$

$$\omega = \left(\frac{2}{a}\frac{\partial a}{\partial P} + \frac{1}{\rho_w}\frac{\partial \rho_w}{\partial P} - \frac{1}{\varepsilon_r}\frac{\partial \varepsilon_r}{\partial P} \right)_{T,\underline{n}} \qquad [3.15]$$

$$\beta = \left(\frac{1}{\rho_w}\left(\frac{\partial \rho_w}{\partial P}\right) - \frac{3}{\varepsilon_r}\left(\frac{\partial \varepsilon_r}{\partial P}\right) \right)_{T,\underline{n}} \qquad [3.16]$$

The only unknown parameters in eq. [3.14-3.16] are the distance of closest approach, *a,* and the derivative of this parameter with respect to pressure. The *a*-parameter can be found from regression of activity coefficient data; however the pressure derivative should be fitted to e.g. volumetric data. In figure 3.3 the apparent molal volume of NaCl has been calculated using eq. [3.14-3.16]. The line was calculated with the pressure derivative of *a* set equal to 0. The dashed line was calculated by fitting $\frac{\partial a}{\partial P}$ to experimental data. In both cases the values used for *a* is 4.0 Å as suggested by Robinson and Stokes[8].

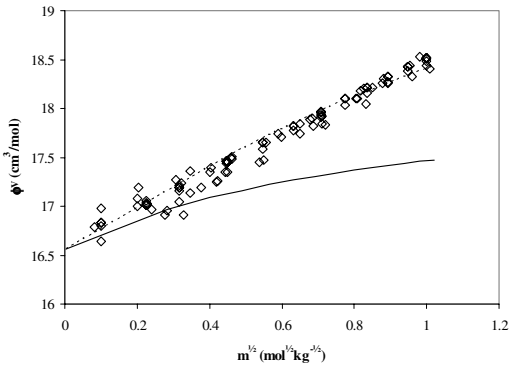

Figure 3.3. The variation of the apparent molal volume of NaCl as function of square root of molality at 25°C. (◇) Exp. datapoints.
(–) Calculated by eq. [3.14], $\frac{\partial a}{\partial P} = 0$.
(- -) Calculated by eq. [3.14], $\frac{\partial a}{\partial P} = 4.5 \cdot 10^{-18} \, (m \cdot bar^{-1})$.

Figure 3.3 shows poor agreement between the calculated results when no pressure dependence of *a* is taken into account. The result obtained with the Debye-Hückel limiting law in fig. 3.1 was in fact better. The calculations where the term $\frac{\partial a}{\partial P}$ has been fitted to the experimental data represent the data with accuracy similar to the one obtained with the limiting law.

The observed deviation in figure 3.3 is a general problem when applying Gibbs excess models to volumetric data. The pressure dependence of the different parameters, e.g. the distance of closest approach parameter or different binary interaction parameters, is unknown and therefore has to be regressed from experimental data. Application of this kind of models therefore often has a tendency to have a substantial amount of parameters with no obvious physical meaning. In the following section this problem is solved by using a slightly more empirical approach

3.2.3 Model Equations

In the work presented here it is assumed that the Masson equation can be used for single ions. Masson[1] found in 1929 that the apparent volume of an electrolyte varies linearly with the square root of the molality in dilute solutions:

$$\phi_{V,S} = \overline{v}_S^{\nabla} + k\sqrt{m_S} \qquad [3.17]$$

This relation has been shown to be valid for many systems in concentrated solutions as well[2]. The relation is purely empirical. However, several authors[6,8] have later derived equations like eq. [3.13] that are very similar to eq. [3.17] and thereby given a theoretical basis for the relation.

Assuming that the Masson equation can be used for single ions the apparent volume of an ion *i* is described by the relation:

$$\phi_{V,i} = \overline{v}_i^{\nabla} + k_i\sqrt{m_i} \qquad [3.18]$$

If the apparent molal volumes of the ions are assumed to be additive, the volume of an aqueous solution of ions can be calculated using the equation:

$$V = V_w + \sum_{i=1}^{N_{ions}} m_i \phi_{V,i} \qquad [3.19]$$

where V_w is the volume of 1 kg of water at the given temperature and pressure.

Eq. [3.19] can be applied to solutions of single valence ions; however, as seen in figure 3.4 the results for multicomponent systems of multivalence ions are not acceptable. Young and Smith[9] suggested a mixing rule for describing the volumetric data of mixed electrolyte solutions. The relation is based on the principle that the mean ionic activity coefficient of any strong electrolyte is the same in all solutions at the same ionic strength. According to Young's rule the apparent molal volume of a mixture of two salts can be calculated using:

$$\phi_V = \frac{m_{S1}\phi_{V,S1} + m_{S2}\phi_{V,S2}}{m_{S1} + m_{S2}} \qquad [3.20]$$

where m_{S1}, m_{S2} are the molalities of the two salts and $\phi_{V,S1}, \phi_{V,S2}$ are the apparent molal volumes of the two salts evaluated at the ionic strength of the total solution.

By applying the mixing rule of Young and Smith to ions rather than salts, eq. [3.19] can be applied to multicomponent solutions of multivalence ions:

$$\phi_{V,i} = \bar{v}_i^{\nabla} + k_i\sqrt{I_m} \qquad [3.21]$$

where I_m is the ionic strength on the molality scale and k_i an ion specific parameter.

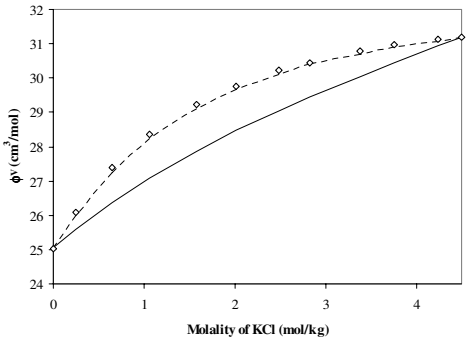

Figure 3.4. The apparent molal volume in solutions of KCl and $CaCl_2$ at I_m = 4.5 mol/kg and 25°C.
(◇) exp. datapoints[10]. (–) calculated by eq. [3.17], (--) calculated by eq. [3.21].

One difference between eq. [3.21] and the relation of Masson eq. [3.17] is the use of ionic strength instead of concentration. However, the most important difference is that eq. [3.21] is based on ion basis rather than salt basis. This means that the two equations behave similarly for binary electrolyte solutions, while the results of eq. [3.21] are much better in multicomponent solutions than the original Masson equation. One example of this is shown in figure 3.4. In this case, the parameters in eq. [3.17] and [3.21] have been regressed for K^+, Ca^{++} and Cl^- from the binary data. The parameters have been applied to data for the apparent molal volume in the KCl-$CaCl_2$ system. The figure shows data for the apparent molal volume at a constant ionic strength; hence only the molality of one of the salts is given. The figure shows excellent agreement between the experimental data and eq. [3.21]. However, there are larger deviations when the original Masson equation is used.

3.3. Parameter Estimation

The IVC-SEP electrolyte databank[11] contains at present time more than 100,000 experimental data related to electrolyte solutions. In this work the database has been extended with 7,000 volumetric data points for the system of interest (see appendix C). These literature data points have mainly been measured by density measurements or directly from measurements of apparent molal volumes.

Prior to the regression of model parameters, a basic statistic analysis of the data has been conducted to exclude obviously incorrect data. The remaining data are listed in table 3.1 (in the back of the chapter).

3.3.1 Parameters at 25°C

The standard state molal volume at 25°C has been reported for many ions by several different authors. In this work the recommended values of Marcus[12] have been implemented in the model and have therefore not been regressed from experimental data. It is not possible to measure the volume of an ion independently due to the electroneutrality criteria. Therefore the properties usually are measured relative to the properties of the H^+ ion. The values of Marcus have therefore been corrected so the standard state molal volume of the H^+ ion is equal to zero and the k parameter of H^+ has also been assigned the value zero.

The use of ionic parameters makes the system internally consistent and it is therefore not necessary to include data for all the different salts in the parameter regression. In this work only data for the following 8 salts have been included in the regression of the model parameters at 25°C; NaCl, $NaNO_3$, Na_2SO_4, KCl, HCl, NH_4Cl, $CaCl_2$, $MgCl_2$. The volumetric properties of these salts are very well documented in the literature and are sufficient to regress accurate parameters for the entire system of ions. The parameters obtained are thus able to describe the density of binary and multicomponent solutions of all 18 salts formed by these ions.

The k_i parameters for all ions have been estimated simultaneously from the chosen experimental data using the objective function:

$$OF = \sum \left(\frac{\phi_{V,Exp.} - \phi_{V,Calc.}}{\phi_{V,Exp.}} \right)^2 \qquad [3.22]$$

3.3.2 Temperature Variation of Model Parameters

The temperature dependence of the standard state molal volumes at infinite dilution, $\overline{v}_i^{\nabla}$, and the k_i parameters were fitted by simple second order polynomial expressions:

$$\overline{v}_i^{\nabla} = \overline{v}_i^{(1)} + \overline{v}_i^{(2)} (t-25) + \overline{v}_i^{(3)} (t-25)^2 \qquad [3.23]$$

$$k_i = k_i^{(1)} + k_i^{(2)} (t-25) + k_i^{(3)} (t-25)^2 \qquad [3.24]$$

The parameters for the temperature dependence were regressed from data for the same 8 salts as mentioned above. However, the amount of data available for the 8 original salts at high temperatures is limited, and additional data for KNO_3 and K_2SO_4 were included in order to increase the accuracy of the parameters in the high temperature area. All parameters were regressed simultaneously using the objective function given in eq. [3.22].

3.4 Results and Discussion

All experimental data and model results are listed in table 3.1 (in the end of the chapter). The parameters regressed from experimental data are given in table 3.2.

Table 3.2. Parameters of eq. [3.21, 3.23-3.24] regressed from experimental data. $\overline{v}_i^{(1)}$ taken from Marcus[12] (has been corrected so that the value of H^+ is equal to zero)

i	$\overline{v}_i^{(1)}$	$\overline{v}_i^{(2)} \cdot 10^2$	$\overline{v}_i^{3} \cdot 10^4$	$k_i^{(1)}$	$k_i^{(2)} \cdot 10^2$	$k_i^{(3)} \cdot 10^4$
H^+	0	0	0	0	0	0
Na^+	-1.2	7.748	-13.80	0.9758	-2.628	6.309
K^+	9	6.331	-7.502	1.094	-2.689	3.919
Mg^{++}	-21.2	1.096	-9.093	1.493	-2.144	4.751
Ca^{++}	-17.9	-1.938	2.789	1.581	3.450	-5.821
NH_4^+	18.2	1.604	-1.957	0.4435	-0.7984	0.5941
Cl^-	17.8	3.692	-7.407	0.9454	-0.0979	0.9162
SO_4^{--}	14	13.36	-27.39	4.837	-2.927	6.793
NO_3^-	29	10.78	-4.537	1.307	-2.751	0.0439

3.4.1 Binary Solutions

The results for the binary systems at 25°C are shown in the figures 3.5-3.7. The figures show that the agreement between model calculations and experimental data is very good for the majority of the salts, even though only a part of the data have been used in the parameter regression.

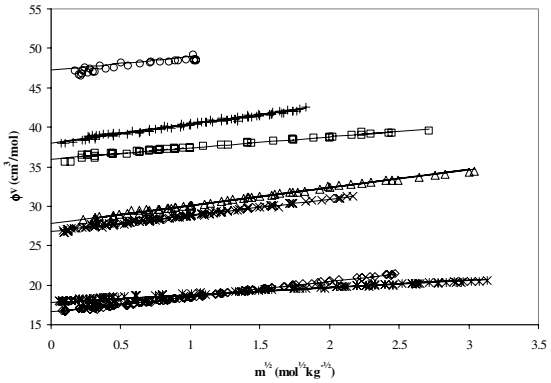

Figure 3.5. Model results for binary systems. 1:1 electrolytes.
(◇) NaCl, (△) $NaNO_3$, (×) KCl, (+) KNO_3, (□) NH_4Cl, (o) NH_4NO_3, (∗) HCl, (–) Model correlation.

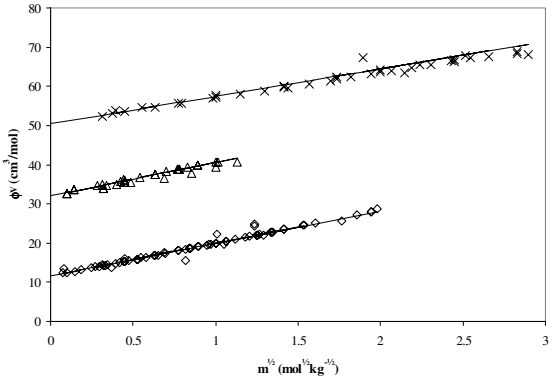

Figure 3.6. Model results for binary systems. 1:2 electrolytes.
(◇) Na_2SO_4, (△) K_2SO_4, (×) $(NH_4)_2SO_4$, (–) Model correlation.

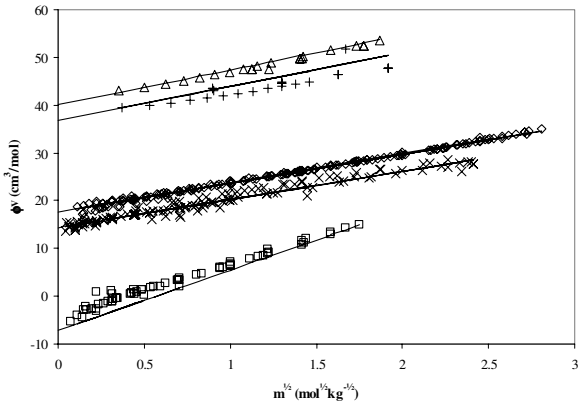

Figure 3.7. Model results for binary systems. 2:1 electrolytes and 2:2 electrolytes.
(◇) CaCl2, (△) $Ca(NO_3)_2$, (×) $MgCl_2$, (+) $Mg(NO_3)_2$, (□) $MgSO_4$, (–) Model correlation.

In the case of Na_2SO_4 is it seen that the model correlation actually holds up to 4 molal, even though the solution at this point is highly supersaturated. There is though, a slight inaccuracy in the calculated results for the $MgSO_4$ and the $Mg(NO_3)_2$ systems. This might be caused by the high degree of association between Mg^{++} and NO_3^- and SO_4^{--}. These types of interactions are not taken into account in the model. An example of how the model could be extended to systems with systems with weaker electrolytes is given in appendix D. However, even in these highly non-ideal systems the average relative error is only 2.5 – 3% in the apparent molal volume. It should be noted, that these deviations would only cause relative errors between calculated and experimental densities of 0.1 ‰ or lower.

The temperature dependence of the apparent molal volume has been modeled using eq. [3.26, 3.28-3.29], and the relative errors for all the relevant data are shown in table 3.1. The table shows that the average relative deviation between calculated and experimental apparent molal volumes for most systems is below 1%.

A graphical representation of the temperature variance and the model capabilities is shown in figure 3.8, where model results are compared with volumetric data of solutions of $NaNO_3$. Optimal values of $\bar{v}_i^{\nabla}$ and k_i for eq. [3.21] were determined for each temperature by regression

of experimental data. In figure 3.8 the optimal values are compared with $\overline{v}_i^{\nabla}$ and k_i values that has been calculated using eq. [3.23] and [3.24] with the parameters given in table 3.2.

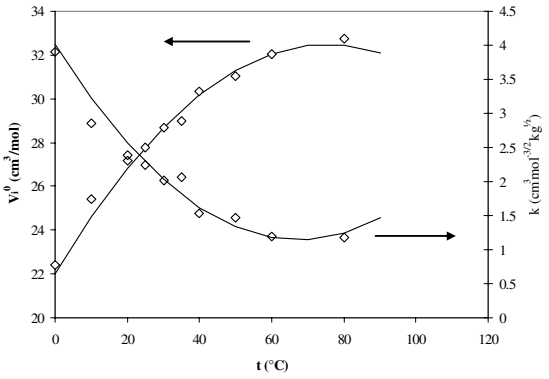

Figure 3.8. k_i and $\overline{v}_i^{\nabla}$ for the $NaNO_3$ system.
(◇) Optimal values at individual temperatures. (–) Calculated by eq. [3.23-3.24]

In the figure it is seen that a better representation of the data might be obtained using a higher degree of the polynomials in eq. [3.23-3.24] used to calculate k_i and $\overline{v}_i^{\nabla}$. One example of a much more comprehensive model applied to volumetric properties of electrolyte solutions is the recent work of Krumgalz et al.[5]. The model of Krumgalz et al. is based on the model of Pitzer[13] and gives extremely precise correlations for many binary solutions of aqueous electrolyte solutions. However, applying the model of Krumgalz to the system investigated in this work would require more than 450 parameters. This can be compared to the less than 50 parameters of the model used in this work. In addition, figure 3.8 show that there is some scattering in the volumetric data. The unreliability of experimental volumetric data is a general problem. One of the reasons for this is that most of the available data are found from density measurements. The apparent molal volume is much more sensitive to experimental inaccuracies than the densities. In semi dilute solutions an error of $1‰$ in the density can easily lead to an error of 25% in apparent molal volume of the electrolyte in the solution. This is the reason why in this work it has been chosen to use simple polynomials instead of more complex relations that most probably would include experimental noise in the parameters.

3.4.2 Multicomponent Solutions

Eq. [3.21] can easily be applied to multicomponent solutions. In figure 3.9 the model has been applied to the system NaCl – K_2SO_4 with an ionic strength of 1.5 mol/kg. The figure shows very good agreement between the calculated results and the experimental data.

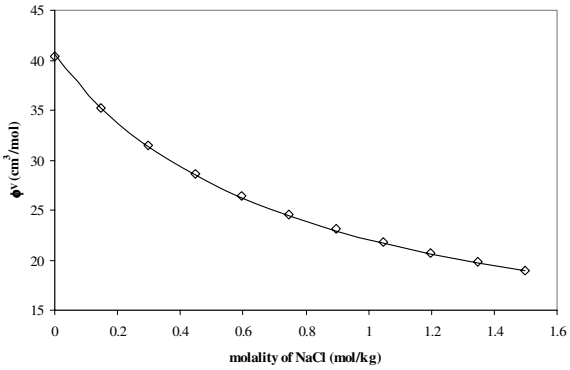

Figure 3.9. The apparent molal volume in solutions of NaCl and K_2SO_4 at I_m = 1.5 mol/kg and 25°C. (◇) Exp. datapoints[14]. (–) Calculated by eq. [3.21].

Table 3.3. Results for the calculation of densities in multicomponent systems.

Species	I_{max}	N_{data}	$100 \cdot \Delta\rho / \rho_{Exp.}$	Source
Na^+, Ca^{++}, Cl^-	6.4	72	0.001	58
K^+, Cl^-, $SO4^{--}$	1.5	10	0.007	13
Na^+, Cl^-, SO_4^{--}	1.5	10	0.01	13
K^+, Ca^{++}, Cl^-	4.5	11	0.07	8
K^+, Ca^{++}, Cl^-, SO_4^{--}	1.5	10	0.02	13
H^+, K^+, Na^+, Cl^-	2.1	15	0.025	74
K^+, Na^+, Cl^-, SO_4^{--}	2.1	9	0.025	51
Na^+, K^+, Cl^-, SO_4^{--}	2.0	9	0.015	51
Na^+, Mg^{++}, Cl^-, SO_4^{--}	2.9	18	0.035	75
Na^+, K^+, Mg^{++}, Ca^{++}, Cl^-	9.2	9	0.11	73

In table 3.3 model results have been compared with multicomponent density data from several different sources. From the table it is seen that even in the very concentrated solutions, the relative deviation from the experimental data is only approximately 1‰. Another example of the model capabilities in concentrated multicomponent solutions is given in figures 3.10-3.11. In these figures calculated densities are compared with experimental values for saturated ternary and quaternary systems. The results presented in table 3.3, in figure 3.10 and in figure 3.11 are pure predictions as only data for binary, more dilute solutions were used in the parameter estimation. For all the included systems it is seen that the deviations between calculated and experimental densities are within the experimental accuracy of the data.

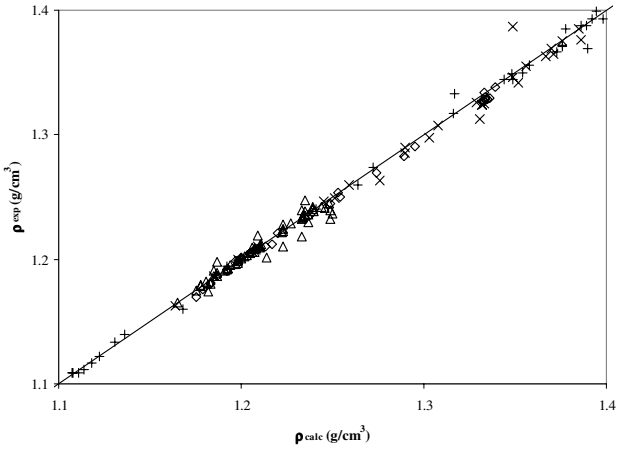

Figure 3.10. Calculated and experimental densities of ternary aqueous systems at saturation (two-salt points). Temperatures between 0-70°C.
(×)[76] Na^+, Cl^-, NO_3^-, (+)[77] Na^+, NO_3^-, SO_4^{--}, (◇)[78] Na^+, Mg^{++}, Cl^-, (△)[79] Na^+, K^+, Cl^-.

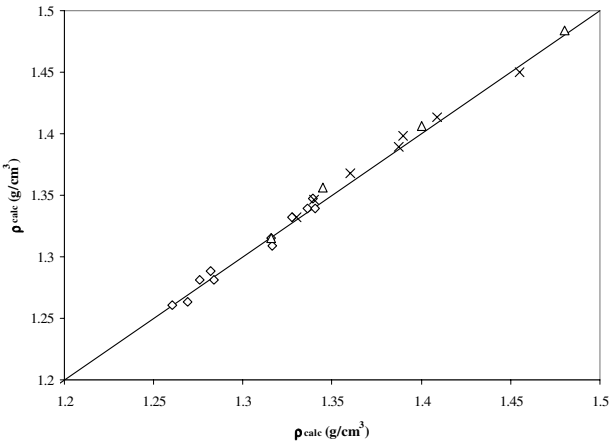

Figure 3.11. Calculated and experimental densities of quaternary aqueous systems at saturation (three-salt points). Temperatures between 0-80°C.
(×)[80] Na^+, Mg^{++}, Cl^-, NO_3^-, (+)[79] Na^+, K^+, NO_3^-, Cl^-, (◇)[79] Na^+, K^+, Mg^{++}, Cl^-.

3.5 Conclusion

A modification of the Masson equation combined with Young's rule based on ion specific parameters has been applied to volumetric data for mixtures of (H^+, Na^+, K^+, NH_4^+, Ca^{++}, Mg^{++}) (Cl^-,NO_3^-,SO_4^{--}). The parameters have been regressed from data in the temperature range 0 – 100°C and concentration range 0 – 11.8 mol/kg, but are shown to be valid up to the point of saturation. The model only requires 5 parameters and the standard state molal volume per ion in the entire range of concentration and temperature. The model parameters have been regressed on the basis of data from only few selected salts. In spite of this, the deviations between model calculations and experimental data for all the salts formed by these ions are in most cases within the experimental accuracy of the data used in the work. The model is easily applied to multicomponent mixtures, and it is shown that the relative errors of the predicted results in both ternary and quaternary systems are well within the experimental accuracy of the data.

Table 3.1. List of experimental data and relative deviation between experimental and calculated results.

Salt	Molality	T (°C)	N_{data}	$100 \cdot \Delta\phi_V / \phi_{V,Exp.}$	Source
NaCl	0.17 – 6.0	0 - 80	96	0.84	15
	0.5 – 5.0	15 - 35	17	0.49	16
	1.0 – 6.1	25 - 40	29	0.30	17
	0.01 – 1.5	0 – 35	44	0.39	18
	0.5 – 5.8	10 – 40	20	0.34	19
	0.05 – 5.8	25 – 50	24	0.61	20
	0.5 – 4.4	0 – 60	19	2.04	21
	0.01 – 1.0	0 – 35	48	0.38	22
	0.05 – 3.7	5 – 25	39	0.39	23
	0.16 – 5.9	15 – 30	26	0.47	24
	0.01 – 2.8	25	40	0.56	25
	0.1 – 5.0	25	8	0.48	26
	0.04 – 2.4	25	5	0.15	27
$NaNO_3$	0.12 – 9.6	0 – 80	177	0.68	15
	0.19 – 5.8	25	12	0.49	28
	0.5 – 4.0	20 – 30	13	0.78	16
	0.6 – 10.4	0 – 80	16	1.14	29
	0.2 – 3.1	30	6	0.21	30
	0.05 - 1	25	11	0.22	31
	0.3 – 9.2	25	9	0.45	32
	0.1 – 10.8	25	18	0.34	33
Na_2SO_4	0.14 – 5.5	25	16	1.50	28
	0.10 – 3.0	15 – 35	17	1.73	16
	0.02 – 2.0	0 - 50	33	2.51	34
	0.07 – 2.4	25 – 75	14	1.57	35
	0.02 – 1.4	0 – 35	74	1.35	18
	0.02 – 0.28	15 – 40	17	3.25	36
	0.9 – 1.8	25	10	0.27	37
	0.2 – 2.0	25	12	0.32	22
	1.1 – 3.9	60	6	1.86	38
KCl	0.14 – 5.2	0 – 80	121	0.54	15

	0.05 – 4.0	15 – 55	38	0.53	16
	0.5 – 4.5	25 – 45	45	0.32	17
	0.06 – 1.0	50	6	1.56	34
	0.71 – 3.5	40 – 60	7	0.45	35
	2.1 – 4.6	20 – 50	8	0.89	39
	0.04 – 1.0	15 – 65	31	1.38	40
	0.10 – 4.7	10 – 40	35	0.34	19
	0.33 – 4.6	20 – 50	36	0.34	20
	1.1 – 4.8	35	4	0.22	41
	0.51 – 4.6	35 – 45	10	0.71	42
	0.05 – 2.9	25	18	0.06	23
	0.08 – 2.1	25	20	0.56	25
	0.06 – 3.0	25	7	0.16	26
	0.09 – 1.4	25	9	0.43	43
	0.1 – 1.0	25	10	0.16	31
	0.009 – 0.6	25	13	0.38	44
	0.2 – 3.0	25	9	0.18	45
	0.07 – 4.3	25	14	0.14	46
KNO_3	0.86 – 3.1	0 – 100	101	0.81	15
	0.05 – 3.0	15 – 45	30	0.34	16
	0.009 – 1.9	30	10	0.30	30
	0.005 – 0.5	5 – 30	110	0.61	47
	0.2 – 3.1	25	11	0.32	45
	0.06 – 2.5	25	35	0.30	48
	0.5 – 3.0	25	10	0.39	49
K_2SO_4	0.12 – 1.3	0 – 100	50	2.2	15
	0.04 – 1.3	0 – 25	20	1.5	50
	0.006 – 1.4	0 – 50	41	1.1	34
	0.06 – 1.3	5 – 95	90	1.2	51
	0.01 – 0.18	15 – 35	20	0.9	52
	0.20 – 2.1	25	7	0.4	31
NH_4Cl	0.19 – 5.9	0 – 100	121	0.45	15
	0.05 – 5.0	15 – 55	101	0.42	16
	0.01 – 0.62	15 – 35	17	0.93	36
	3.0 – 8.0	50 - 100	98	0.4	53

	0.2 – 1.0	25	8	0.03	31
	0.1 – 7.4	25	14	0.13	33
NH_4NO_3	0.13 – 5.4	0 – 80	125	1.9	15
	0.04 – 1.1	25	20	1.0	54
	1.1 – 10.9	25	7	3.0	55
	0.05 – 12.7	25	16	2.5	56
$(NH_4)_2SO_4$	0.13 – 6.5	0 – 100	147	1.2	15
	0.1 – 10.0	15 – 55	110	1.1	16
	1.0 – 8.0	25	7	0.8	57
$CaCl_2$	0.18 – 6.0	0 – 100	154	2.8	15
	0.05 – 6.0	15 – 55	42	2.6	16
	1.41 – 6.41	25	24	0.20	58
	0.05 – 5.0	25	8	0.27	26
	0.02 – 7.9	25	76	0.61	43
	0.01 – 0.33	25	8	1.58	59
	0.67 – 7.4	25	14	0.60	60
$Ca(NO_3)_2$	0.12 – 2.0	6 – 30	44	0.93	15
	0.12 – 2.6	17.5	30	1.7	50
	1.3 – 10.3	25 – 60	52	1.4	61
	0.03 – 1.9	20 – 35	25	1.1	50
	1.3 – 8.4	25	8	1.7	50
	1.5 – 3.5	25	5	0.52	50
$MgCl_2$	0.2 – 4.5	0 – 100	128	2.5	15
	0.54 – 3.3	25	7	0.62	17
	0.003 – 0.9	0 – 50	45	3.0	34
	0.05 – 1.5	25	25	0.54	18
	0.005 – 0.97	0 – 30	37	1.8	18
	1.0 – 5.7	25 – 60	23	1.7	62
	0.05 – 0.97	25	9	0.28	31
	0.004 – 0.34	25	8	0.90	59
	0.002 – 5.8	25	23	1.0	63
$Mg(NO_3)_2$	0.14 – 2.1	0 – 40	62	3.2	15
	0.15 – 3.7	0 – 25	30	2.9	50
	0.8 – 3.7	25	5	2.1	64
HCl	0.27 – 11.8	0 – 100	151	0.81	15

	0.56 – 4.5	0 – 60	42	0.96	65
	0.56 – 5.2	0 – 50	59	0.58	66
	0.09 – 1.0	5 - 35	35	0.61	67
	0.61 – 8.5	25	8	0.52	57
	0.01 – 0.23	25	8	0.99	68
	0.13 – 10.2	25	38	0.67	69
	0.004 – 0.19	25	27	0.55	70
HNO_3	0.16 – 6.8	0 - 100	228	2.87	15
	0.64 – 11.4	25	23	3.12	71
	0.11 – 1.15	25	20	0.91	72

3.6 References

(1) Masson, D. O. Solute molecular volumes in relation to solvation and ionization. *Phil. Mag.* **1929**, 8, 218.

(2) Root, Wm. C.. Equation relating density and concentration. J. Am. Chem. Soc. **1933**, 55, 850.

(3) Söhnel, O.; Novotny, P. *Densities of Aqueous Solutions of Inorganic Substances. Phys. Sci. Data 22*; Elsevier: Tokyo, **1985**.

(4) Kumar, A. Volume properties of aqueous electrolytes. 1. Examination of apparent molal volume data by the Pitzer model. *J. Chem. Eng. Data*. **1987**, 32, 106.

(5) Krumgalz, B.S; Pogorelskii, R.; Sokolov, A.; Pitzer, K.S. Volumetric Ion Interaction Parameters for Single-Solute Aqueous Electrolyte Solutions at Various Temperatures. *J. Phys. Chem. Ref. Data*. **2000**, 29, 1123.

(6) Redlich, O.; Rosenfeld, P. The theory of the molal volume of a dissolved electrolyte. II. *Z. Elektrochem. Phys. Chem.* **1931**, 37, 705.

(7) Harvey, A.H., Perskin, A.P., Klein, S.A., **1996**. NIST/ASME steam properties formulation for general and scientific use.

(8) Robinson R.A. and R.H. Stokes, Electrolyte Solutions, 2nd edition, Butterworth and Co., London, **1970**.

(9) Young, T.F.; Smith, M.B. Thermodynamic Porperties of Mixtures of Electrolytes in Aqueous Solutions. *J. Phys. Chem.* **1954**, 58, 716.

(10) Kumar, A. Densities and apparent molal volumes of aqueous potassium chloride-calcium chloride mixtures at 298.15 K. *J. Chem. Eng. Data.* **1986**, 31, 21.

(11) http://www.ivc-sep.kt.dtu.dk/databank/databank.asp

(12) Marcus, Y. Ion Properties. Marcel Dekker. New York, **1997.**

(13) Pitzer, K.S. Thermodynamics of electrolytes. I. Theoretical basis and general equations. *J. Phys. Chem.* **1973**, 77, 268.

(14) Millero, F.J.; Sotolongo, S. PVT properties of concentrated aqueous electrolytes. 7. The volumes of mixing of the reciprocal salt pairs potassium chloride, potassium

sulfate, sodium chloride, and sodium sulfate at 25°C and I = 1.5 M. *J. Chem. Eng. Data,* **1986**, 31, 470

(15) Washburn, E.W. International Critical Tables of Numerical Data, Physics, Chemistry and Technology. McGraw-Hill Book Company, New York, **1928**.

(16) Isono, T. Measurements of Density, Viscosity and Electrolyte Conductivity of Concentrated Aqueous Electrolyte Solutions. *Rikakaku Kenkyusho Hokoku.* **1980**, 56, 103.

(17) Romankiw, L.A.; Chou, I.M. Densities of aqueous sodium chloride, potassium chloride, magnesium chloride, and calcium chloride binary solutions in the concentration range 0.5-6.1 m at 25, 30, 35, 40, and 45°C. *J. Chem. Eng. Data.* **1983**, 28, 300.

(18) Chen, C.-T.A.; Chen, J.H.; Millero, F.J. Densities of NaCl, $MgCl_2$, Na_2SO_4 and $MgSO_4$ Aqueous Solutions at 1 atm. from 0 to 50° and from 0.001 to 1.5m. *J. Chem. Eng. Data.* **1980**, 25, 307.

(19) Lengyel, S.; Tamás, J.; Giber, J.; Holderith, J. Study of Viscosity of Aqueous Alkali Halide Solutions. *Acta Chim. Hung.* **1964**, 40, 125.

(20) Goncalves, F.A.; Kestin, J. The Viscosity of NaCl and KCl in the range 25-50°C. *Ber. Bunsenges. Phys. Chem.* **1977**, 81, 1156

(21) Lyle, T.R.; Hosking, R. The Temperature Variations of the Specific Molecular Conductivity and the Fluidity of Sodium Chloride Solutions. *Phil. Mag. Ser.* **1902**, 6, 487.

(22) Millero, F.J. The Apparent and Partial Molal Volume of Aqueous Sodium Chloride Solutions at Various Temperatures. *J. Phys. Chem*. **1970**, 74, 356.

(23) Vaslow, F. The Apparent Molal Volume of the Lithium and Sodium Halides. Critical-type Transitions in Aqueous Solution. *J. Phys. Chem*. **1969**, 73, 3745.

(24) Dessauges, G.; Miljevic, N.; Van Hook, W.A. Isotope effects in aqueous systems. 9. Partial molar volumes of sodium chloride/water and sodium chloride/water-d2 solutions at 15, 30, and 45°C. *J. Phys. Chem.* **1980**, 84, 2587.

(25) Olofsson, I.V. Apparent molar heat capacities and volumes of aqueous sodium chloride, potassium chloride, and potassium nitrate at 298.15 K. Comparison of Picker flow calorimeter with other calorimeters. *J. Chem. Thermodyn*. **1979**, 11, 1005.

(26) Gates, J.A.; Wood, R.H. Densisties of Aqueous Solutions of NaCl, $MgCl_2$, KCl, NaBr, LiCl and $CaCl_2$ from 0.05 to 5.0 mol/kg and 0.1013 to 40 MPa at 298.15K. *J. Chem. Eng. Data.* **1985**, 30, 44.

(27) Wirth, H.E. Apparent and partial molal volumes of sodium chloride and hydrochloric acid in mixed solutions. *J. Am. Chem. Soc.* **1940**, 62, 1128.

(28) Lobo, V.M.M; Quaresma J.L. Handbook of Electrolyte Solutions. Elsevier, New York, **1989**.

(29) Puchkov, L.V.; Matashkin, V.G. Density of lithium nitrate-water and sodium nitrate-water solutions at 25-300.deg. *Zhurnal Prikladnoi Khimii*. **1970**, 43, 1848.

(30) Barchiesi, M.A.; Berchiesi, G.; Lobbia, G.G. Apparent Molal Volumes of Alkali Metal Nitrates at 30°C. *J. Chem. Eng. Data.* **1974**, 19, 326.

(31) Millero, F.J.; Ward, G.K.; Chertirkin, P.V. Relative Sound Velocities of Sea Salts at 25°C. *J. Acoust. Soc. Am.* **1977**, 61, 1492.

(32) Kartzmark, E.M. Conductances, densities, and viscosities of solutions of sodium nitrate in water and in dioxane-water, at 25.deg. *Can. J. Chem*. **1972**, 50, 2845.

(33) Pearce, J.N.; Hopson, H. The vapor pressures of aqueous solutions of sodium nitrate and potassium thiocyanate. *J. Phys. Chem.* **1937**, 41, 535.

(34) Millero, F.J; Knox, J.H. Apparent Molal Volumes of Aqueous NaF, Na_2SO_4, KCl, K_2SO_4, $MgCl_2$ and $MgSO_4$ Solutions at 0° and 50°. *J. Chem. Eng. Data.* **1973**, 18, 407.

(35) Korosi, A.; Fabuss, B.M. Viscosities of Binary Aqueous Solutions of NaCl, KCl, Na_2SO_4 and $MgSO_4$ at Concentrations amd Temperatures of interest in Delalination Processes. *J. Chem. Eng. Data*, **1968**, 13, 548.

(36) Kaminsky, M. The concentration and temperature dependence of the viscosity of aqueous solutions of strong electrolytes. III. KCl, K_2SO_4, $MgCl_2$, $BeSO_4$, and $MgSO_4$ solutions. *Z. physik. Chem.* **1957**, 12, 206.

(37) Lühdemann, R. The Dependence on Concentration of the Equivalent Refraction of a Few Salts and Acids in Aqueous Solution. *Z. Phys. Chem*. **1935**, B29, 133.

(38) Trimble, H.M. Solubility of potassium permanganate in solutions of potassium sulfate and of sodium sulfate. *J. Am. Chem. Soc.* **1922** , 44, 451.

(39) Suhrmann, R.; Wiedersich, I. The Effect of Foreign Ions on the Conductivity of Hydrogen Ion in Aqueous Solutions. *Z. Annorg. Allg. Chem.* **1953**, 272, 167.

(40) Out, D.J.P; Los, J.M. Viscosity of Aqueous Solutions of Univalent Electrolyes from 5 to 95°. *J. Sol. Chem.* **1980**, 9, 19

(41) Scott, A.F.; Wilson, R.W. The apparent volumes of salts in solution and their compressibilities. *J. Phys. Chem.* **1934**, 38, 951.

(42) Firth, J.G.; Tyrrell, H.J.V. Diffusion Coefficients for Aqueous Silver Nitrate Solutions at 25°, 35° and 45° from Diaphragm-cell Measurements. *J. Chem. Soc.* **1962**, 2042.

(43) Zhang, H.-L.; Chen, G.-H.; Han, S.-J. Viscosity and Density of H_2O + NaCl + $CaCl_2$ and H_2O + KCl + $CaCl_2$ at 298.15 K. *J. Chem. Eng. Data.* **1997**, 42, 526.

(44) MacInnes, D.A.; Dayhoff, M.O. The partial molal volumes of potassium chloride, potassium and sodium iodides, and of iodine in aqueous solution at 25°. J. Am. Chem. Soc. 1952, 74, 1017.

(45) Epikhin, Y.A.; Stakhanova, M.S.; Karapetyants, M.K. Volume and heat capacity changes in aqueous salt solutions. III. The KCl-KNO_3-H_2O system. *Zhurnal Fizicheskoi Khimii*. **1964**, 38, 692.

(46) Shibata, E.; Oda, S.; Furukawa, S. Thermodynamic study of chemical change. VI. Thermodynamic investigation of potassium chloride. *Nippon Kagaku Kaishi*. **1931**, 51, 71.

(47) Halasey, M.E. Partial Molal Volumes of Potassium Salts of the Hofmeister Series. *J. Phys. Chem.* **1941**, 45, 1252.

(48) Pena, M.P.; Vercher, E.; Martinez-Andreu, A. Apparent Molar Volumes of Potassium Nitrate and Sodium Nitrate in Ethanol + Water at 298.15 K. *J. Chem. Eng. Data*. **1998**, 43, 626.

(49) Doan, T.H.; Sangster, J. Viscosities of Concentrated Aqueous Solutions of Some 1:1, 2:1, and 3:1 Nitrates at 25°C. *J. Chem. Eng. Data.* **1981**, 26, 141.

(50) Timmermans, J. The Physico-chemical constants of binary systems in concentrated solutions, 3,, Systems with metallic compounds. Interscience. New York, 1960

(51) Dedick, E.A.; Hershey, J.P.; Sotolongo, S.; Stade, D.J.; Millero, F.J. The PVT properties of concentrated aqueous electrolytes. IX. The volume properties of potassium chloride and potassium sulfate and their mixtures with sodium chloride and sodium sulfate as a function of temperature. *J. Sol. Chem*. **1990**, 19, 353.

(52) Kaminsky, M. Concentration and Temperature Dependence of the Viscosity of Aqueous Solutions of Strong Electrolytes. III. KCl, K_2SO_4, $MgCl_2$, $BeSO_4$ and $MgSO_4$ solutions. *Z. Phys. Chem*. **1957**, 12, 206.

(53) Rashkovskaya, E.A.; Chernen'kaya, E.I. Densities of ammonium bicarbonate, sodium bicarbonate, and ammonium chloride and ammonia salt solutions at 20-100°. *Zhurnal Prikladnoi Khimii.* **1967**, 40, 301.

(54) Campbell, A.N.; Friesen, R.J. Conductance in the Range Medium Concentration. *Can. J. Chem.* **1959**, 37, 1288.

(55) Campbell, A.N.; Kartzmark, E.M. The Normal Boiling Points and Other Physical Properties of Strong Solutions of Silver Nitrate and of Ammonium Nitrate. *Can J. Research*, **1950**, 28B, 161

(56) Campbell, A.N.; Gray, A.P.; Kartzmark, E.M. Conductances, Densities, and Fluidities of Solutions of Silver Nitrate and of Ammonium Nitrate at 35°C. *Can. J. Chem.* **1953**, 31, 617.

(57) Goldsack, D.E.; Franchetto, A.A. The Viscosity of Ceoncentrated Electrolyte Solutions. III. A Mixture Law. *Electrochimica Acta*. **1977**, 22, 1287.

(58) Oakes, C.S.; Simonson, J.M.; Bodnar, R.J. The system sodium chloride-calcium chloride-water. 2. Densities for ionic strengths 0.1-19.2 $mol \times kg^{-1}$ at 298.15 and 308.15 and at 0.1 MPa. *J. Chem. Eng. Data.* **1990**, 35, 304.

(59) Perron, G.; Desnoyers, J.E. Apparent Molal Volumes and Heat Capacities of Alkaline Earth Chlorides in Water at 25°C. *Can. J. Chem.* **1974**, 52, 3738.

(60) Kumar, A.; Atkinson, G.; Howell, R.D. Thermodynamics of concentrated electrolyte mixtures. II. Densities and compressibilities of aqueous sodium chloride-calcium chloride at 25°C. *J. Sol. Chem.* **1982**, 11, 857.

(61) Ewing, W.W.; Mikovsky, R.J. Calcium nitrate. V. Partial molal volumes of water and calcium nitrate in concentrated solution. *J. Am. Chem. Soc.* **1950**, 72, 1390.

(62) Ezrokhi, L.L. Viscosity of Aqueous Solutions of the Individual Salts of Sea Water Systems. *J. App. Chem. USSR*. **1952**, 25, 917

(63) Miller, D.G.; Rard, J.A.; Eppstein, L.B.; Albright, J.G. Mutual Diffusion Coefficients and Ionic Coefficients l_{ij} of $MgCl_2$ - H_2O at 25°C. *J. Phys. Chem.* **1984**, 88, 5739.

(64) Herz, W. Internal Friction of Salt Solutions. *Z. Anorg. Chinie.* **1914**, 89, 393.

(65) Åkerlöf, G.; Teare, J.W. A note on the density of aqueous solutions of hydrochloric acid. *J. Am. Chem. Soc.* **1938**, 60, 1226.

(66) Haase, R.; Sauermann, P.-F.; Dücker, K.-H. Conductivities of Concentrated Electrolyte Solutions. II. Nitric Acid. *Z. Physik. Chem.* **1965**, 46, 129.

(67) Hershey, J.P.; Damesceno, R.; Millero, F.J. Densities and compressibilities of aqueous hydrochloric acid and sodium hydroxide from 0 to 45°C. The effect of pressure on the ionization of water. J. Sol. Chem. 1984, 13, 825.

(68) Pogue, R.; Atkinson, G. Apparent molal volumes and heat capacities of aqueous hydrogen chloride and perchloric acid at 15-55°C. *J. Chem. Eng. Data*. **1988**, 33, 495.

(69) Rizzo, P.; Albright, J.G.; Miller, D.G. Measurements of Interdiffusion Coefficients and Densities for the System HCl + H_2O at 25 °C. *J. Chem. Eng. Data.* **1997**, 42, 623.

(70) Redlich, O.; Bigeleisen, J. Molal Volumes of Solutes VI. Potassium Chlorate and Hydrochloric Acid. *J. Am. Chem. Soc.* **1942**, 64, 758.

(71) Haase, R.; Sauermann, P.F.; Duecker, K.H. Conductivities of concentrated electrolyte solutions. II. Nitric acid. *Z. Phys. Chem.* **1965**, 46, 129.

(72) Hovey, J.K.; Hepler, L.G.; Tremaine, P.R. Apparent molar heat capacities and volumes of aqueous perchloric and nitric acids, tetramethylammonium hydroxide and potassium sulfate at 298.15 K. *Ther. Acta* **1988**, 126, 245.

(73) Krumgalz, B.S.; Millero, F.J. Physicochemical study of Dead Sea waters. II. Density measurements and equation of state of Dead Sea waters at 1 atm. *Marine Chemistry.* **1982**, 11, 477.

(74) Ruby, C. E.; Kawai, J. Densities, equivalent conductances and relative viscosities at 25°, of solutions of hydrochloric acid, potassium chloride and sodium chloride, and of their binary and ternary mixtures of constant chloride-ion-constituent content. *J. Am. Chem. Soc.* **1926**, 48 1119.

(75) Millero, F.J.; Connaughton, L.M.; Vinokurova, F.; Chetirkin, P.V. PVT properties of concentrated aqueous electrolytes. III. Volume changes for mixing the major sea salts at I = 1.0 and 3.0 at 25°C. *J. Sol. Chem.* **1985**, 14(12), 837-51.

(76) Mayeda, T.J. Equilibrium of the system water and the chlorides and sulfates of sodium and magnesium at 105°. *J. Soc. Chem. Ind., Japan*. **1920**, 23, 573.

(77) Benrath, A.; Pitzler, H.; Ilieff, N.; Beu, W.; Schloemer, A.; Clermont, J.; Kojitsch, S.; Benrath, H. Über das reziproke salzpaar $MgSO_4$-$Na_2(NO_3)_2$-H_2O. I. *Z. Anorg. Chem.* **1928**, 170, 257.

(78) Kurnakov, N. S.; Manoev, D. P.; Osokoreva, N. A. Solubility of the carnallite system. *Kali*, **1932**, No. 2 25.

(79) Osokoreva, N. A.; Opuikhtina, M. A.; Shoikhet, D. N.; Plaksina, E. F.; Zaslavskii, A. I. Equilibria of the solutions in the system NaCl-KCl-$MgCl_2$-H_2O. *Tr. Gos. Inst. Prikl. Khim*. **1932**, 16, 24.

(80) Frowein, F.; von Mühlendahl, E. Die lösungen des doppelt-ternären Salzgemisches. *Z. Angew. Chem.* **1926**, 39, 1488.

4. Application of the Extended UNIQUAC Model to Acidic Solutions.

This chapter is a rewriting of the article "*Modeling of vapor-liquid-solid equilibria in acidic aqueous solutions*" co-authored with Kaj Thomsen and published in Industrial and Engineering Chemical Research. 2003, 42, 4260.

The phase behavior (vapor - liquid equilibria (VLE) and solid – liquid equilibria (SLE)) and thermal properties of aqueous solutions of ions like (K^+, Na^+, NH_4^+, Ca^{2+}, Cl^-) in the presence of phosphoric acid (H_3PO_4, $H_2PO_4^-$, HPO_4^{2-}) and nitric acid (HNO_3, NO_3^-) are described by means of the Extended UNIQUAC model. Model parameters are evaluated on the basis of more than 2000 experimental data points. There is good agreement between calculated and experimental data points. The model parameters are valid in the temperature range from -18 - +122°C and in the concentration range up to 12 molal for the acids HNO_3 and H_3PO_4.

4.1 Introduction

The phase behavior of multicomponent aqueous electrolyte systems is important in many processes in the chemical industry. Developing models for describing these kinds of systems are relevant in order to be able to optimize processes as well as equipment in these types of industries.

Most of the existing work on modeling aqueous electrolyte solutions has primarily considered neutral or slightly acidic solutions. However, in industries such as the mineral and fertilizer industry, many processes involve highly acidic solutions. The intention of this work is to extend the existing parameters of the Extended UNIQUAC model to acidic environments.

The binary phosphoric acid – water system has previously been modeled by Jiang[1], and Cherif et al.[2]. The binary nitric acid – water system has previously been modeled by Rains et al.[3]. To my knowledge no multicomponent model including phosphoric acid, nitric acid, and other ions has previously been presented in the open literature.

In industrial applications such as the production of potassium phosphate from phosphate rock the major components are K^+, Ca^{2+}, H^+, NO_3^-, $H_2PO_4^-$. For such applications, a model that is capable of describing multicomponent mixtures is necessary. The model parameters

determined in this thesis are intended for the use in this type of applications. In previous works[4,5] it has been shown that the Extended UNIQUAC model gives very reasonable predictions in systems with more than 3 ions present even though the model only contains unary and binary parameters. This model is therefore very suitable for multicomponent solutions.

4.2 The Extended UNIQUAC Model

As mentioned in chapter 2, in this thesis the excess Gibbs energy of the aqueous phase is described using the Extended UNIQUAC model[4]. The extended UNIQUAC model has previously been applied to describe the excess Gibbs energy of aqueous electrolytes solutions containing (K^+, Na^+, H^+, NH_4^+, Cl^-, NO_3^-, HSO_4^- ,SO_4^{2-}, OH^-, CO_3^{2-}, HCO_3^-, NH_2COO^-)[4,5]. In this thesis the model parameters are extended to aqueous systems of electrolytes containing phosphoric acid (H_3PO_4, $H_2PO_4^-$, HPO_4^{2-}), and nitric acid (HNO_3, NO_3^-) together with (K^+, Na^+, NH_4^+, Ca^{2+}, Cl^-). The extended UNIQUAC parameters for Ca^{2+} have been determined on the basis of data for aqueous solutions of $CaCl_2$, $CaNO_3$ and ternary solutions that in addition contain NaCl, $NaNO_3$, KCl, KNO_3, NH_4Cl and NH_4NO_3.

4.2.1 Model Equations

The model consists of a combinatorial and a residual term similar to the original UNIQUAC model but also includes a Debye-Hückel term taking into account the long range ion-ion interactions:

$$\frac{G^{Excess}}{RT} = \frac{G^{Excess}_{Combinatorial}}{RT} + \frac{G^{Excess}_{\text{Residual}}}{RT} + \frac{G^{Excess}_{Debye-Hückel}}{RT} \qquad [4.1]$$

The Debye-Hückel term is given by

$$\frac{G^{E}_{Debye-Hückel}}{RT} = -x_w M_w \frac{4A_{DH}}{b^3}\left[ln(1 + b\sqrt{I_m}) - b\sqrt{I_m} + \frac{b^2 I_m}{2} \right] \qquad [4.2]$$

where x_w is the mole fraction of water, M_w kg mol^{-1} is the molar mass of water, b is a constant equal to 1.50 (kg mol^{-1})^{½}, A_{DH} is the Debye-Hückel parameter and I_m is the ionic strength (mol (kg H_2O)$^{-1}$).

The combinatorial term is:

$$\frac{G^E_{Combinatorial}}{RT} = \sum_i x_i \ln\left(\frac{\phi_i}{x_i}\right) - \frac{z}{2}\sum_i q_i x_i \ln\left(\frac{\phi_i}{\theta_i}\right) \qquad [4.3]$$

z = 10 is the coordination number. ϕ_i is the volume fraction of component i, and θ_i is the surface area fraction of component i:

$$\phi_i = \frac{x_i r_i}{\sum_k x_k r_k}; \quad \theta_i = \frac{x_i q_i}{\sum_k x_k q_k} \qquad [4.4]$$

r_i and q_i are respectively the volume and surface area parameters for the component i.

The residual, enthalpic term is:

$$\frac{G^E_{Residual}}{RT} = -\sum_i x_i q_i \ln\left(\sum_k \theta_k \Psi_{ki}\right) \qquad [4.5]$$

where

$$\Psi_{ki} = exp\left(-\frac{u_{ki} - u_{ii}}{T}\right) \qquad [4.6]$$

The binary interaction parameters, u_{ki}, are given by:

$$u_{ki} = u^0_{ki} + u^t_{ki}(T - 298.15) \qquad [4.7]$$

The model only requires UNIQUAC volume and surface area parameter for each species and a binary interaction energy parameter for each pair of species. In order to reduce the number of parameters, the u_{ii} for water and for cations have been set to zero[4,5].

The number of parameters used in the Extended UNIQUAC model is small compared to the number of parameters required by other models such as the Pitzer model. In a recent paper by Clegg and Brimblecombe[6], Vapor-Liquid-Solid equilibria in aqueous electrolyte multicomponent solutions is modeled at 298.15K. In their work they modeled the H^+ - NH_4^+ - Na^+ - SO_4^{2-} - NO_3^- - Cl^- - H_2O system using the multicomponent model of Pitzer and Simonson[7]. This modeling required more than 100 binary and ternary interaction parameters. If temperature dependency was introduced into the model, the number of parameters would

increase by a factor of 4 to 5. Compared to this, less than 40 unary and binary parameters are required in the Extended UNIQUAC model for the same system at a single temperature and less than 80 parameters if the temperature dependency is included. As it can be expected from the large number of parameters, the Pitzer model usually gives a more accurate reproduction of experimental data than the Extended UNIQUAC model. An extensive amount of data is required in order to determine these parameters.

4.2.2 Model Application

Three different kinds of equilibria are taken into account in this work:

Speciation equilibria:

$$H_2O(l) \rightleftarrows H^+(aq) + OH^-(aq)$$

$$H_3PO_4(aq) \rightleftarrows H^+(aq) + H_2PO_4^-(aq)$$

$$H_2PO_4^-(aq) \rightleftarrows H^+(aq) + HPO_4^{2-}(aq)$$

$$HNO_3(aq) \rightleftarrows H^+(aq) + NO_3^-(aq)$$

As this work only deals with acidic systems, the formation of phosphate ions is not included.

A large number of different solids can be formed in the systems considered in this work. The corresponding solid-liquid equilibria are listed in the section dealing with experimental data. The only vapor – liquid equilibrium considered in this work is:

$$H_2O(l) \rightleftarrows H_2O(g).$$

Speciation equilibrium calculations are performed simultaneously with all solid-liquid and vapor-liquid equilibrium calculations and are preceding the calculation of properties like osmotic coefficients.

The equilibrium constants for all three types of equilibria are calculated from Gibbs energy of formation for the species and are evaluated at temperatures different from 298.15 K using the Gibbs – Helmholtz equation[4] as shown in chapter 2.

In this thesis thermal property data are included in the parameter regression, hence thermal property data can be reproduced by the model. This is an improvement compared to many of the previously works. Both in the recent works of Clegg and Brimblecombe[6] using a Pitzer model, Zhao et al.[8] using a Wilson model, or Jaretun and Aly[9] using an NRTL model, thermal property data were not used for determining the model parameters.

4.3 Parameter Estimation

The extension of the model to new species implies that a suitable amount of experimental data is included in the parameter optimization procedure. In this work a variety of different data was included. These data included speciation data, osmotic coefficients, water activity, SLE data and a number of different types of thermal properties data. Most of the data used for the parameter regression was found in the existing databank for aqueous electrolyte solutions[10]. However, the databank was extended to include the solubility of different species in acidic solutions as well as the speciation of such solutions. Unfortunately, the amount of available experimental data for the solubility of the investigated salts in solutions of HNO_3 and H_3PO_4 is very limited.

Several values of the thermodynamic properties of the species needed for describing the system could not be found in the literature. Therefore, values of the standard state free energy of formation, the standard state enthalpy of formation, and the standard state heat capacity for several salts were estimated from experimental data. The three parameter correlation[4,11] given in chapter 2 was used for the temperature dependency of the standard state heat capacity of HNO_3(aq).

The available experimental data were evaluated, and it was concluded that the data were adequate for estimating the interaction parameters marked with a "+" in table 4.1. The values of the remaining parameters were set to a suitably large value resulting in a negligible contribution to the excess Gibbs function from the interaction of the two species.

The parameter estimation was carried out by a least-square minimization procedure as described by Thomsen et al.[4] and Thomsen[11].

Table 4.1: List of estimated parameters.

	Na^+	K^+	Ca^{2+}	NH_4^+	H^+	Cl^-	NO_3^-	$H_2PO_4^-$	HPO_4^{2-}
$H_2PO_4^-$	+	+	+	+	+	+	+	+	+
HPO_4^{2-}	+	+	+	+	+			+	+
H_3PO_4	+	+			+			+	
HNO_3	+	+	+	+	+		+		

In order to obtain the best possible quantitative fit of the experimental data, different types of weighting factors and deviation calculations were applied to the different types of data. The parameters were finally fitted to a minimum in deviation between experimental and calculated data as shown in table 4.2.

In tables 4.3 and 4.4 (in the end of the chapter) all the deviations are calculated according to the minimization scheme in table 4.2.

The concentrations used in the various tables are total molality, m_T, which is defined as the sum of the molalities of the pure components in their apparent form. This means that in the H_3PO_4 – water system, m_T is the sum of the molalities of H_3PO_4 , $H_2PO_4^-$, and HPO_4^{2-}. This concentration definition is especially convenient when dealing with weak electrolytes as it does not depend on the degree of dissociation etc. In some works[2] this concentration definition is referred to as "apparent molality".

Table 4.2: Deviation minimization scheme.

Type of data	Deviation
Solid – liquid equilibria	Absolute deviation in weight percent
Heat of solution ($\Delta_s H$)	Absolute deviation in kJ/mol
Osmotic coefficients (ϕ)[a]	Relative deviation
Degree of dissociation (α)	Absolute deviation
Apparent molal relative heat. cap. of salt ($C_{p,\varphi}$)	Absolute deviation in J/mol
Water activity (γ_w)	Relative deviation
Apparent molal relative enthalpy of salt (L_φ)	Absolute deviation in J/mol

[a]Osmotic coefficient data are defined according to the definitions given in the original references from where each data point is taken.

4.4 Experimental Data

This section gives a detailed overview of the experimental data used to determine the parameters of the model.

Only data up to approximately 12 molal of acid exists for the solubility of e.g. KH_2PO_4 in aqueous H_3PO_4 and of KNO_3 in aqueous HNO_3. The model parameters presented are therefore only valid for aqueous solutions with H_3PO_4 or HNO_3 concentrations less than 12 molal. This concentration range corresponds to the concentrations that are used in the fertilizer industry.

4.4.1 Binary Systems

The available data for the binary systems are shown in table 4.3 (found in the end of the chapter).

Phosphoric acid

For the phosphoric acid - water system the following speciation is considered:

$$H_3PO_4(aq) \rightleftarrows H^+(aq) + H_2PO_4^-(aq)$$
$$H_2PO_4^-(aq) \rightleftarrows H^+(aq) + HPO_4^{2-}(aq)$$

The speciation in aqueous solutions of phosphoric acid has been investigated by Elmore et al.[12], Preston and Adams[13], and Cherif et al.[14]. However, the three different works do not agree completely on the speciation of the system. Elmore et al.[12] include the formation of a dimer:

$$H_2PO_4^-(aq) + H_3PO_4(aq) \rightleftarrows H_3P_2O_8^-(aq)$$

In the work of Cherif et al.[14] the results are interpreted with and without the presence of the dimer and in the work of Preston and Adams[13] the presence of the dimer is not considered at all. The results from the different works are shown in fig. 4.1. The data from Preston and Cherif are converted from molarity into molality using density parameters from Söhnel and Novotny[15].

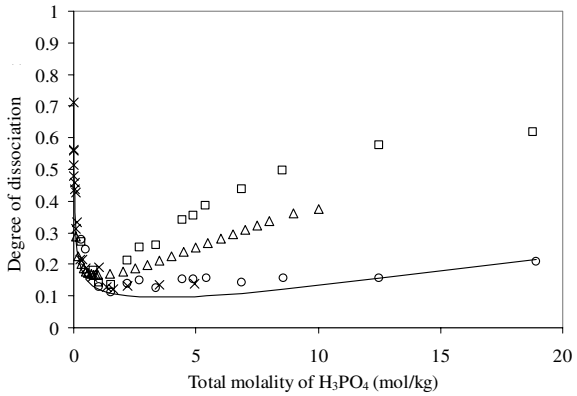

Figure 4.1 The degree of dissociation at 25° as a function of the total molality of H_3PO_4 in the solution. (△) Elmore[12], (×) Preston[13], (o) Cherif[14] without dimer, (□) Cherif[14] including dimer. (–) Extended UNIQUAC.

The figure shows a discrepancy between the data of Elmore et al.[12] and the data of Cherif et al.[14] when the dimer is taken into consideration. However, the data series from the two works[13,14] show a very good agreement when the dimer is ignored. Even though the works of Cherif et al.[14] and of Preston and Adams[13] give a strong indication of the formation of a dimer it was decided to neglect the formation of the dimer in this work. This decision was based on the fact that there is a large discrepancy between the experimental data describing the properties of the dimer. A number of additional model parameters and standard state thermodynamic data would have to be determined on the basis of these contradictory data. The fact that the model gives good results without considering the dimer does not prove or disprove the existence of the dimer in real solutions.

Nitric acid

The speciation considered for the nitric acid – water system is:

$$HNO_3(aq) \rightleftarrows H^+(aq) + NO_3^-(aq)$$

The speciation in aqueous solutions of nitric acid has been investigated by Haase et al.[53] and Krawetz[55]. The data from the two sources at 25°C and 50°C are compared in figure 4.2. The

data from Krawetz[55] have been converted from the molarity scale to the molality scale using density parameters from Söhnel and Novotny[15]. The figure shows good agreement between the two sources.

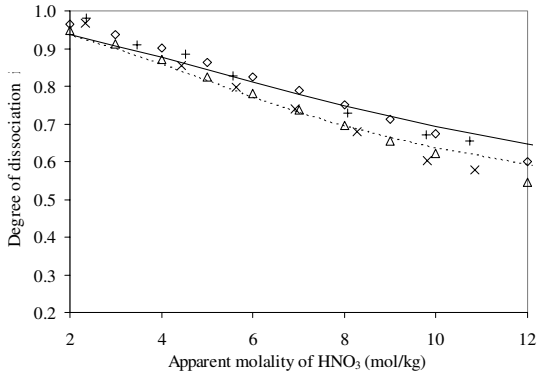

Figure 4.2 The degree of dissociation as function of the total molality of HNO_3 in the solution. (◇) Haase[53] 25°C, (△) Haase[53] 50°C, (+) Krawetz[55] 25°C, (×)Krawetz[55] 50°C, (–) Extended UNIQUAC 25°C. (--) Extended UNIQUAC 50°C

Potassium salts of phosphoric acid:

The solid-liquid equilibria considered for these systems are:

$$K^+(aq) + H_2PO_4^-(aq) \rightleftarrows KH_2PO_4(s)$$
$$2K^+(aq) + HPO_4^{2-}(aq) \rightleftarrows K_2HPO_4(s)$$

$$2K^+(aq) + HPO_4^{2-}(aq) + 3H_2O \rightleftarrows K_2HPO_4 \bullet 3H_2O(s)$$
$$2K^+(aq) + HPO_4^{2-}(aq) + 6H_2O \rightleftarrows K_2HPO_4 \bullet 6H_2O(s)$$

There is a variety of different sources of both SLE data and osmotic coefficient data for the KH_2PO_4 – water system. The data from all these various sources seem to be consistent both numerically and with respect to the nature of the solid phases. Hence, all available data were used in the parameter regression. The solubility of K_2HPO_4 in water has been investigated by Ravich[32] and consists of a branch representing the formation of ice and three branches corresponding to hexahydrate, trihydrate and anhydrous K_2HPO_4 (figure 4.3).

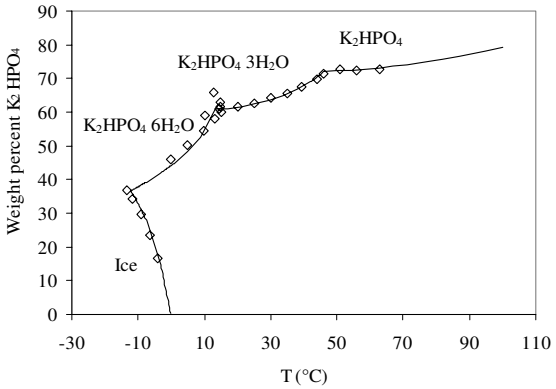

Figure 4.3. Solubility of K_2HPO_4 in water. (◇) exp. data. (–) Extended UNIQUAC.

Ammonium salts of phosphoric acid:

The following equilibria have been considered for these systems:

$$NH_4^+(aq) + H_2PO_4^-(aq) \rightleftarrows NH_4H_2PO_4(s)$$

$$2NH_4^+(aq) + HPO_4^-(aq) \rightleftarrows (NH_4)_2HPO_4(s)$$
$$2NH_4^+(aq) + HPO_4^-(aq) + 2H_2O \rightleftarrows (NH_4)_2HPO_4(s) \bullet 2H_2O$$

Ammonium monophosphate does not form hydrates while the diphosphate forms an anhydrous as well as a hydrated form.

Sodium salts of phosphoric acid.

The solid-liquid equilibria included for this system are:

$$Na^+(aq) + H_2PO_4^-(aq) \rightleftarrows NaH_2PO_4(s)$$
$$Na^+(aq) + H_2PO_4^-(aq) + H_2O \rightleftarrows NaH_2PO_4 \bullet H_2O(s)$$
$$Na^+(aq) + H_2PO_4^-(aq) + 2H_2O \rightleftarrows NaH_2PO_4 \bullet 2H_2O(s)$$

$$2Na^+(aq) + HPO_4^{2-}(aq) \rightleftarrows Na_2HPO_4(s)$$
$$2Na^+(aq) + HPO_4^{2-}(aq) + 2H_2O \rightleftarrows Na_2HPO_4(s)\cdot 2H_2O(s)$$
$$2Na^+(aq) + HPO_4^{2-}(aq) + 7H_2O \rightleftarrows Na_2HPO_4(s)\cdot 7H_2O(s)$$
$$2Na^+(aq) + HPO_4^{2-}(aq) + 12H_2O \rightleftarrows Na_2HPO_4(s)\cdot 12H_2O(s)$$

The data for the solubility of NaH_2PO_4 in water are plotted in figure 4.4. The figure shows that there is very good agreement between the experimental SLE data from various sources.

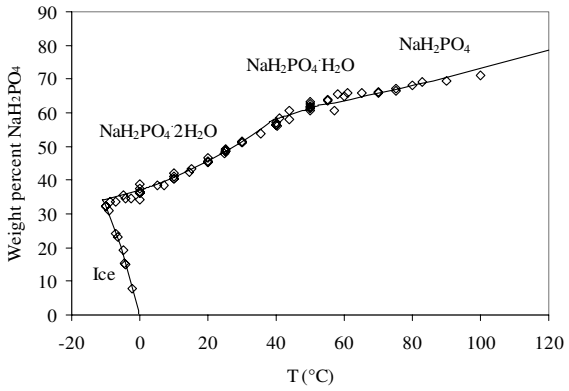

Figure 4.4. Solubility of NaH_2PO_4 in water. (◇) exp. data. (–) Extended UNIQUAC.

The experimental data for both the diphosphate and the monophosphate form verify the existence of the various hydrated forms considered for this system. The osmotic coefficients of aqueous solution of NaH_2PO_4 at 25°C have been reported by 6 different investigators which all show the same general trend for the system.

4.4.2 Ternary Data

The available data for the solubility of KH_2PO_4, NaH_2PO_4, $CaHPO_4$ and $Ca(H_2PO_4)\cdot 2H_2O$ in aqueous solutions of H_3PO_4 and of $NaNO_3$, KNO_3, $Ca(NO_3)_2$ and NH_4NO_3 in aqueous nitric acid solutions are summarized in table 4.4 (given in appendix 4.B).

Systems with phosphoric acid:

The additional equilibria included for these systems are:

$$Na^{+}(aq) + H_2PO_4^{-}(aq) + H_3PO_4(aq) \rightleftarrows NaH_2PO_4 \bullet H_3PO_4(s)$$
$$Ca^{2+}(aq) + HPO_4^{2-}(aq) \rightleftarrows CaHPO_4(s)$$
$$Ca^{2+}(aq) + H_2PO_4^{-}(aq) + 2H_2O \rightleftarrows Ca(H_2PO_4)\bullet 2H_2O$$

For all the data a clear salting in effect is observed when adding phosphoric acid to the solutions. The salting in effect is significant in KH_2PO_4 solutions as seen in figure 4.5 while it is less expressed in NaH_2PO_4 solutions.

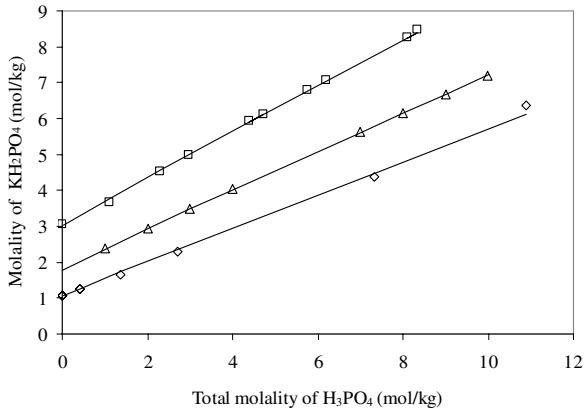

Figure 4.5. Solubility of KH_2PO_4 in aqueous solutions of H_3PO_4.
(◇) exp. data at 0°C, (△) exp. data at 25°C, (□) exp. data at 50°C. (–) Extended UNIQUAC.

Systems with nitric acid:

For the nitric acid systems there is no clear trend in the salting in or salting out effects. For $NaNO_3$ solutions a very clear salting out effect is observed as shown in figure 4.6. The solubility of KNO_3 is not significantly affected by adding nitric acid to the solution. In low concentrations of nitric acid a small salting out effect is observed. However, at higher concentrations a salting in effect is noted. For NH_4NO_3 solutions a salting out effect is

observed up to approximately 7-8 molal HNO_3, whereas at higher concentrations a clear salting in effect is seen.

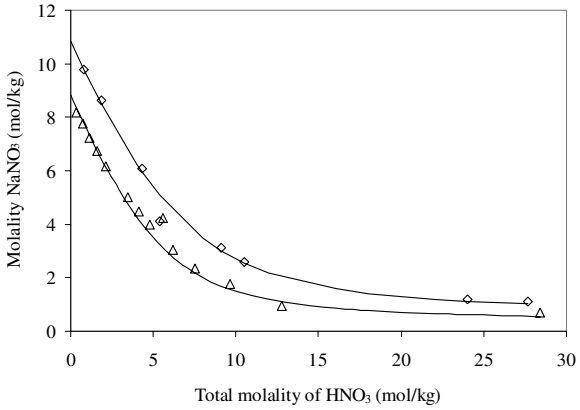

Figure 4.6. Solubility of $NaNO_3$ in aqueous solutions of HNO_3.
(◇) exp. data. (–) Extended UNIQUAC.

Mixed ternary systems:

In order to determine ion-ion interactions in phosphoric acid solutions containing additional salts, ternary data have been included in the parameter regression. Additional solid-liquid equilibrium was included for the multicomponent systems:

$$Na^+(aq) + NH_4^+(aq) + HPO_4^-(aq) + 4H_2O \rightleftarrows NaNH_4HPO_4 \bullet 4H_2O(s)$$

4.5 Results and Discussion

The values of the thermodynamic properties for ions and salts that were fitted to experimental data in this work are given in table 4.5 (end of the chapter). For some hydrated salts the heat capacity has been calculated from the corresponding anhydrous salt using an additive rule where 36.2 J/(mol K) is added pr. water molecule. The value 36.2 J/(mol K) approximately corresponds to the heat capacity of H_2O(s).

Table 4.6, and tables 4.7-4.8 (end of chapter) include the 66 new binary interaction parameters and 8 new r and q parameters that were determined in this work.

Table 4.6: Extended UNIQUAC r, q and heat capacity parameters.

	r	q	a	b	c
H_3PO_4 (aq)	1.6982	3.4643	80.000	0	0
HNO_3 (aq)	14.736	12.544	-652.638	1.38818	29085.77
$H_2PO_4^-$	8.3088	8.1975	108.000	0	0
HPO_4^{2-}	12.392	11.004	69.622	0	0

4.5.1 Model Correlations

The modeling results are generally very good for all binary systems included in the parameter regression as shown in table 4.3. Figures 4.1 and 4.2 show model calculations of speciation in aqueous H_3PO_4 and HNO_3 solutions. The model fits the data acceptably in both cases. In the case of H_3PO_4-water, the model correlates the dissociation data well up to 19 in molality even though only data up to 12 in molality were used in the regression. However, there seems to be a slight overestimation for the HNO_3-water system. The main reason for this is probably that the main focus was on the representation of SLE data. Hence, the speciation data were given less weight in the parameter regression.

Another example of the model calculations in binary systems is given in figure 4.3 and 4.4 where the solubility of K_2HPO_4 and Na_2HPO_4 in water is shown. The figures show that the model correlations are good for all the different hydrated and anhydrous forms of the salts.

The deviations between calculated results and experimental data for 5 of the 6 sources of osmotic data for the NaH_2PO_4-water system are very reasonable. However, the somewhat larger deviation of the data from Pavicevic et al.[41] is caused by a few data points with very high deviation. Overall though, the data are well correlated by the model.

From table 4.4 it is seen that the overall representation of the solubility of the different salts in aqueous solutions of phosphoric acid is good. For all systems the model correlates the right trend of the salting in effects for increasing concentrations of H_3PO_4. One example is given in

figure 4.5 where the solubility of KH_2PO_4 in aqueous H_3PO_4 is shoen. The figure reveals an excellent correlation of the solubility.

In general the model represents the solubility data in aqueous nitric acid well. The solubility of $NaNO_3$ in aqueous nitric acid is shown in figure 4.6. The model calculations are very accurate up to high concentrations of HNO_3 even though only data up to 12 in molality of HNO_3 were included in the parameter optimization.

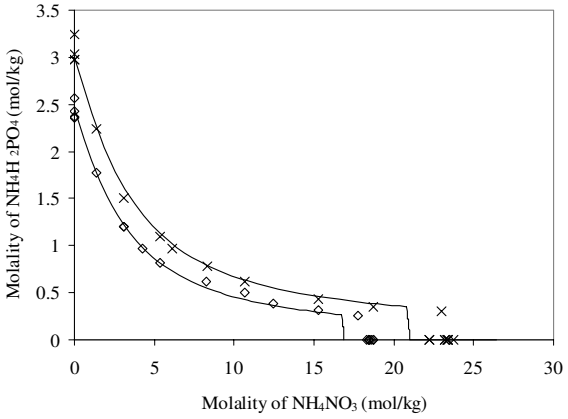

Figure 4.7. Solubility in the ternary aqueous system $NH_4H_2PO_4$ – NH_4NO_3.
(◇) exp. data at 10°C. (×) exp. data at 20°C. (–) Extended UNIQUAC.

There is however a discrepancy between the model correlations and the experimental data for the NH_4NO_3-HNO_3 system. The model shows a continuous salting in effect and is incapable of representing the salting out effect at low HNO_3 concentration. This discrepancy might be caused by the formation of complexes of NH_4NO_3 and HNO_3 in the investigated concentration range as reported by Treushchenko et al.[64]. As the apparent complexes between NH_4NO_3 and HNO_3 have not been included in the model due to insufficient experimental data this could lead to the inaccurate representation of the NH_4NO_3 – HNO_3 – water data.

The included ternary data are all well represented by the model as seen in table 4.4. Figure 4.7 shows the model correlation for the ternary system $NH_4H_2PO_4$ – NH_4NO_3- water. The model

calculations at high concentrations of NH_4NO_3 are inaccurate. This inaccuracy is caused by the original parameters[5] for NH_4^+ and NO_3^-. An improvement was not attempted here.

4.6 Conclusion

The Extended UNIQUAC model has been successfully applied to describe the phase behavior and thermal properties of various acidic aqueous solutions of electrolytes over a wide range of temperatures. The model is capable of describing the dissociation of both H_3PO_4 and HNO_3 in aqueous solutions and of describing the solubility of several different salts in aqueous solutions of these two acids. In addition the model reproduces the thermal properties of these solutions with high accuracy. In the following chapters these parameters will be used in describing the aqueous phase thermodynamics in relation with ion exchange equilibria.

Table 4.3: Experimental data used for parameter estimation. Binary systems.

System H_2O +	m_{Total}	T (°C)	No. of Data Points	Type of Data	Source	Deviation
H_3PO_4	0.3 -19.9	25	15	α	(13)	0.04
	0 – 5.0	25	20	α	(14)	0.06
	0.5 – 8.3	25	9	L_φ	(16)	49.1
	0.5 – 8.3	15 - 80	55	$C_{p,\varphi}$	(17)	11.7
	0.1 – 9.9	0 - 25	33	ϕ	(18)	5.20
	1.1 – 9.5	25	7	γ_w	(19)	1.21
	0.6 – 8.4	25 - 80	29	γ_w	(20)	1.79
	0.9 – 7.9	0	4	γ_w	(21)	0.79
HNO_3	2 – 28	25 – 75	48	ϕ	(53)	2.42
	0.1 – 3.0	25	17	ϕ	(26)	0.68
	0 – 12	0 – 50	18	α	(55)	0.03
	0 – 12	25 – 75	30	α	(53)	0.02
	0 – 0.15	25	7	$C_{p,\varphi}$	(56)	7.83
	0 – 18.5	25	45	$C_{p,\varphi}$	(57)	18.0
	0 – 6.9	0 – 120	405	$C_{p,\varphi}$	(54)	4.33
KH_2PO_4	1.0 – 4.6	0 - 75	4	SLE	(22)	1.31
	1.0 – 1.6	-3 - 20	5	SLE	(23)	0.44
	0.3 – 2.0	-3 - 32	24	SLE	(24)	0.59
	1.1 – 6.1	0 - 90	14	SLE	(25)	0.99
	0.1 – 1.6	25	13	ϕ	(26)	0.53
	0.1 – 1.3	25	13	ϕ	(27)	0.61
	0 – 1.8	25	20	ϕ	(28)	0.49
	0 – 0.2	37	3	ϕ	(29)	0.59
	0.8 – 5.8	110	16	ϕ	(30)	2.25
	0 – 1.8	25	18	$\Delta_s H$	(31)	0.37
K_2HPO_4	1.2 – 15.4	-12 - 63	21	SLE	(32)	2.41
	0.1 – 1.0	25	10	ϕ	(26)	0.81
	0.1 – 1.1	25	11	ϕ	(27)	1.03
	0 – 0.4	37	7	ϕ	(29)	1.41

	0.6 – 5.5	110	26	ϕ	(30)	2.06
	3.1 – 10.0	25	7	$\Delta_s H$	(33)	1.21
$NH_4H_2PO_4$	1.7 – 3.8	-4 - 30	6	SLE	(34)	0.45
	0.4 – 18.7	-4 - 110	22	SLE	(35)	2.41
	0.4 – 3.8	-4 - 30	27	SLE	(24)	0.81
	0.2 – 3.4	25	28	$\Delta_s H$	(31)	0.49
$(NH_4)_2HPO_4$	2.9-14.0	-6.9 – 121.9	41	SLE	(67)	1.75
NaH_2PO_4	4.7 – 16.6	0 - 75	3	SLE	(22)	0.97
	0.7 – 8.7	-10 - 30	23	SLE	(34)	1.33
	2.0 – 12.9	-9 - 57	10	SLE	(36)	3.40
	7.7 – 12.8	25 - 50	2	SLE	(37)	1.29
	3.7 – 20.4	-9 - 100	19	SLE	(35)	1.84
	4.3 – 18.7	0 - 83	16	SLE	(38)	4.48
	4.8 – 20.6	0 - 99	40	SLE	(39)	0.92
	0 – 6.5	25	30	ϕ	(28)	0.55
	0.1 – 6.0	25	23	ϕ	(26)	0.55
	0.2 – 6.3	25	8	ϕ	(40)	1.03
	0.1 – 2.3	25	13	ϕ	(27)	0.58
	0.7 – 3.9	25	16	ϕ	(41)	3.59
	0.8 – 10.8	110	26	ϕ	(30)	0.92
Na_2HPO_4	0.1 – 7.2	-4.7 - 99.8	97	SLE	(72)	0.73
	0.1 – 1.0	25	10	ϕ	(26)	1.47
	0.1 – 1.1	25	11	ϕ	(27)	1.72
	0.6 – 8.2	110	24	ϕ	(30)	6.15

Table 4.4: Experimental data used for parameter estimation. Ternary systems.

System H_2O +	m_{Total}	T (°C)	No. of Data Points	Type of Data	Source	Deviation
$NaNO_3$ – HNO_3	10.4 – 22.1	25 – 65	12	SLE	(58)	1.31
	9.8 – 14.0	0 – 20	4	SLE	(59)	2.16
	8.3 – 11.4	0	11	SLE	(65)	0.99
	9.4 – 21.0	15 – 75	8	SLE	(66)	0.66
KNO_3 – HNO_3	8.4 – 14.5	50	9	SLE	(46)	2.25
	4.1 – 15.2	25- 50	9	SLE	(60)	2.97
	1.7 – 10.4	0	6	SLE	(65)	1.38
	1.48 – 16.6	0 - 15	14	SLE	(66)	1.10
$Ca(NO_3)_2$ – HNO_3	17.2 – 26.6	25	9	SLE	(61)	0.39
	18.0 – 20.4	25	3	SLE	(62)	1.22
	12.9 – 16.6	0	2	SLE	(63)	1.35
NH_4NO_3 – HNO_3	14.7 – 17.9	0	4	SLE	(65)	7.70
	14.6 – 30.8	0 – 30	16	SLE	(66)	10.3
NaH_2PO_4 – H_3PO_4	2.4 – 37.8	0 - 34	5	SLE	(42)	4.69
	6.2 – 37.1	0 – 50	25	SLE	(43)	3.31
KH_2PO_4 – H_3PO_4	1.1 – 21.0	0 – 25	18	SLE	(44)	0.44
	1.9 – 4.9	25	10	SLE	(45)	0.28
	3.1 – 16.8	50	10	SLE	(46)	0.28
	1.7 – 12.7	25	19	SLE	(47)	1.34
$Ca(OH)_2$ – KH_2PO_4 – H_3PO_4	3.7 – 7.6	25	4	SLE	(48)	4.49
	2.3 – 36.1	25- 51	18	SLE	(49)	3.36
	2.1 – 43.7	25 - 51	18	SLE	(50)	3.21

$Ca(OH)_2$ – KH_2PO_4 – H_3PO_4	2.2 – 11.2	25	30	SLE	(45)	2.58
KH_2PO_4 – KNO_3	1.4 - 4.6	0 - 30	21	SLE	(24)	0.49
	3.0 – 10.4	40 - 60	14	SLE	(46)	2.51
KH_2PO_4 – KCl	1.9 – 6.9	0 - 75	22	SLE	(22)	0.39
NaH_2PO_4 – $NaNO_3$	3.4 – 11.6	-18 – 30	114	SLE	(34)	1.03
	12.9 – 13.7	50	10	SLE	(51)	2.49
NaH_2PO_4 – NaCl	4.8 – 15.5	0 - 75	17	SLE	(24)	1.18
	6.4 – 11.1	40	5	SLE	(52)	0.65
	6.7 – 11.7	25 - 50	19	SLE	(37)	2.33
NaH_2PO_4 – $NH_4H_2PO_4$	1.6 – 10.4	-10 - 30	75	SLE	(34)	1.88
	3.9 – 12.3	40	16	SLE	(68)	1.46
	2.4 – 14.1	25	16	SLE	(69)	2.15
$NH_4H_2PO_4$ – NH_4NO_3	2.8 – 28.9	-10 - 30	42	SLE	(24)	1.03

Table 4.5: Standard thermodynamic properties for solid salts (s) and species in aqueous solution (aq).

	$-\Delta_f G^0 \left(kJ\ mol^{-1}\right)$	$-\Delta_f H^0 \left(kJ\ mol^{-1}\right)$	$C_P^0 \left(J\ mol^{-1}\ K^{-1}\right)$
NaH_2PO_4(s)	1387.854	1520.426	116.860[a]
$NaH_2PO_4 \cdot H_2O$(s)	1626.145	1809.727	153.000[b]
$NaH_2PO_4 \cdot 2H_2O$(s)	1864.505	2107.005	189.000[b]
$NaH_2PO_4 \cdot H_3PO_4$(s)	2519.885	2800.564	180.000[c]
Na_2HPO_4(s)	1609.383	1748.100	150.500[a]
$Na_2HPO_4 \cdot 2H_2O$(s)	2088.572	2337.691	222.900[b]
$Na_2HPO_4 \cdot 7H_2O$(s)	3280.214	3811.880	403.900[b]
$Na_2HPO_4 \cdot 12H_2O$(s)	4470.081	5324.452	584.900[b]
NaNH4$HPO_4 \cdot 4H_2O$(s)	2394.762	2826.641	360.000[c]
KH_2PO_4(s)	1416.434	1550.681	90.414
K_2HPO_4(s)	1645.157	1794.833	97.082
$K_2HPO_4 \cdot 3H_2O$(s)	2363.708	2679.245	205.700[b]
$K_2HPO_4 \cdot 6H_2O$(s)	3077.146	3578.376	314.300[b]
$NH_4H_2PO_4$(s)	1210.494	1427.108	142.260
$(NH_4)_2HPO_4$(s)	1260.425	1588.761	197.000[c]
$(NH_4)_2HPO_4 \cdot 2H_2O$(s)	1734.931	2178.370	269.400[b]
$CaHPO_4$(s)	1684.005	1776.435	110.040[a]
$Ca(H_2PO_4)_2 \cdot H_2O$(s)	3060.574	3374.698	205.700[c]
H_3PO_4(aq)	1142.580	1296.219	80.000[c]
HNO_3(aq)	105.158	208.55	-[d]
$H_2PO_4^-$(aq)	1130.603	1279.999	108.000[e]
HPO_4^{2-}(aq)	1090.191	1306.822	69.622

[a] Value from NIST[70].

[b] Calculated by additivity rule.

[c] Value chosen due to lack of experimental data.

[d] A three parameter correlation was used for the heat capacity of HNO_3(aq)

[e] Value from Marcus[72]

Table 4.7

Parameters $u_{ij}^{(0)} = u_{ji}^{(0)}$ Parameter values in bold letters were determined in this work, remaining parameters are from a previous work[5].

	H_2O	NH_3	H_3PO_4	HNO_3	Na^+	K^+	Ca^{2+}	NH_4^+	H^+	Cl^-	NO_3^-	OH^-	$H_2PO_4^-$	HPO_4^{2-}
H_2O	0	-	-	-	-	-	-	-	-	-	-	-	-	-
NH_3	371.6025	1140.188	-	-	-	-	-	-	-	-	-	-	-	-
H_3PO_4	**0.249377**	10^{10}	**2964.381**	-	-	-	-	-	-	-	-	-	-	-
HNO_3	**255.1375**	10^{10}	10^{10}	**564.1982**	-	-	-	-	-	-	-	-	-	-
Na^+	733.2863	1461.773	**2952.152**	**289.7742**	0	-	-	-	-	-	-	-	-	-
K^+	535.0227	1511.982	**-130.5168**	**119.3235**	-46.19374	0	-	-	-	-	-	-	-	-
Ca^{2+}	166.7021	2500	10^{10}	**631.8481**	-182.2332	-402.9549	0	-	-	-	-	-	-	-
NH_4^+	52.73045	3598.826	10^{10}	**172.3940**	384.0513	1469.491	**2879.923**	0	-	-	-	-	-	-
H^+	10^5	10^{10}	10^{10}	10^{10}	10^{10}	10^{10}	10^{10}	10^{10}	0	-	-	-	-	-
Cl^-	1523.393	1598.045	10^{10}	10^{10}	1443.229	1465.178	**2316.383**	1385.387	10^{10}	2214.814	-	-	-	-
NO_3^-	936.5346	1001.175	10^{10}	**1365.819**	770.4277	772.9943	**1005.026**	757.0215	10^{10}	2175.016	1870.133	-	-	-
OH^-	600.4952	2046.797	10^{10}	10^{10}	1398.137	1805.749	**-449.0293**	1877.901	10^{10}	1895.521	1379.954	1562.881	-	-
$H_2PO_4^-$	**103.5017**	10^{10}	**-0.332928**	10^{10}	**1918.884**	**608.8342**	**2178.778**	**76.838**	10^{10}	**1877.565**	**1351.315**	**2509.133**	**199.3348**	-
HPO_4^{2-}	**-122.6830**	10^{10}	10^{10}	10^{10}	**561.0501**	**738.3592**	**38.84894**	**-264.089**	10^{10}	10^{10}	10^{10}	**327.8494**	**2.627895**	**-89.30536**

Table 4.8

Parameters $u_{ij}^{(1)} = u_{ji}^{(1)}$ Parameter values in bold letters were determined in this work, remaining parameters are from a previous work[5].

	H_2O	NH_3	H_3PO_4	HNO_3	Na^+	K^+	Ca^{2+}	NH_4^+	H^+	Cl^-	NO_3^-	OH^-	$H_2PO_4^-$	HPO_4^{2-}
H_2O	0	-	-	-	-	-	-	-	-	-	-	-	-	-
NH_3	6.61937	4.0165	-	-	-	-	-	-	-	-	-	-	-	-
H_3PO_4	**1.2163**	0	**0.88186**	-	-	-	-	-	-	-	-	-	-	-
HNO_3	**-0.52850**	0	0	**-0.92492**	-	-	-	-	-	-	-	-	-	-
Na^+	0.48719	-0.98534	**12.764**	**1.0780**	0	-	-	-	-	-	-	-	-	-
K^+	0.99356	-10.495	**2.7887**	**1.6397**	0.11899	-0.04293	-	-	-	-	-	-	-	-
Ca^{2+}	-5.7699	0	0	**-5.6454**	-3.3839	-3.3100	0	-	-	-	-	-	-	-
NH_4^+	0.50922	6.5432	0	**-1.2050**	-0.55447	1.0968	**1.7222**	0	-	-	-	-	-	-
H^+	0	0	0	0	0	0	0	0	0	-	-	-	-	-
Cl^-	14.631	15.540	0	0	15.635	15.329	**9.2428**	14.796	0	14.436	-	-	-	-
NO_3^-	5.7882	10.919	0	**7.9255**	6.7914	7.4222	**7.3612**	6.6152	0	13.449	4.1240	-	-	-
OH^-	8.5455	0.09037	0	0	20.278	27.283	**1.5431**	0.34921	0	13.628	6.6369	5.6169	-	-
$H_2PO_4^-$	**0.10055**	0	**-0.92808**	0	**26.324**	**2.8510**	**-11.351**	0	0	**13.495**	**5.6452**	**-0.05796**	**-0.50305**	-
HPO_4^{2-}	**-0.78930**	0	0	0	**1.5429**	**12.947**	**-27.477**	0	0	0	0	**11.974**	**0.13741**	**-2.7550**

4.7 References

(1) Jiang, C. Thermodynamics of aqueous phosphoric acid solution at 25°C. *Chem. Eng. Sci.* **1996**, 51, 689.

(2) Cherif, M.; Mgaidi, A.; Ammar, N. M.; Abderrabba M.; Fürst, W. Modelling of the equilibrium properties of the system H_3PO_4 – H_2O: representation of VLE and liquid phase composition. Fluid Phase Equilibria, **2000**, 175, 197.

(3) Rains, W. O.; Counce, R. M.; Spencer, B. B. Application of the Brunauer-Emmett-Teller isotherm to the water-nitric acid system for the determination of mean ionic activity coefficients. *Chem. Eng. Comm.* **1999**, 171, 169.

(4) Thomsen, K.; Rasmussen, P.; Gani, R. Correlation and Prediction of thermal properties and phase behaviour for a class of aqueous electrolyte systems. *Chem. Eng. Sci.* **1996**, 51, 3675.

(5) Thomsen, K.; Rasmussen P. Modeling of vapor-liquid-solid equilibrium in gas-aqueous electrolyte systems. *Chem. Eng. Sci*. **1999**, 54, 1787.

(6) Clegg, S. L.; Brimblecombe, P.; Wexler A. S. Thermodynamic Model of the System H^+ - NH_4^+ - Na^+ - SO_4^{2-} - NO_3^- - Cl^- - H_2O at 298.15K. *J. Phys. Chem.* **1998**, 102, 2155.

(7) Pitzer, K. S.;Simonson, J. M. Thermodynamics of Multicomponent, Miscible, Ionic Systems: Theory and Equations. *J. Phys. Chem.* **1986**, 90, 3005.

(8) Zhao, Ensheng; Yu, Ming; Sauvé, Robert E.; Khoshkbarchi, Mohammad K. Extension of the Wilson model to electrolyte solutions. *Fluid Phase Equilibria* **2000**, 173, 161.

(9) Jaretun, A.; Aly, G. New local composition model for electrolyte solutions: multicomponent systems. *Fluid Phase Equilibria*, **2000**, 175, 213.

(10) http://www.ivc-sep.kt.dtu.dk/databank/databank.asp.

(11) Thomsen, K. Aqueous Electrolytes: Model Parameters and Process Simulation. Ph.D. Thesis. Technical University of Denmark, Lyngby, 1997.

(12) Elmore, K. L.; Hatfield, J. D.; Dunn, R. L.; Jones, A.D. Dissociation of Phosphoric Acid at 25°C. *J. Phys. Chem.* **1965**, 69, 3520.

(13) Preston, C. M.; Adams, W. A. A Laser Raman Spectroscopic Study of Aqueous Phosphoric Acid. *Can. J. Spectroscopy*. **1977**, 22, 125.

(14) Cherif, M.; Mgaidi, A.; Ammar, N.; Géraldine, V.; Fürst, W. A New Investigation of Aqueous Orthophosphoric Acid Speciation Using Raman Spectroscopy. *J. Sol. Chem.* **2000**, 29, 255.

(15) Söhnel, O.; Novotny, P. *Densities of Aqueous Solutions of Inorganic Substances. Phys. Sci. Data 22*; Elsevier: Tokyo, 1985.

(16) Egan, E. P.; Luff, B. B. Heat of solution of orthophosphoric acid. *J. Phys. Chem.* **1961**, 65, 523.

(17) Egan, E. P.; Luff, B. B.; Wakefield, Z. T. Heat capacity of phosphoric acid solutions, 15 to 80°. *J. Phys. Chem.* **1958**, 62, 1091.

(18) Platford, R. F. Thermodynamics of aqueous solutions of orthophosphoric acid from the freezing point to 298.15K. *J. Sol. Chem.* **1975**, 4, 591.

(19) Elmore, K. L.; Mason, C. M.; Christensen J. H. Activity of orthophosphoric acid in aqueous solution at 25°C from vapor pressure measurements. *J. Am. Chem. Soc*. **1946**, 68, 2528.

(20) Kablukov, I. A.; Zagwosdkin, K. I. Die Dampfspannungen der Phosphorsäurelösungen. *Z. anorg. allg. Chem*. **1935**, 224, 315-321

(21) Dieterici, C. Über die Damppfdrucke wässerigen Lösungen bei 0°C. *Ann. Phys. (Leipzig)*. **1893**, 286, 47.

(22) Brunisholz, G.; Bodmer, M. Contribution a l'etude du systême quinaire H^+ - Na^+ - K^+ - Cl^- - PO_4^{3-}. *Helv. Chim. acta.* **1963**, 46, 2566.

(23) Babenko, A. M.; Vorob'eva, T. A. Study of solubility in the system NaH_2PO_4 - KH_2PO_4 - H_2O. *J. Appl. Chem. USSR*. **1975**, 48, 2519.

(24) Bergman, A. G.; Bochkarev, P.F. Physico-chemical study of the equilibria of the aqueous reciprocal system of nitrates, monophosphates and chlorides of potassium and ammonium. *Izv. Akad. Nauk SSSR, Ser. Khim. Nauk.* **1938**, 1, 237.

(25) Kazantsev, A. A. The solubility of potassium dihydrophosphate in water. *Zh. Obshch. Khim.* **1938**, 8, 1230.

(26) Robinson, R. A.; Stokes, R.H. *Electrolyte Solutions*; Butterworths: 1965

(27) Scatchard, G.; Breckenridge, R. C. Isotonic Solutions. II The chemical Potential of water in aqueous solutions of potassium and sodium phosphates and arsenates at 25°. *J. Phys. Chem.* **1954**, 58, 596.

(28) Hamer, W.J.; Wu, Y.-C. Osmotic Coefficients and Mean Activity Coefficients of Uni-univalent Electrolytes in Water at 25°C. *J. Phys. Chem. Ref. Data.* **1972**, 1, 1047.

(29) Burge, D. E. Osmotic coefficients in aqueous solutions, studies with the vapor pressure osmometer. *J. Phys. Chem*. **1963**, 67, 2590.

(30) Holmes, H. F.; Simonson, J. M.; Mesmer, R. E. Aqueous solutions of the mono- and di-hydrogenphosphate salts of sodium and potassium at elevated temperatures. Isopiestic results. *J. Chem. Thermodynamics*. **2000**, 32, 77.

(31) Egan, E.P.; Luff B. B. Heat of solution of Monoammonium and Monopotassium Phosphates at 25°C. *J. Chem. Eng. Data*. **1963**, 8, 181.

(32) Ravich, M. I. The solubility polytherms of secondary and tertiary potassium orthophosphate in water. *Izv. Akad. Nauk SSSR Ser. Khim*. **1938**, 1, 137

(33) Luff, B. B.; Reed, R. B. Enthalpy pf solution of dipotassium orthophosphate at 25°. *J. Chem. Eng. Data*. **1978**,23, 56.

(34) Shpunt, C.J. A reciprocal Aqueous System - Ammonium Monophosphate - Sodium Nitrate, water, I and II. *Zh. Prikl. Khim.* **1940**, 13, 9.

(35) Linke, W. F.; Seidell, A. *Solubilities of Inorganic and Metal-Organic Compounds*. (1965)

(36) Babenko, A. M.; Vorob'eva, T. A. Study of solubility in the system NaH_2PO_4 - KH_2PO_4 - H_2O. *J. Appl. Chem. USSR*. **1975**, 48, 2519.

(37) Girich, T. E.; Gulyamov, Yu. M.; Ganz, S. N.; Miroshnik, O. S. Sodium$^+$, chloride$^-$, dihydrogen phosphate$^-$ -water system at 298 and 323 K. *Voprosy Khimii i Khimicheskoi Tekhnologii*. **1979**, 57, 58.

(38) Apfel O. Dissertation, Technischen Hochschule, Darmstadt, 1911.

(39) Imadsu, A. The solubility of Sodium Dihydrogen Phosphate and the transition point of the hydrates. *Memoirs of the College of Science and Engineering, Kyoto.* **1912**, 3, 257.

(40) Platford, R.F. Thermodynamics of the system H_2O-NaH_2PO_4-H_3PO_4. *J. Chem. Eng. Data.* **1976**, 21, 468.

(41) Pavicevic, V;. Ninkovic, R.; Todorovic, M.; Osmotic and activity coefficients of {yNaH_2PO_4 + (1-y)Na_2SO_4} (aq) at the temperature 298.15K. *Fluid Phase Equilibria*. **1999**, 164, 275.

(42) Parravano, N.; Mieli, A. Fosfati acidi. *Gaz. Chim. Ital*. **1908**, 38, 535.

(43) Lilich, L. S.; Vanyusheva, L. N.; Chernykh, L. V. The Sodium dihydrogen phosphate-phosphoric acid-water system at 0, 25, 50°C. *Russ. J. Inorg. Chemistry.* **1971**, 16, 1482.

(44) Ravich, M. I. The solubility isotherm for 0°C in the triple system K_2O-P_2O_5 - H_2O. *Izv. Akad. Nauk SSSR, Ser. Khim*. **1938**, 1, 167.

(45) Flatt, R. ; Brunisholz, G.; Bourgeois, J. Contribution l'etude du systême quinaire Ca,NH4,H,NO3,PO4,H2O. *Helvetica Chimica Acta*. **1956**, 39, 841.

(46) Christensen, S. G. Technical University of Denmark, unpublished results.

(47) Berg, L. G. The solubility isotherm for 25° (50°) of the triple system K_2O-P_2O_5-H_2O. *Izv. Akad. Nauk SSSR, Ser. Khim.* **1938**, 1, 147.

(48) Chikina, M. V.; Nikolskaya Yu. P. System H_3PO_4 - $Ca(OH)_2$ - H_2O at 25°C. *Izv. Sib. Otd. Akad. Nauk SSSR, Ser. Khim. Nauk*. **1973**, 43.

(49) Belopolskij, A. P.; Serebrennikova, M. T.; Bilevic, A. V. Vapor pressures and solubility in the in the system CaO - P_2O_5 - H_2O. *Zh. Prikl. Khim.* **1940**, 13, 1.

(50) Bassett Jr., H. Beitriege zum Studium der Calciumphosphate III. *Z. anorg. allg. Chemie*. **1908**, 59, 1.

(51) Kol'ba, V. I.; Zhikharev, M. I.; Sukhanov, L. P. The NaH_2PO_4 - $NaNO_3$ - H_2O system at 50°C. *Zh.Neorg.Khim.* **1981**, 26, 828.

(52) Khallieva, Sh. D. Solubility in ternary aqueous-salt systems of potassium dihydrogen phosphate-sodium dihydrogen phosphate-water; sodium dihydrogen phosphate-sodium chloride-water, and potassium dihydrogen phosphate-potassium chloride-water at 40°C *Izv. Akad. Nauk SSSR, Ser. Khim.* **1977**, 3, 125.

(53) Haase, R.; Dücker K. -H.; Küppers H. A. Aktivitätskoefficienten und Dissoziationskonstanten wässriger Salpetersäure und Überchlorsäure, *Bericte der Bunsengesellschaft für Physikalische Chemie*. **1965**, 69, 97.

(54) Clegg, S. L.; Brimblecombe, P. Equilibrium partial pressures and mean activity and osmotic coefficients of 0-100% nitric acid as a function of temperature. *J. Phys. Chem.* **1990**, 94, 5369.

(55) Krawetz, A. *Raman Spectral Study in Aqueous Solution of Nitric Acid.* Thesis. University of Chicago, 1955.

(56) Enea, O.; Singh, P. P.; Woolley, E. M.; McCurdy, K.G.; Hepler, L. G. Heat capacities of aqueous nitric acid, sodium nitrate, and potassium nitrate at 298.15 K: ΔCp° of ionization of water. *J. Chem. Thermodynamics*. **1977**, 9, 731.

(57) Parker, V. B. *Handbook of Chemistry and Physics*; CRC-Press, New York, 1980.

(58) Kurnakow, N. S.; Nikolajew, W. J. Singuläre Falte des Natriumnitrats. *Z. Phys. Chem.* **1927**, 130, 193.

(59) Saslawsky, A. J.; Ettinger, J. L.; Eserowa, E. A. Gemeinesame Löslichkeit der Aluminium-, Natrium-, Kalium- und Eisennitrate im Wasser in Gegenwart von Salpetersäure. *Z. Anorg. Chem.* **1935**,225, 305.

(60) Saad, D.; Padova, J.; Marcus, Y. Thermodynamics of Mixed Electrolyte Solutions VI. An Isopiestic Stud of a psudo-ternary system. *J. Sol. Chem.* **1975**, 4, 983.

(61) Bassett Jr., H.; Taylor, H. S. Calcium Nitrate Part I: The two component system Calcium Nitrate - Water. Part II. The three component system Calcium Nitrate - Nitric Acid - Water at 25°C. *J. Chem. Soc.* **1912**, 101, 576.

(62) Flatt, R.; Fritz, P. Contribution l'etude du systême quinaire Ca, NH_4, H, NO_3, PO_4, H_2O. *Helv. Chim. Acta.* **1950**, 33, 2045.

(63) Flatt, R.; Brunisholz, G.; Fell, G.. Contribution l'etude du systême quinaire Ca, NH_4, H, NO_3, PO_4, H_2O. *Helvetica Chimica Acta.* **1954**, 37, 2363.

(64) Treushchenko, N. N.; Pozin M. E.; Bel'chenko, G. V.; Ivanova, É. Ya. Vapor Pressure of the System HNO_3-NH_4NO_3-H_2O. *J. of Applied Chemistry of the USSR*. **1997**, 44, 1775.

(65) Engel, R. Action de l'acide azotique sur la solubiliti des azotates alcalins, *Hebd. Sîances Acad. Sci*. **1887**, 104, 911.

(66) Kazantzev, A. Über die Einwirkung von Salpetersäure auf die Löslichkeit der Nitrate in Wasser. *Trudy Institut Chistykh Khimicheskikh Reaktivov*. **1923**, 2, 10.

(67) Eysseltová J.; Dirkse T. P. IUPAC – NIST Data Series 66. Ammonium Phosphates. Journal of Physical and Chemical Reference Data. **1998**, 27, 1289.

(68) Lazrak, R.; Nadifiyine, M.; Tanouti, B.; Mokhlisse, A.; Guion, J.; Tenu, R.; Berthet, J.; Counioux, J. J. Etude par conductimetrie des isothermes 40°C des systemes ternaires: M_2HPO_4 – M'_2HPO_4-H_2O (M,M ' = Na, K, NH_4. *J. of Solid State Chemistry.* **1995**, 119, 68.

(69) Platford R. F. Thermodynamics of System H_2O-NaH_2PO_4-$(NH_4)_2HPO_4$ at 25°C. *J. Chem. Eng. Data.* **1974**, 19, 166.

(70) NIST Chemical Thermodynamics Database Version 1.1 (1990). U. S. Department of Commerce, National Institute of Standards and Technology, Gaithesburg, MD 20899.

(71) Shiomi, Ts. *Mem. Col. Sci. Emp.* (Kyoto), **1908**, 67, 1589.

(72) Markus, Y. *Ion Properties*. Marcel Dekker Inc. New York, 1997.

5. Introduction to Ion Exchange Equilibria

A short introduction to the ion exchange phenomena is given. The most basic principles of reactions involving ion exchange systems are introduced, and the most common definitions are introduced. The two most commonly approaches to the modeling of ion exchange equilibria are presented.

5.1 Introduction

Observations of the ion exchange phenomena date back to ancient times. The correct mechanism of the equilibria was however not established until the middle of the nineteenth century, and it is only in the last few decades, after the introduction of the synthetic ion exchangers, that the subject has expanded and become a true science from which extensive industrial applications have emerged. The first large scale industrial ion exchange process was softening of water, and water treatment is still the largest single application. However, the number of new applications for which ion exchange processes are used increases rapidly. Examples of areas with increasing interest in ion exchangers are the mineral, pharmaceutical and agricultural industries. This chapter gives a short introduction to the area of ion exchange equilibria and the most important definitions needed for the understanding of the following chapters will be introduced. For a more detailed description of ion exchange systems in general and ion exchange equilibria, the reader is referred to the extensive books of Helfferich[1] and Dorfner[2].

5.2 Type and Structure

Ion exchangers can in general be divided into two groups; inorganic and organic ion exchangers. Inorganic ion exchangers are usually made up from crystalline alumosilicates with cations held on the surface. Organic ion exchangers, often called ion exchange resins, are in most cases constructed from different polymeric materials and are at present time by far the most common type of ion exchangers used in both science and industry. The main reason for this is the capability of tailor making the exchanging material for special purposes when using synthetic ion exchangers. The organic ion exchange resins are therefore of main interest in

this thesis, and the following section mainly deals with the structure of organic ion exchange resins.

5.2.1 Ion Exchange Resins

In general, a polymeric ion exchange resin consists of an arrangement of linear macromolecules intermolecularly crosslinked to form an infinite network. The crosslinking makes the network insoluble in the solvent it is exposed to. The most important factors when trying to understand the properties of an ion exchange resin is:

- the raw materials used for producing the matrix of the resin
- the crosslinking agent
- the type and amount of fixed ionic groups

One of the most important starting materials for the construction of strongly acidic and basic ion exchange resins is styrene. The styrene is usually polymerized with itself and with divinylbenzene (DVB) as crosslinking agent. The stiffness of the resin matrix is a function of the amount of crosslinks and is often given in % of DVB used in the polymerization process. Different ionogenic groups could be added to the resin surface. By adding e.g. sulfuric acid to the matrix, sulfuric groups are formed on the resin surface:

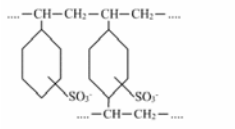

The result of the polymerization process is a large insoluble polymeric molecule. The degree of homogeneity depends on the starting materials and the conditions during the polymerization. There are several different morphological variants of the resin matrixes. The two extremes are the gel type and the macroporous resins, which will be discussed in the following sections.

5.2.1.1 Gel Type Resins

The gel type resins are usually made up by polystyrene materials and have a relatively low degree of crosslinking. During the polymerization process, a network of styrene and DVB is obtained, which is, from a macroscopically point of view, homogeneous and elastic of nature. The matrix is macroporous in the dry state, but when in contact with a good solvent the matrix swells reversibly to form a gel. In this form, the matrix could be considered as having a fairly uniform structure. The matrix of the gel resin has no substantial porosity until it is swollen in a suitable medium. Even though there is not an actual porosity in these types of resins, the channels that exist as a result of swelling could be used for solutes to enter the resin phase.

These types of resins are soft and compressible in their swollen state and the level of swelling depends on the degree of crosslinking and the nature of the solvent. A picture of a gel type resin is shown in figure 5.1. The figure clearly shows that light penetrates the resin which is due to the homogeneity and softness of the matrix.

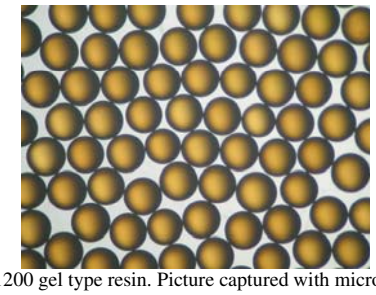

Figure 5.1 Amberjet 1200 gel type resin. Picture captured with microscope at Rohm & Haas experimental lab.

5.2.1.2 Macroreticular Resins

Macroreticular resins are produced using an adequate solvent during the polymerization so that a porous structure is formed. Compared to gel type resins macroporous exchangers are generally more rigid, less compressible and change their volume less when solvent is added. These kinds of resins consist of macromolecular chains which are heavily crosslinked. The structure can be regarded as having a discrete and accessible internal surface and surface area even in the dry state. Good solvents for the primary polymer may cause the resin to swell in

spite of the high degree of crosslinking. The different types of macroreticular resins differ on a microscopic level. However, on a macroscopic level they are usually very alike. The regions in the resin with high matrix density are the reason for considerable mechanical strength. The porosity in the resin may be defined as an intrinsic porosity. The overall structure and properties of this type of resin are very non-uniform. A typical example of a macroreticular resin is shown in figure 5.2.

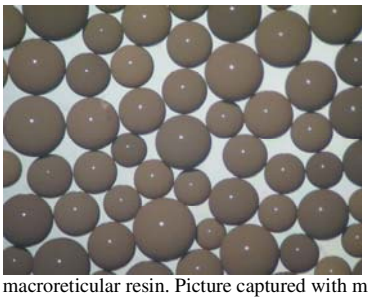

Figure 5.2 Amberlyst 35W macroreticular resin. Picture captured with microscope at Rohm & Haas experimental lab. Light is reflected on the resin surface and causes white dots.

The figure shows that the resin is not permeable for light due to the heterogeneity of the matrix. In a good solvent the exchanging ionic substances are allowed to diffuse quickly through the matrix. However, in a bad solvent the diffusion requires motion of the polymer walls and is generally considered a slow diffusion.

5.3 Definitions and Principles

An ion exchange reaction may be defined as the reversible interchange of ions between a solid phase (the ion exchanger) and a solution phase. The ion exchanger is usually insoluble in the medium in which the reaction occurs. This means that ion exchangers could be characterized as a solid material which carries exchangeable cations or anions. Carriers of exchangeable cations are called cation exchangers and carriers of anions are called anion exchangers. A cation exchange process could be represented by the following equilibrium:

$$AR + B^{+}(aq) + X^{-}(aq) \rightleftarrows BR + A^{+}(aq) + X^{-}(aq) \qquad [5.1]$$

where R denotes the resin or ion exchanger phase.

The participating ions (in this case the cations) are called counter-ions and the non-participating ions (in this case the anion) are usually called co-ions. The amount of fixed ionogenic groups on the ion exchange surface is called the capacity and is usually given in meq/g of exchanging material. The reaction is also graphically represented in figure 5.3.

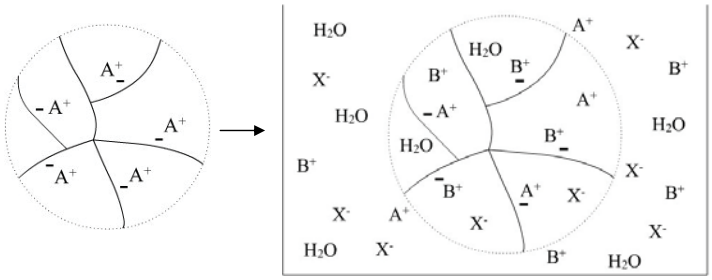

Figure 5.3 Graphical representation of an ion exchange reaction. The resin in its initial form is brought in contact with an aqueous solution of salt with a competing cation.

The relation between the two different counter-ions is called the selectivity. The molal selectivity coefficient is defined as:

$$K_B^A = \frac{m_{AR}^{|z_B|} \cdot m_B^{|z_A|}}{m_{BR}^{|z_A|} \cdot m_A^{|z_B|}} \qquad [5.2]$$

5.3.1 Swelling

When the ion exchanger is brought into contact with a liquid phase it may shrink or swell depending on its initial state and the interactions with the surrounding liquid phase. The main driving force for the solvent uptake is the hydration of the ionic species in the resin and the tendency of the liquid in the pores to dilute itself. The concentration of ionic components inside the resin phase is usually much higher than in the surrounding bulk phase. The resin will therefore take up solvent in order to dilute the resin phase solution. During the absorption of solvent the resin matrix stretches to make room for the solvent molecules. This phenomenon is also called swelling. The expanded matrix causes a pressure on the pore phase and the equilibrium is attained when the swelling pressure balances the driving force of the

solvent uptake. This means that the degree of swelling is mainly a function of the concentration of ions in the surrounding liquid phase, the capacity of the resin and the softness of the ion exchanger matrix. Examples of this phenomenon are shown in figure 5.4 and 5.5.

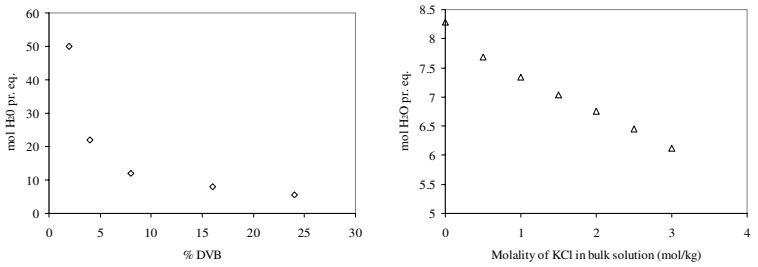

Figure 5.4 and 5.5. Absorption of water in polystyrene resins as a function of the degree of crosslinking and concentration of salt in the surrounding bulk solution.
(◇) Data from Boyd and Soldano[3], (△) data from Christensen and Thomsen[4].

Figure 5.4 shows that the higher the degree of crosslinking, the lower is the sorption of water. The reason for this is that the energy used for stretching the matrix increases with decreasing flexibility of the matrix, and this is why the uptake of water is less at equilibrium. In figure 5.5 the solvent uptake is given as a function of the concentration of salt in the bulk solution. When the concentration of salt in the bulk phase increases, the concentration difference between the two phases decreases. The driving force for the uptake is therefore smaller and solvent uptake is reduced.

5.3.2 Sorption of Solutes

Depending on the aqueous phase concentration and pore volume of the ion exchanger, the different solute species can partition between the pure solvent phase and the ion exchanger phase. In the ideal case solutes would be sorped in the resin phase until the concentration in the two different phases would equal. However, this is rarely seen due to effects from the size of the molecules and the interactions with the fixed ionic groups and counter-ions.

The sorption of ionic species is somewhat lower than for non-ionic solutes. The reason for this is the electrostatic forces arising from the presence of fixed ionic groups and the counter-

ions in the resin phase. In figure 5.3 the concentration of the anion X^- is higher outside the resin than inside and the concentration of the cations A^+ and B^+ are higher in the resin phase than in the bulk phase. If the components were neutral, the concentration differences would even out by diffusion like in the case of non-ionic species. However, migration of cations into the bulk solution and of anions into the resin phase would cause an electric potential difference between the two phases. This is the so-called Donnan effect. The equilibrium is attained when the tendency of the ions to diffuse between the two phases is leveled out by the forces of the electric field. The Donnan potential has thereby the effect that co-ions are repelled from the resin phase solution, and at equilibrium the concentration of co-ions inside the resin is usually much lower than in the external solution. An example of this behavior is given in figure 5.6 where data for the absorption of KCl on a gel type resin are shown.

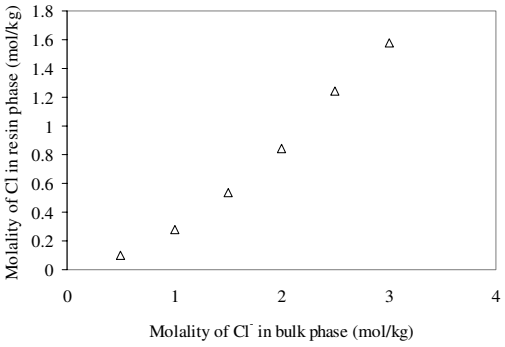

Figure 5.6 Absorption of KCl in an Amberjet 1200 resin on K-form.
(△) data from Christensen and Thomsen[4].

The data in figure 5.6 clearly shows that the Donnan effect excludes the co-ion from the internal solution, and that it is most dominant at low concentrations.

5.4 Modeling of Ion Exchange Equilibrium

Usually two different approaches are used for the description of the ion exchange phenomenon. In one of the approaches the ion exchange process is described as an osmotic equilibrium and in the other as a heterogeneous reaction. Usually the osmotic approach gives

more rigorous models and a higher degree of information about the ion exchanger phase, but therefore also demands more complex experimental data for regression of model parameters etc.

5.4.1 Heterogeneous Approach

A common assumption in the heterogeneous approach is that the maximum uptake of ions by an ion exchanger is limited to the number of functional groups in the ion exchanger. This means that there is no uptake of ions with the same charge as the functional groups. In addition to this, it is assumed that the amount of solvent in the ion exchanger is independent of the ionic form of the exchanger, i.e. the swelling is constant during the exchange reaction. This means that the reaction could be considered a pure heterogeneous reaction between ions held in a "solid solution" and ions in a liquid solution. The reaction is shown schematically in figure 5.7. The model approach is very simple and takes only the selectivity of the ion exchanger for the different counter-ions into account. This means that no information of the absorption of solutes and solvent and of the swelling of the ion exchanger is given when this approach is used. The application of the approach to ion exchange data usually consists of a thermodynamic model for the description of the aqueous phase thermodynamics and some kind of empirical correlation of the non-ideality of the "solid solution"[5,6].

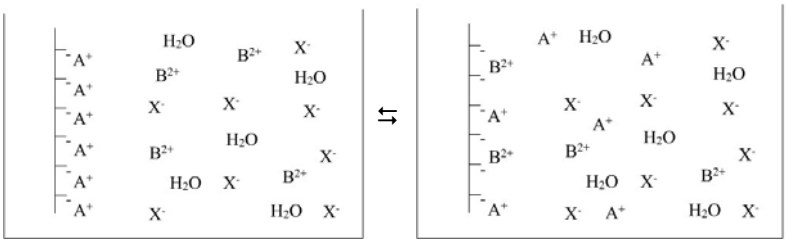

Figure 5.7: Ion exchange reaction according to the mass action law.

The assumption of the model holds for the prediction and the correlation of equilibria between ion exchangers like zeolites and resins with a high degree of crosslinking and aqueous solutions with low to moderate concentrations of ions. At low bulk phase concentrations, the amount of sorped solutes is negligble, and the amount of solvent in the resin could be

considered almost constant during the reaction due to the rigid structure of the ion exchange matrix. However, the approach is often used for the description of other systems as well. The main reason for this is that the data measured in the industry often lacks information about complete solvent/solute distribution between the two phases. Therefore, it is more often convenient to use a more simple approach for the modeling of the available data. In chapter 6 this approach is used for the modeling of both binary and ternary ion exchange isotherms for a variety of different ion exchange systems.

5.4.2 Osmotic Approach

In the osmotic approach the resin phase is considered a liquid phase encaged in an elastic structure. The elastic structure plays the same role as a semi permeable membrane in an osmotic equilibrium. The elastic structure allows the solvent to freely pass. However, only some solute molecules are allowed to pass. As in the case of osmotic equilibrium, there is a pressure difference between the gel phase and the surrounding fluid. When the resin is in equilibrium with a liquid phase the equilibrium conditions consist of a chemical equilibrium, but include an additional mechanical equilibrium as the energy of the resin matrix structure depends of the volume of the gel phase. When in contact with a liquid phase, the resin therefore swells or shrinks until mechanical equilibrium is reached.

The equilibrium could be represented using the model of Gregor[3] shown in figure 5.8. In the left hand side the resin pore is illustrated with the functional groups ,⊖, that are incapable of leaving the resin phase. In the right hand side of the figure an infinite solution is surrounding the resin particle. The matrix of the resin particle is represented by elastic springs which are stretched when the resin swells.

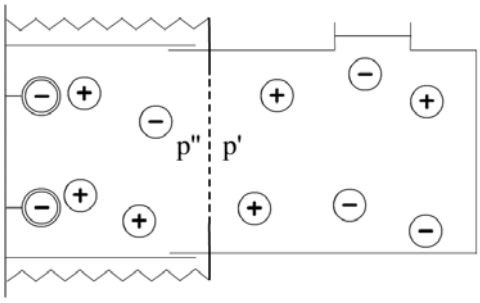

Figure 5.8 Osmotic approach for the description of ion exchange equilibria according to Gregor[3]

Usually the models for the description of ion exchange equilibria using this kind of approach consist of a thermodynamic model for the modeling of the two liquid phases and a mechanical model for taking the energy of elasticity of the resin matrix into account[8,9,10]. The osmotic approach gives a very detailed level of information of the ion exchange equilibrium and could be used for a higher understanding of the forces related to these kinds of reactions. However, the drawback of this model is that very detailed data for the swelling and complete distribution of all species between the two phases is needed for regression of model parameters. In chapter 7 the osmotic approach is used for the modeling of the distribution of water and ions between a bulk phase and different ion exchange resins.

5.5 Conclusion

The most basic principles of reactions involving ion exchange systems have been summarized in this chapter. Besides, the two most common approaches for the modeling of ion exchange equilibria have been presented. In the following chapters these two approaches will be presented in more detail and the capabilities and modeling aspects will be discussed by applying the approaches to both new and existing experimental data.

5.6 References

(1) Helfferich, F. Ion Exchange. Dover. New York, 1995.

(2) Dorfner, K. Ion Exchange. Walter de Gruyter. New York, 1991.

(3) Boyd, G.E.; Soldano, B.A., *Z. Elektrochem.*, **1953**, 57, 162

(4) Christensen, S.G.; Thomsen, K. Experimental measurement and modeling of the distribution of solvent and ions between an aqueous phase and an ion exchange resin. Accepted for publication in *Fluid Phase Equilibria*.

(5) Shallcross, D.C.; Herman, C.C.; McCoy B.J. Improved model for the prediction of multicomponent ion exchange equilibria. Chem. Eng. Sci. 1988, 43, 279.

(6) Högfeldt, E. Ten Years Experience of a Simple Three-Parameters Model to Fit Ion Exchange Data. Reac. Pol. 1989, 11, 199.

(7) Gregor, H.P. A general thermodynamic theory of ion-exchange processes. *J. Am. Chem. Soc.* **1948**, 70, 1293.

(8) Maurer, G. ; Prausnitz, J.M. Thermodynamics of Phase Equilibrium for Systems Containing Gels. Fluid Phase Equilibria. 1996, 115, 113.

(9) Thiel, J.; Maurer, G. Swelling Equilibrium of Poly(acrylamide) Gels in Aqueous Salt and Polymer Solutions. Fluid Phase Equilibria. 1999, 165, 225.

(10) Tiihonen, J.; Markkanen, I.; Kärki, A.; Äänismaa, P.; Laatikainen, M.; Paatero, E. Modelling the Sorption of Water-Ethanol Mixtures in Cross-Linked Ionic and Neutral Polymers. Chem. Eng. Sci. 2002, 57, 1885.

6. Modeling Ion Exchange Isotherms Using a Heterogeneous Approach

Ion exchange isotherms have been modeled using an approach in which the ion exchanger is considered a solid solution phase. The aqueous phase has been modeled using the Extended UNIQUAC model, while the ion exchanger phase has been models using the Margules 1 coefficient model. The thermodynamic equilibrium constant has been calculated individually from the experimental data by a very simple approach. The method has been successfully applied to a variety of both binary and ternary ion exchange systems including new experimental isotherms for the (H^+) - (Na^+, K^+, Ca^{++}) with (Cl^-, NO_3^-, SO_4^{--}, $H_2PO_4^-$) as co-ions at 1N and 25°C.

6.1 Introduction

Ion exchange resins have been used commercially for more than a century and are at present time used extensively in the industry for separation and purification processes. A description of the equilibrium between a multi ionic solution and an ion exchanging material is essential for the development of new and existing ion exchange processes. Especially the choice of design and operating conditions require a detailed knowledge of the ion exchange selectivity. The amount of experimental data necessary for describing the ion exchange equilibria increases tremendously with each exchanging ionic species added to the system. Theoretical models that allow the prediction of multicomponent equilibria from corresponding binary experimental equilibria data are therefore very useful when designing ion exchange processes.

As mentioned in the previous chapter usually two different approaches for the description of the ion exchange phenomenon are seen in the literature. In one of the approaches the ion exchange process is described as an osmotic equilibrium and in the other as a heterogeneous reaction. Usually the osmotic approach gives more rigorous models and a higher degree of information of the ion exchanger phase. However, due to lack of data, works dealing with the osmotic approach very often use assumptions from the heterogeneous approach. In addition to this, it is very common in the industry only to measure the exchange isotherms of the ion exchange system. The measured data lack information of e.g. swelling and solvent sorption which plays an important role in the osmotic approach. Therefore, it is difficult to use this

method on the given data. It is therefore of interest for the industry to develop simple but less rigorous methods for describing ion exchange isotherms.

In this chapter ion exchange isotherms are modeled using an approach where the exchanging phase is treated as a solid solution. The approach is fairly empirical, but is capable of consistently describing the ion exchange isotherm based on very few parameters. Additionally, the method is capable of performing reasonable predictions with varying concentrations. Only very few data exist showing the co-ion effect on the ion exchange equilibrium in systems where ion-pairing/speciation takes place. Therefore, new exchange isotherms have been experimentally measured for different H^+ - $M^{+/++}$ systems with Cl^-, NO_3^-, $H_2PO_4^-$, SO_4^{--} as co-ions at 25°C. These new data are also correlated and the model is successfully capable of predicting the correct trend for the ion exchange isotherms dependence on the different co-ions.

6.2 Experimental Section

The measurement of ion exchange equilibria isotherms is far from a new discipline and can usually be measured by simple means. Several standard procedures exist for measurement of these types of data, and the methods used in this thesis are closely related to these standard methods. Ion exchange equilibria are usually measured by equilibrating the ion exchanger with a solution of both the competing counter-ion species, and then analyzing the ionic composition of the ion exchanger after separating it from the solution. The amount of the two different counter-ions can subsequently to the separation be found by displacing the two competing ions with a solution containing a third counter-ion.

The experiments could be performed either in batch form with closed flasks[1] or in columns. In this work the column method is chosen. The method is convenient for performing many successive experiments with the same resin, which is the case in this work. In addition to this it is easy to ensure a stable temperature with a heating jacket. Two of the most important sources of experimental error are the conditioning of the resin and making certain that equilibrium is obtained before the wash and elution of the column is performed. In this work the macroporous resin Amberlyst 40CW is used. The resin has been chosen mainly because it is used in many industrially relevant processes e.g. the production of fertilizer salts. Bulk

solutions of 1N were used in all experiments due to the fact that most of the used salts do not precipitate at this concentration at 25°C.

6.2.1 Preparation of Experimental Equipment:

Glassware:

All glassware used in this work was of class A grade and was prior to use washed in dilute nitric acid followed by washing with ultra pure (UP) water in order to remove all traces of impurities.

Electrolyte solutions:

Electrolyte stock solutions of 1N were prepared in 1L volumetric flasks with salts of analytical grade where UP water with a resistivity of 18.2 MΩ·cm was used as a solvent.

Resin conditioning:

The required amount of resin was first washed with 5 bed volumes of water in order to remove impurities originating from the polymerization process. The resin was converted into the desired form by passing the resin with at least 10 bed volumes of a 1N solution until complete conversion of the resin was obtained. Subsequently the resin was washed with 10 bed volumes of water to remove any absorbed salt.

6.2.2 Measurement of the Physical/Chemical Properties of the Resin:

A good number of standardized experimental methods are available for the measurement of the most common properties of ion exchange resins. The experimental methods used in this work are similar to the different official test methods found in the literature[1].

6.2.2.1 Equilibrium Water Content Measurement:

50mL of resin was equilibrated with UP water for 30 min and transferred to a 6 cm Buchner funnel loaded with medium porosity filter paper. The funnel was placed on a vacuum flask covered with a rubber stopper and connected to a humidifying tower. Vacuum was applied at 40 ± 2 torr for 5 min. The prepared resin was transferred to a dry tared weighing dish and the wet weight was recorded. The sample was dried at 105 ± 2 °C for 12 hr. Finally the resin was

cooled in a desiccator and the dry weight recorded. The fraction of water in the resin when equilibrated with pure water was then calculated by the following equation:

$$q_w = 1 - \frac{w_R^{dry}}{w_R^{wet}} \qquad [6.1]$$

6.2.2.2 Capacity Measurement:

A sample of the resin was treated in the same way as for the equilibrium water content measurement. Afterwards a known weight, approximately 15g, of the resin was converted to H^+ form by placing the sample in a column and passing 1L of 1N HCl through the column with a flowrate of 25mL/min. After the conversion, the sample was rinsed with 1L of UP water. Next 1L of 0.5 N $NaNO_3$ was passed through the column with a flowrate of 25mL/min in order to elute the H^+ from the sample. Exactly 1L of effluent was collected in a volumetric flask. Next, 100mL of the effluent was transferred to a titration beaker. The sample was titrated with 0.1000N NaOH. After this, the capacity can be found according to the following equation:

$$q = \frac{10 \cdot c_{NaOH} \cdot V_{NaOH}}{w_R^{wet} \cdot (1 - q_w)} \qquad [6.2]$$

The equation expresses the amount of functional groups per grams of dry resin. The coefficient 10 in the equation relates to the fact that only 100mL of the 1L solution are titrated.

6.2.3 Measurement of Ion Exchange Isotherms

A sample of the resin Amberlyst 40CW on the appropriate form was treated in the same way as for the equilibrium water content measurement. Afterwards, a known amount of wet resin, approximately 70 grams, was transferred to a thermostatically controlled column at 25±0.1°C with internal diameter of 1.5cm and 30cm in internal height. Inert glass beads were used for topping of the column in order to improve the liquid flow in the column. The solution with the two competing counter-ions of interest was passed through the column with 5mL/min until the effluent had the same composition as the feed. The column was then briefly purged with pure water to displace the interstitial solutions. After the purge the two counter-ions were displaced from the exchanger by passing a concentrated solution (3N) of NaCl at 5mL/min.

The displacement was continued until there was no trace of H^+ in the eluent. A test showed that approximately 4 bed volumes of NaCl were necessary to elute all the counter-ions of interest from the column.

The amount of H^+ in the eluent was analyzed by titration with 0.1N NaOH (see appendix E) and the amount of the competing counter-ion was calculated using the total capacity of the column:

$$n_{H^+} = 10 \cdot c_{NaOH} \cdot V_{NaOH} \qquad [6.3]$$

$$n_{M^{+/++}} = \frac{w_{\text{resin}} \cdot q}{1000} - n_{H^+} \qquad [6.4]$$

To test that equilibrium actually was obtained before purge and elution, the experiment was carried out from both sides of the equilibria isotherm and the results compared.

6.3 Theory

6.3.1 Equilibrium Conditions

We consider the ion exchange equilibrium between an aqueous solution containing the ions A^{z_A} and B^{z_B} and the ion exchanger R^-. If it is assumed that the swelling of the ion exchanger is constant and that the only uptake of ions is directly connected to the stochiometric ion exchange reaction, the equilibrium can be described as a pure heterogeneous chemical reaction where ions in the solution shift place with ions bound to the surface of the ion exchanger:

$$|z_B| A^{z_A} + |z_A| BR_{z_B} \rightleftarrows |z_B| AR_{z_A} + |z_A| B^{z_B} \qquad [6.5]$$

where *R* denotes the ion exchanger phase.

The criterion for phase equilibria in terms of chemical equilibrium is given by:

$$|z_B| \mu_{A^{z_A}} + |z_A| \mu_{BR_{z_B}} - |z_A| \mu_{B^{z_B}} - |z_B| \mu_{AR_{z_A}} = 0 \qquad [6.6]$$

In the aqueous phase we define the chemical potential in terms of molality:

$$\mu_i = \mu_i^{\nabla}(T,p) + RT\,ln\left(m_i\gamma_i^{\nabla}\right) \qquad [6.7]$$

μ_i^{∇} is the chemical potential of component *i* in the standard state, based on the asymmetrical convention and the molality scale.

For the ion exchanger phase, the chemical potential is defined as:

$$\mu_i = \mu_i^{0}(T,p) + RT\,ln(x_i\gamma_i^{0}) \qquad [6.8]$$

x_i is the mole fraction of component *i* on the resin surface, μ_i^{0} is the standard chemical potential of the ion exchanging component based on the symmetrical convention and the mole fraction scale, hence the standard state of e.g. component *A* is the ion exchanger on pure *A* form.

The thermodynamical equilibrium constant for equation [6.5] is according to eq. [6.7 – 6.8] defined as:

$$K_A^B = \frac{\left(m_B\gamma_B\right)^{z_A}}{\left(m_A\gamma_A\right)^{z_B}} \cdot \frac{\left(x_{AR_{z_A}} f_{AR_{z_A}}\right)^{z_B}}{\left(x_{AR_{z_B}} f_{AR_{z_B}}\right)^{z_A}} \qquad [6.9]$$

where $x_{AR_{z_A}} = \frac{n_{AR_{z_A}}}{n_{AR_{z_A}} + n_{BR_{z_B}}}$

The apparent equilibrium constant K_C is a convenient definition as it only consists of parameters that can be measured experimentally or calculated using appropriate models:

$$K_C = \frac{\left(m_B\gamma_B\right)^{z_A}}{\left(m_A\gamma_A\right)^{z_B}} \cdot \frac{\left(x_{AR_{z_A}}\right)^{z_B}}{\left(x_{AR_{z_B}}\right)^{z_A}} \qquad [6.10]$$

This means that the following equation applies:

$$K_A^B = K_C \frac{\left(f_{AR_{z_A}}\right)^{z_B}}{\left(f_{AR_{z_B}}\right)^{z_A}} \qquad [6.11]$$

Equation [6.11] states that the ratio between the activity coefficients in the resin phase can be found from experimental ion exchange isotherm data if a suitable model for the aqueous solution activity coefficients is used.

In some works the equivalent fraction is used for the resin phase instead of mole fractions. The equivalent fraction is defined as:

$$y_{AR_{z_B}} = \frac{z_A n_{AR_{z_B}}}{z_B n_{BR_{z_B}} + z_A n_{AR_{z_A}}}$$

6.3.2 Aqueous Phase Thermodynamics

Single-ion activities are not defined rigorously within chemical thermodynamics and the possibility of measuring single ion activity coefficients in ionic solutions are still a subject of substantial discussion[2]. It would therefore be most appropriate to introduce equation [6.9] in terms of the activities of the two salts in the aqueous phase or in terms of mean ionic activity coefficients. However, as shown in appendix F, it is only a matter of notation whether or not the co-ions are included in the expression for the thermodynamic equilibrium constant.

The activity of one electrolyte in a solution of another electrolyte is a matter that has been studied by several different investigators during the past two centuries. The most important experimental methods for determining this property are the measurement of one salt's solubility in solutions of other salts or by measurement of osmotic coefficients or mean activity coefficients of the multicomponent solution. In the case of SLE data this type of data contains information about the activities of the individual salts in multicomponent solutions. This is realized by observing the solubility product of the salt $C_\chi A_\alpha$ in an aqueous solution:

$$C_\chi A_\alpha(s) \rightleftarrows \chi C(aq) + \alpha A(aq) \qquad [6.12]$$

The solubility product is given as:

$$K_{C_\chi A_\alpha} = a_C^\chi a_A^\alpha \qquad [6.13]$$

where the activity of the ions are defined as $a_i = m_i \gamma_i^\nabla$. Eq. [6.13] means that SLE data of a multicomponent solution give information of the activity of the salt $C_\chi A_\alpha$ in the solubility

point independently of the other ions in the solution. The osmotic coefficient and mean molal activity coefficient however do not include any information of the activity of one of the salts in the mixture, but only a value of the total or mean activity of the solution. The mean activity coefficient is defined in the following manner:

$$\ln \gamma_{\pm} = \frac{1}{n} \sum_{N_{ions}} \ln \gamma_i \qquad [6.14]$$

Values of mean activity coefficients of multicomponent electrolyte solutions could be found from e.g. experimental electromotive force measurements. However, as seen from eq. [6.14], this value includes no information of the activity of neither the individual salts nor the different ions. This means that when regressing parameters of a thermodynamic model to these types of data, there is no guarantee that the model is capable of calculating the relationship between the activities of the different salts correctly.

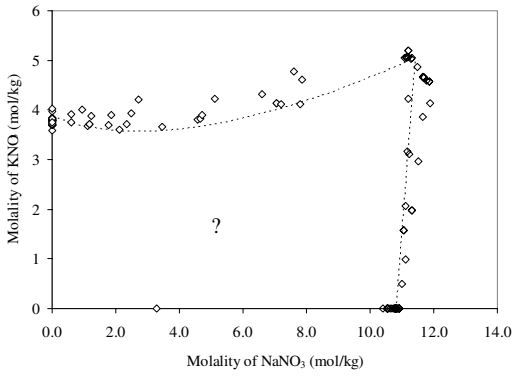

Figure 6.1. Experimental data for the solubilities in aqueous solutions of $NaNO_3$ and KNO_3 at 25°C.

The phase diagram for the ternary aqueous system $NaNO_3$ – KNO_3 is shown in figure 6.1. In the case of single salt solutions, osmotic coefficients are adequate for obtaining data of single salt activities, and in the ternary system, SLE data provide the relevant information. This means that in this case it is possible to gather information about the individual salt activities in the borderlines of the area marked with a question mark. However, in the entire area inside the borders only information of the overall activity of the solution exists. This implies that

even though two different thermodynamic models are capable of calculating the mean activity coefficient of a ternary mixture correct, it is not certain that the models give the same ratio between the activities of the two salts in the solution. An example of this is given in figure 6.2 where the Pitzer and the Extended UNIQUAC model have been applied to the ternary system Na^+ - K^+ - NO_3^- at a total molality of 2 moles of salt pr. kg water. The parameters used in the Pitzer model have been regressed on the basis of osmotic coefficient data[3] while SLE data, osmotic coefficients and thermal data have been used for regression of the parameters in the Extended UNIQUAC[4] model.

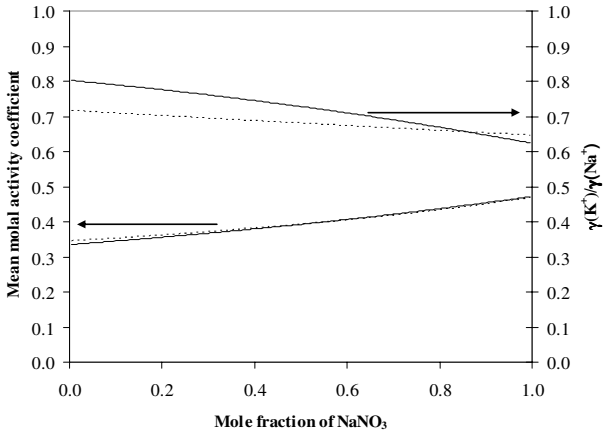

Figure 6.2: Mean molal activity coefficients and relation between the cationic activity coefficients in the system $NaNO_3$ – KNO_3 with a total molality of 2m.
(–) Extended UNIQUAC model (--) Pitzer model.

Figure 6.2 shows that the two different models give very similar values of the mean activity coefficient of the aqueous ternary solution. However, the ratio between the activity coefficients of the two cations is somewhat different for the two models. This is seen more clearly in figure 6.3 where relative deviations between results calculated with the Pitzer model and the Extended UNIQUAC models are shown. The deviations given in the figure are:

$$AAD = 100 \cdot \left((\gamma_{\pm})_{UNIQUAC} - (\gamma_{\pm})_{Pitzer} \right) / (\gamma_{\pm})_{UNIQUAC} \qquad [6.15]$$

$$AAD = 100 \cdot \left(\left(\frac{\gamma_{Na^+}}{\gamma_{K^+}} \right)_{UNIQUAC} - \left(\frac{\gamma_{Na^+}}{\gamma_{K^+}} \right)_{Pitzer} \right) / \left(\frac{\gamma_{Na^+}}{\gamma_{K^+}} \right)_{UNIQUAC} \qquad [6.16]$$

The figure shows that the relative deviation between the fractions of the two cation activity coefficients calculated with the two different models is very large, even though the relative deviation in mean activity coefficient for the mixture is rather small.

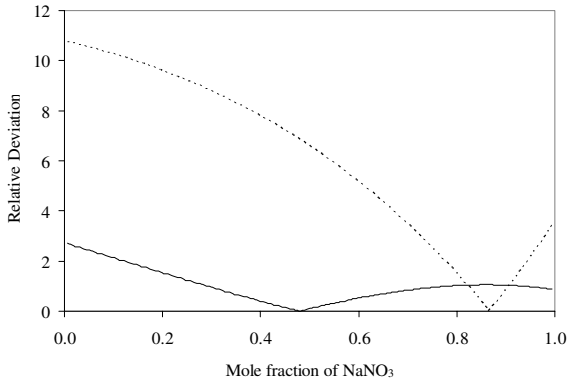

Figure 6.3: Deviation between Extended UNIQUAC and Pitzer model in the $NaNO_3$ – KNO_3 system. (–) eq. [6.15], (--) eq. [6.16]

The calculation has been repeated for the aqueous NaCl - $CaCl_2$ system at a total molality of 1m and the results are shown in figure 6.4. In this case, the deviation in the calculated fractions between the two cation activity coefficients using the two different models is up to 65% even though the deviations in mean activity coefficients of the mixture do not exceed 3%.

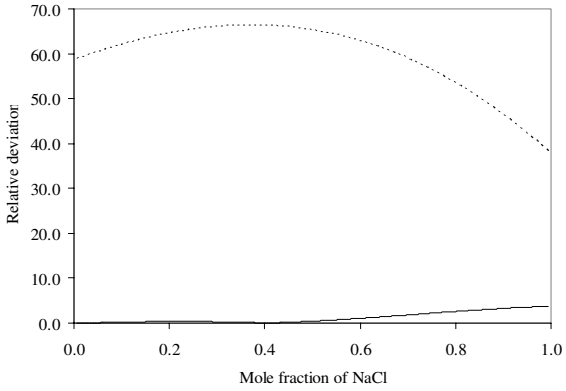

Figure 6.4: Deviation between Extended UNIQUAC and Pitzer model in the NaCl – $CaCl_2$ system. (–) eq. [6.15], (--) eq. [6.16]

In the work presented here, the activity coefficients of the ions in the aqueous phase are described using the Extended UNIQUAC model. As described in chapter 4, the extended UNIQUAC model has previously been applied to describe the excess Gibbs energy of aqueous electrolytes solutions containing many different ions[4,5,6]. One of the strengths of the Extended UNIQUAC is that model parameters are valid in a very large interval in temperature and concentration. To a comparison, most of the available parameters for the Pitzer model are only valid at 25°C, and only in some cases at concentrations up to saturation[7]. Another advantage of the Extended UNIQUAC model is that both binary and ternary SLE data have been included in the parameter regression. This means that the model at least is capable of describing the relationship between the activities of the two salts at the saturation point.

6.3.2.1 Influence of Speciation and Ion Pairing on the Equilibria

The influence of speciation on the ion exchange equilibria has been discussed in several different works. In many works these types of equilibria are included in the model by calculating the free ion concentration e.g. from experimental stability constants for the ion pairs[8,9]. However, this is a problematic approach when the free component concentrations of the ions are combined with aqueous solution activity coefficients that are calculated using activity coefficient models with the most commonly reported parameters. This is illustrated

by examining the definition of the activity of an electrolyte. If we consider a salt $C_\chi A_\alpha$ that can form ion pairs, following equilibria occur in aqueous solutions:

$$C_\chi A_\alpha(s) \rightleftarrows \chi C(aq) + \alpha A(aq) \quad [6.17]$$

$$\chi C(aq) + \alpha A(aq) \rightleftarrows C_\chi A_\alpha(aq) \quad [6.18]$$

The activity of the electrolyte $C_\chi A_\alpha$ that forms ion pairs in aqueous solution can be expressed in two equivalent ways:

$$a_{C_\chi A_\alpha} = \left(m_{C,T}\gamma_{C,T}\right)^\chi \left(m_{A,T}\gamma_{A,T}\right)^\alpha = \left(m_{C,F}\gamma_{C,F}\right)^\chi \left(m_{A,F}\gamma_{A,F}\right)^\alpha \quad [6.19]$$

The subscripts F and T refer to respectively the free concentrations and the total or stochiometric concentrations of each species. The free concentration of a species is defined as the total concentration minus the amount of the species bound in ion pairs. For the majority of the most common salts, parameters for e.g. the Pitzer model have been regressed using experimental data where the reported property (SLE, osmotic coefficient, mean molal activity coefficient etc.) are given as a function of the total molality of the salt[4,7]. This means that the activity coefficients calculated by the model are most likely related to the total molality of the ion, and that ion pairing/speciation implicit is included in the fitted parameters, and hence in the activity coefficients calculated by the model. If we once again consider the solubility of the salt $C_\chi A_\alpha$ in water, then the solubility product is given as:

$$K_{C_\chi A_\alpha} = a_C^\chi a_A^\alpha = \left(m_C\gamma_C\right)^\chi \left(m_A\gamma_A\right)^\alpha \quad [6.20]$$

When the parameters of a thermodynamic model are fitted to e.g. SLE data, the activity coefficients used in the parameter fitting are dependent on the definition of the components in the aqueous phase. If the salt in eq. [6.20] is assumed to be a folly dissociated electrolyte and the parameters of the thermodynamic model are regressed on the basis of this assumption, then the same assumption should be used when the activity of the given salt later on is calculated using the model parameters. This relation has not until now been a subject of discussion within the area of ion exchange thermodynamics. However, the problematic approach of using free ion concentrations with thermodynamic models based on complete dissociated salts is seen in many published works.

Based on the discussion in this section we therefore in this thesis use the same component concentrations in the aqueous phase for calculating the activities that were used when regressing the parameters for the applied thermodynamic model. This will maintain a thermodynamic consistent in the modeling work.

6.3.3 Ion Exchanger Phase Thermodynamics

The objective of the excess Gibbs energy model for the ion exchanger phase is to equate the excess Gibbs energy to a simple function of composition.

Several different approaches have been proposed for the modeling of the nonideality of the components in the ion exchanger phase. However, due to the fact that there are no experimental means of determining the activity coefficients of the components in the ion exchanger phase, all the models presented at present time are more or less empirical. Some of the proposed models have been taken from the thermodynamic theory of liquids[1,10], while others are statistical approaches derived for the use in ion exchange systems[11,12]. The requirements for the resin phase thermodynamic model are unambiguous. The Gibbs excess energy is a function of the solid-phase mole fraction and for any solid-phase species AR_{z_A} and the Gibbs excess energy should be zero for $x_{AR_{z_A}} = 1$. Usually the excess energy models can be divided into three algebraic forms: polynomial, fractional and logarithmic. The choice of model depends on the degree of nonideality in the system and is in general a question of describing the property:

$$\ln K_C = f(x_{AR_{z_A}})$$

In some works[12] it is proposed to divide ion exchange systems into 4 classes:

1. Ideal systems. Systems with a constant value of K_C and with activity coefficients equal to unity.
2. Regular systems. Systems with a linear expression of $\ln K_C$ as function of the solid phase molefraction and with a second power dependency of the activity coefficients on the solid phase molefractions.

3. Irregular statistic systems. Systems in which $\ln K_C$ could be expressed by an equation of the second power and in which the activity coefficients could be described by equations of the third power.

4. Irregular nonstatistical systems. Systems in which the counter-ions do not distribute statistically between the different exchange sites and therefore require special treatment of the non ideality.

It is a well known problem that it is difficult to obtain exact experimental results at low concentrations of one of the two components. In addition to this, most of the available data for ion exchange isotherms are somewhat scattered due to experimental uncertainties. An example of this is given in figures 6.5 and 6.6.

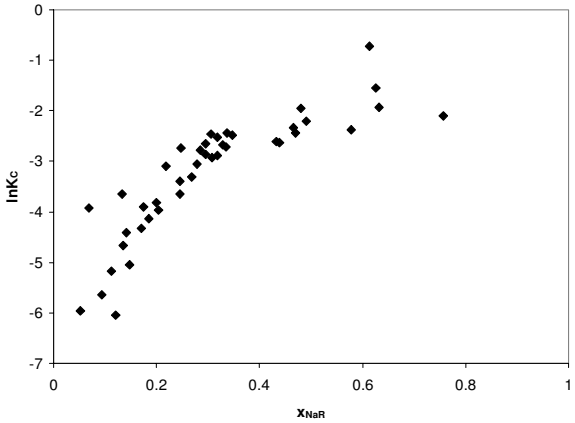

Figure 6.5. Na^+ - Ca^{++} ion exchange on Clinoptolite at a total molality of 0.5N. Apparent equilibrium constant as function of mole fraction of Ca^{++} on the resin. Data from Pabalan and Bertetti[13].

In the figures 6.5. and 6.6, the apparent equilibrium constant has been calculated for Na^+ - Ca^{++} ion exchange from data of two different sources. The equilibrium constant has been calculated according to eq. [6.10] and the activity coefficients of the aqueous solution have been calculated using the Extended UNIQUAC model. The data used in figure 6.5 is from the extensive work of Pabalan and Bertetti[13]. The figure shows a huge scattering of the data. This makes it very difficult to identify what type of system the data represents. There is no doubt

that a 3. degree polynomial would represent the data in figure 6.5 better than a straight line. However, there is no assurance that the representation would not include a large part of the experimental noise of the data.

Figure 6.6 shows the apparent equilibrium constant in the Ca^{++} - Na^{+} system calculated on the basis of data from Shallcross et al.[14] The data shows clearly a linear trend in the mole fraction range of 0.2 – 0.8. However, as the mole fraction goes towards 0 or 1, the data are more scattered due to the experimental procedures. This is typical for many ion exchange data and is the reason why it is very often difficult to decide what type of system the data represent. Very often the system is classified as being more irregular than it actually is due to the experimental scattering.

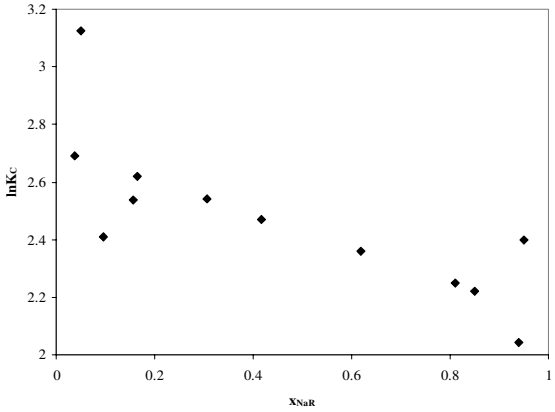

Figure 6.6. Na^{+} – Ca^{++} ion exchange on Amberlite 252 at a total molality of 1.0N. Apparent equilibrium constant as function of mole fraction of Na^{+} on the resin. Data from Shallcross et al.[14].

The impact of this scattering is seen in the regressed parameters of the thermodynamic model of the ion exchanger phase. In many cases it is seen that the regressed parameters are highly intercorrelated; hence the system could just as well have been correlated using a simpler model. In this thesis it is chosen to treat all systems as regular systems. This means that the apparent equilibrium constant could be represented by a straight line, and that the Gibbs Excess energy of the ion exchanger phase could be calculated using a polynomial expression of the 2. degree.

The Margules 1 coefficient equation[15] is therefore used for describing the non-ideality in the ion exchanger phase. Using this equation reduces the number of parameters and thereby also reduces the numerical difficulties compared to previous works[8,9,11,16]:

$$ln\,\gamma_i^0 = \sum_j \frac{\Lambda_{ij}}{RT}(x_j^2) \qquad [6.21]$$

where Λ_{ij} is an ion exchanger specific parameter and $\Lambda_{ii} = 0, \Lambda_{ij} = \Lambda_{ji}$. R is the gas constant and T is the absolute temperature in K. For comparison, the Wilson model used in many previous works includes 2 parameters and is given by the equation:

$$\ln \gamma_i^0 = 1 - \ln \sum_j x_j A_{ji} - \sum_k x_k \frac{A_{ik}}{\sum_j x_j A_{jk}} \qquad [6.22]$$

where $A_{ii} = 0, A_{ij} \neq A_{ji}$

6.3.4 Calculation of the Thermodynamic Equilibrium Constant

It is a very widespread procedure to estimate the thermodynamic equilibrium constant independently from the resin phase activity coefficients[1,8]. The main reason for this is that a high correlation between the different estimated parameters is often observed when regressing the resin phase activities simultaneously with the thermodynamic equilibrium constant. The most common approach is to eliminate the resin phase activity coefficients leading to an expression for the equilibrium constant only dependent on experimentally measurable values and the solution phase activity coefficients. Gaines and Thomas[17] were some of the first scientists who decoupled the thermodynamic equilibrium constant from the resin phase activities. They showed that by solving the Gibbs-Duhem equation for the ion exchanger phase following expression could be obtained (see appendix G):

$$ln\,K = \int_0^1 ln\,K_C\, dy_{BR_{ex}} \qquad [6.23]$$

which is similar to the expression presented by Arsinger et al.[18].

Ioannidis et al.[8] presented a slightly different decoupling method based on the same basic principles. Their motivation was that usually the experimental datapoints in the endpoints of

the isotherm are subject to large experimental errors which could result in an inaccurate numerical integration of eq. [6.23]. However, by assuming that all the given systems are regular and that $\ln K_C = f(x_{AR_{z_A}})$ thereby could be fitted as a straight line, the error related to the experimental datapoints is minimized. In this work we have chosen to use equation [6.23] for determining the thermodynamic equilibrium constant. A straight line has been fitted to the experimental data followed by numerical integration between the two pure states.

6.4 Results and Discussion

The resin properties are calculated from the measured experimental data on the basis of eq. [6.1-6.2]. The properties are given in table 6.1.

Table 6.1: Properties of the used macroreticular resin.

	Amberlyst 40CW
% DVB	16.5
Capacity (H-Form) (eq /kg dry)	5.34
Water content (H-form) (%)	48.3

The experimental isotherm data are calculated using eq. [6.3-6.4]. The validity of the method was tested by measuring the isotherms from both endpoints. In figure 6.7 the data for the H^+ - K^+ system are shown. In one set of data, resin on K^+ form has initially been used, and then a 1N solution of KCl and HCl in different relative fractions has been passed through the column. In the other set of data the resin was initially in H^+ form.

The figure shows that the deviation between data from the two different series of experiments is very small. It can be concluded that equilibrium is obtained between the ion exchange resin and the bulk solutions with the given method. Isotherms have been measured for the H^+ - K^+, H^+ - Na^+ and H^+ - Ca^{++} systems with both Cl^-, NO_3^-, SO_4^{--} and $H_2PO_4^-$ as co-ions except in the case of the H^+ - Ca^{++} in which SO_4^{--} has been omitted due to the low solubility of $CaSO_4$. All data is given in appendix H. The data for Cl^- and NO_3^- as co-ions are in all experiments represented by almost identical isotherms and the NO_3^- data are therefore omitted in the further discussion.

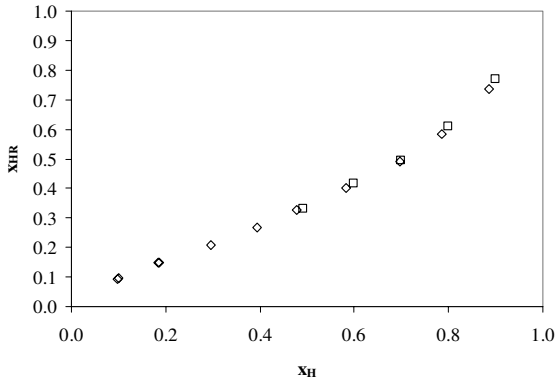

Figure 6.7: Exchange isotherm for the system H^+ - K^+ in 1N chloride solutions.
(◇) resin initially on K^+ form, (□) resin initially on H^+ form.

6.4.1 Binary Systems

The Margules 1 coefficient model has been applied to a large number of ion exchange data, including the data measured in this work. In all examples the aqueous phase thermodynamics have been calculated with the Extended UNIQUAC model with the parameters given in chapter 4 or in previous published articles[4,5,6,19]. The thermodynamic equilibrium constant has been calculated according to eq. [6.23]. All molarity concentrations have been converted into molality using the correlation and parameters given in chapter 3.

6.4.1.1 Impact of the Resin Phase Thermodynamic Model

The Margules 1 coefficient model eq. [6.20] and the Wilson model eq. [6.21] have been applied to a number of ion exchange isotherm data. The deviations for each system have been calculated using eq. [6.24] and the results are given in table 6.2.

$$SD = \sum ABS\left(\frac{K_{\exp} - K_{calc}}{K_{\exp}}\right), \quad K = \frac{m_{B^{z_B}} x_{AR_{z_A}}}{m_{A^{z_A}} x_{BR_{z_B}}} \qquad [6.24]$$

The table shows that the deviation is between 5-14% for both models. This degree of deviation is very common for ion exchange data[8,21], and is mainly due to scattering in the data

which is a result of the experimental methods used. The table also shows that the magnitude of the deviation is the same for the two models. This verifies the previously mentioned fact that when applying the Wilson model to this type of data, the two parameters are highly intercorrelated.

Table 6.2: Comparison of correlations using the Wilson and Margules 1. coefficient model.

Type of exchange	Anions	Ionic Strenght (mol/L)	Margules 1 par.	Wilson	Data ref
			SD	SD	
Na - K	Cl, NO_3	0.005, 0.05, 0.5	0.141	0.132	13
Na - H	Cl	0.01, 0.05, 0.5	0.117	0.115	9
K – H	Cl	0.01, 0.05, 0.5	0.102	0.112	9
K - Na	Cl	0.01, 0.05, 0.5	0.067	0.065	9
Ca - H	Cl	0.1, 0.2, 0.5, 1.0	0.075	0.072	14
Ca - K	Cl	0.1, 1.0	0.056	0.046	14
Na - H	Cl, NO_3, SO_4	0.7	0.077	0.061	14
Na - Mg	Cl, SO_4	0.05, 0.2	0.053	0.058	20
Na - Zn	Cl, SO_4	0.05, 0.2	0.084	0.078	20
Mg - Zn	Cl, SO_4	0.05, 0.2	0.065	0.064	20
Sr - Na	Cl	0.005, 0.05, 0.5	0.058	0.055	13
Sr – K	Cl	0.05	0.084	0.078	13
Sr - Ca	Cl	0.05	0.057	0.053	13
Ca - Na	Cl	0.052	0.132	0.124	20
Mg Na	Cl	0.052	0.121	0.119	20

6.4.1.2 Predictions at Varying Concentrations

To test the methods capability to perform predictions at varying concentrations, it has been applied to $Na^+ – Ca^{++}$ ion exchange data from two different sources. The Margules parameter and equilibrium constant for both systems are given in table 6.3. In figure 6.8 the method has been applied to data from Pabalan et al[13]. who have measured the exchange on the inorganic ion exchanger clinoptolite at different normalities at 25°C. The capacity of the solid material is reported as 2.04 meq/g. The model parameters are regressed on the basis of the data at 0.005N and are used for prediction of the isotherms at 0.05N and 0.5N

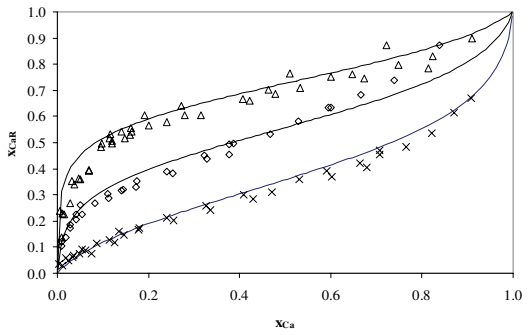

Figure 6.8: Ca^{++} - Na^{+} exchange on clinoptolite at 25°C. Experimental data from Pabalan. (×) 0.5N, (◇) 0.05N, (△) 0.005N. (–) calculated results with model parameters regressed from 0.005N data

The calculated equilibrium constant is 0.195 which is very close to the value of 0.192 reported by Pabalan et al.[13] The figure shows that the predictions represent the data with minor deviations even when taking high degree of scattering in the data into consideration.

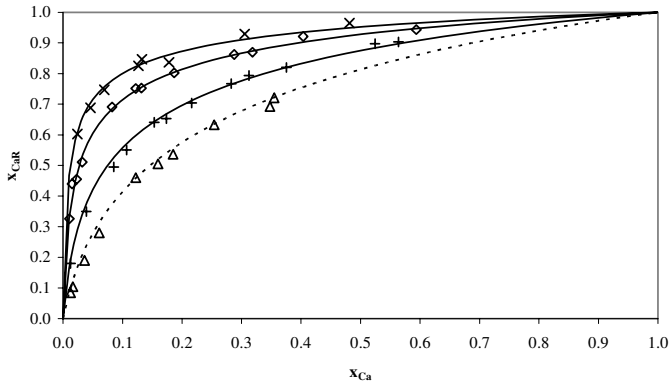

Figure 6.9: Ca^{++} - Na^{+} exchange on Amberlite 252. Experimental data of Shallcross et al.[14]. (△) 1.0N, (+) 0.5N, (◇) 0.2N, (×) 0.1N, (–) calculated results.

Shallcross et al.[14] have measured Ca^{++} - Na^{+} exchange isotherms on the gel type resin Amberlite 252 and report a calculated equilibrium constant of 14.6 which is slightly larger than the value of 12.8 calculated in this work. Figure 6.9 shows the experimental data compared with model predictions. The model parameters have been regressed from the 1.0N data. The results in figure 6.9 indicate that model parameters regressed at a given concentration give reliable predictions at various other concentrations.

Table 6.3: Margules parameter and equilibrium constant for binary systems.

System	Λ	K_{eq}	Exp. data ref.
Ca^{++} - Na^{+}	-2.367	0.195	13
Ca^{++} - Na^{+}	-0.205	12.76	14
Cu^{++} - Na^{+}	-0.772	6.217	22
H^{+} - K^{+}	-0.232	0.372	-
H^{+} - Na^{+}	-0.147	0.550	-
H^{+} - Ca^{++}	0.619	0.0198	-

6.4.1.3 Influence of Speciation on Equilibria

As mentioned previously the speciation could influence the ion exchange isotherms. If ion pairing is present, fewer ions are available in the solution for the ion exchange reaction on the surface. This influence is incorporated in the method by calculating the amount and activity coefficients of each species with the Extended UNIQUAC model. One example of a system in which a high degree of speciation exists, is the Cu^{++} - Na^{+} exchange in chloride media measured by Rao and David[22] on a Dowex 50 ion exchanger. Cu^{++} and Cl^{-} form a complex in aqueous solutions:

$$Cu^{++}(aq) + Cl-(aq) \rightleftarrows CuCl^{+}(aq),\ K_{stability} = \frac{[CuCl^{+}]}{[Cu^{++}][Cl^{-}]}$$

Where [X] is the concentration in moles/l.

The stability equilibrium constant of this system is very dependent on the concentration of the solution and is for example reported[23] to be 0.6 (L/mol) at 0.5N and up to 1.3 (L/mol) at 4N. This means that the relative amount of free Cu^{++} ions decreases at higher concentrations.

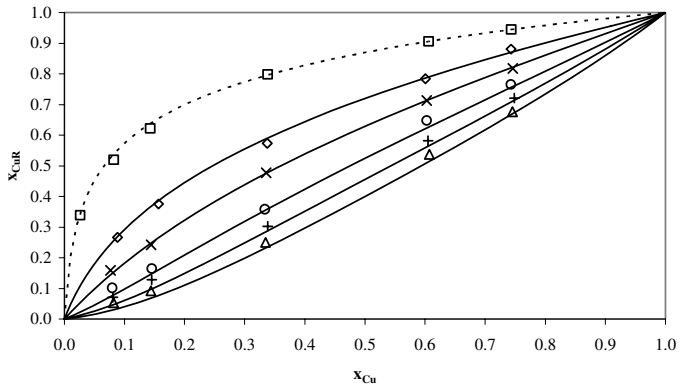

Figure 6.10: Cu^{++} - Na^{+} ion exchange in aqueous chloride solutions. Experimental data from Rao and David[22], (△) 4.0N, (+) 3.0N, (o) 2.0N, (×) 1.0N, (◇) 0.5N, (□) 0.1N, (–) calculated results.

Figure 6.10 shows the model predictions compared with experimental results. The Margules parameter and the equilibrium constant are regressed from the data at 0.1N, and the isotherms at higher concentrations have been predicted on the basis of these parameters. Even though the speciation in the system changes with the concentration, the model excellently captures the trend in the experimental data. This emphasizes the fact mentioned previously, that it is not necessary to convert the concentrations using speciation data, when speciation was not originally considered in the aqueous thermodynamic model.

Another example, in which the speciation has an impact on the ion exchange equilibria is systems where the choice of co-ion influences the aqueous speciation. In e.g. the H^{+} - $M^{+/++}$ system, the amount of free H^{+} ions depends on whether the co-ion is Cl^{-}, SO_4^{--} or $H_2PO_4^{-}$. This is illustrated in figure 6.11 where the experimental results for the H^{+} - K^{+} system are shown. The molefraction of H^{+} in the aqueous phase is calculated on basis of the total concentration of H^{+}, *i.e.* no speciation has been taken into account when calculating this value.

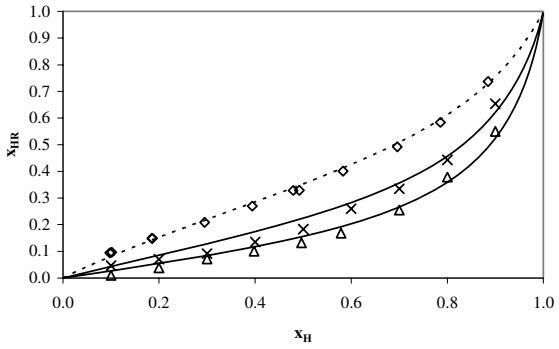

Figure 6.11. H^+ - K^+ ion exchange on Amberlite 40CW at 25°C and 1N.
(◇) Cl^-, (×) SO_4^{--}, (△) $H_2PO_4^-$, (–) calculated results.

The figure clearly shows the effect of the lower concentrations of free H^+ ions in the case of $H_2PO_4^-$ than in the case of Cl^- due to the weak acid properties of H_3PO_4. The experimental data have been modeled by regressing the Margules parameter and equilibrium constant from the chloride data. The extended UNIQUAC model has been applied for the calculation of the speciation and activity coefficients according to the conventions used when the parameters originally were regressed[4,19]. The results show that by only changing the aqueous phase thermodynamics, the model is capable of predicting the correct trend for the SO_4^{--} and $H_2PO_4^-$ data. The predictions slightly overshoot the experimental data; worst in the SO_4^{--} case. The reason for this could be that the Extended UNIQUAC model originally had some problems of fitting the properties of aqueous H_2SO_4 solutions[4]. The procedure has been repeated for the H^+ - Na^+ and H^+ - Ca^{++} systems. The results are shown in figure 6.12 and 6.13. The trend in the predictions is the same as in the previous case; predictions have the right trend, however overshoot the experimental data slightly.

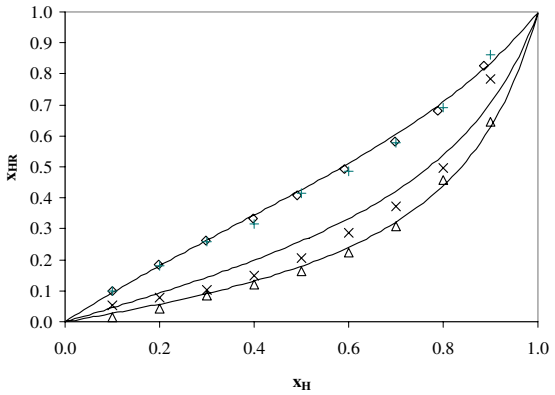

Figure 6.12. H^+ - Na^+ ion exchange on Amberlite 40CW at 25°C and 1N.
(◇) Cl^-, (×) SO_4^{--}, (△) $H_2PO_4^-$, (–) calculated results.

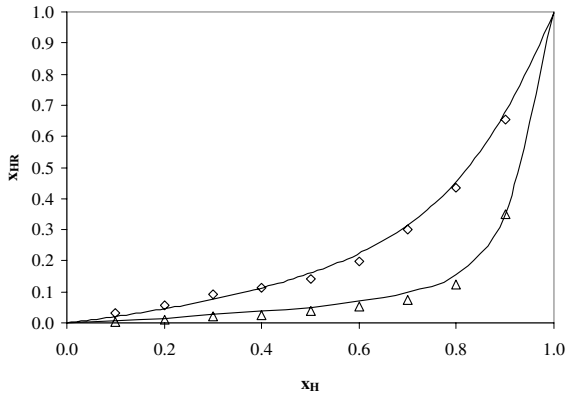

Figure 6.13. H^+ - Ca^{++} ion exchange on Amberlite 40CW at 25°C and 1N.
(◇) Cl^-, (×) SO_4^{--}, (△) $H_2PO_4^-$, (–) calculated results.

6.4.2 Ternary Systems

One way of testing the method's validity is by applying it to ternary systems. Eq. [6.9] could easily be extended to multicomponent systems. One of the forces of the method is that ternary systems could be predicted on the basis of binary exchange data. In addition to this, the thermodynamic equilibrium constant for the three binary systems should follow the Triangle Rule:

$$K_A^B K_B^C (K_A^C)^{-1} = 1$$

When the data do not follow the Triangle Rule, it is usually due to a wrong data reduction method when the thermodynamic equilibrium coefficient is calculated. In this work the method has been tested on the Na^+ - Mg^{++} - Zn^{++} system in aqueous chloride solution measured by Rhee[20]. Figure 6.14 shows the experimental data and model calculations. The two parameters have been found from data measured at 0.2N and are given in table 6.4. The parameters show that the thermodynamic equilibrium constants fulfill the triangle rule:

$$K_{Na}^{Mg} K_{Mg}^{Zn} (K_{Na}^{Zn})^{-1} = 0.97$$

The value of 0.97 is very close to unity taking the scattering of the experimental data into consideration. In other works this test usually shows values that are more than 10% from the value of unity[9,13,20,21]. This is an indication that the method used in this work for calculating the thermodynamic equilibrium constant independently from ion exchanger activities gives more accurate and more consistent values when compared to previous works.

Table 6.4: Parameters for the ternary system Na^+ - Mg^{++} - Zn^{++} at 0.2N and 25°C

System	K	Λ
Na^+ - Mg^{++}	0.513	-0.643
Mg^{++} - Zn^{++}	0.699	0.208
Na^+ - Zn^{++}	0.371	-0.652

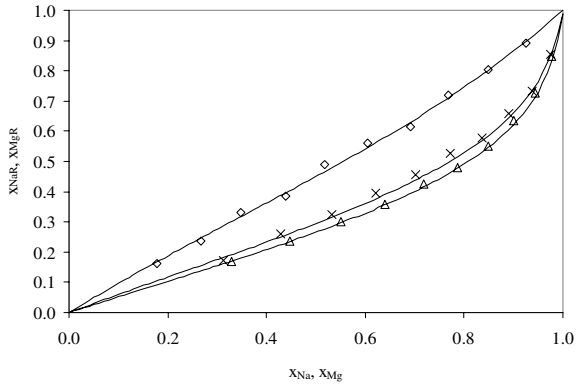

Figure 6.14. Ion Exchange in aqueous chloride solution at 0.2N. Data from Rhee.
(×) Na^{+} - Mg^{++}, (◇) Mg^{++} - Zn^{++}, (△) Na^{+} - Zn^{++}. (–) calculated results.

The thermodynamics of the ternary system has been predicted using the model parameters regressed from the binary data. The result is shown in figure 6.15. In the data of Rhee[20], the total concentration of Mg^{++} has been held constant at 0.05N and the Zn^{++} - Na^{+} exchange has then been measured. The figure shows a good prediction of the ternary system.

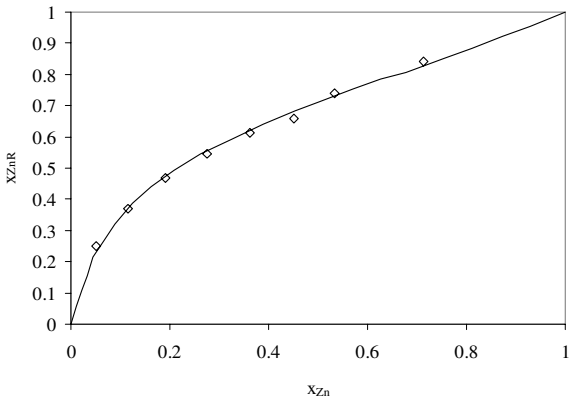

Figure 6.15. Na^{+} - Mg^{++} - Zn^{++} Ion Exchange in aqueous chloride solution at 0.2N. Data from Rhee[20].
Concentration of Mg^{++} is constant 0.05N for all data. (–) predicted results.

6.5 Conclusion

Ion exchange isotherms have been modeled using an approach in which the ion exchanger is considered a solid phase. The aqueous phase has been modeled using the Extended UNIQUAC model, while the ion exchanger phase has been modeled using the Margules 1 coefficient model. The thermodynamic equilibrium constant has been calculated individually from the experimental data by a very simple approach using the equations originally derived by Gaines and Thomas.

The method has been applied to 15 ion exchange systems, and the results show that using the simple Margules model gives very similar results than when using a model with more parameters like e.g. the Wilson model.

The work shows that excellent predictions can be obtained at varying concentrations with parameters regressed at one concentration.

New experimental isotherms have been measured for the H^+ - (Na^+, K^+, Ca^{++}) with (Cl^-, NO_3^-, SO_4^{--}, $H_2PO_4^-$) as co-ions at 1N and 25°C. These new experiments illustrate the impact of speciation on ion exchange equilibria isotherms. The experimental data have been modeled by regressing parameters from the chloride data and the predictions for the isotherms with other co-ions are very reasonable. The conclusions from these calculations are that speciation is implicit included in the aqueous phase activity coefficients. This means, that the conventions used when the parameters of the aqueous thermodynamic model originally were regressed should always be used when activities later on are calculated using the same model parameters.

The approach could easily be extended to a multicomponent system and has in this work been successfully applied to a ternary system. The method gives good predictions in the ternary system from the binary parameters, and the results show that the three thermodynamic equilibrium constants calculated from the binary systems obey the Triangle rule within 3%. This result is better than previously reported results and indicates that the simple method for obtaining the thermodynamic equilibrium constant used in this work gives consistent values. However, the method should be applied to more ternary systems before any final conclusion can be made.

6.6 References

(1) Helfferich, F. Ion Exchange. Chapter 4. Dover Publications, Mineola, USA, **1995**.

(2) Malatesta, F. The Impossibility of Measuring Individual Ion Activity Coefficients Using Ion Selective Electrodes. *J. Sol. Chem.* **2000**, 29, 2000.

(3) Kim H.-T.; Frederick W.J. Evaluation of Pitzer Ion Interaction Parameters of Aqueous Mixed Electrolyte Solutions at 25 °C. 2. Ternary Mixing Parameters. *J. Chem. Eng. Data.* **1988**, 33, 278.

(4) Thomsen, K. Aqueous Electrolytes: Model Parameters and Process Simulation. Ph.D. Thesis. Technical University of Denmark, Lyngby, 1997.

(5) Thomsen, K.; Rasmussen, P.; Gani, R. Correlation and Prediction of thermal properties and phase behaviour for a class of aqueous electrolyte systems. *Chem. Eng. Sci.* **1996**, 51, 3675.

(6) Thomsen, K.; Rasmussen P. Modeling of vapor-liquid-solid equilibrium in gas-aqueous electrolyte systems. *Chem. Eng. Sci*. **1999**, 54, 1787.

(7) Pitzer, K.S. Activity Coefficients in Electrolyte Solutions. CRC Press, Florida, 1991

(8) Ioannidis S.; Anderko A.; Sanders S.J. Internally Consistant Representation of Binary Ion Exchange Equilibria. *Chem. Eng. Sci.*, **2000**, 55, 2687.

(9) Mehablia A. Multicomponent Ion Exchange Equilibria. Ph.D. Thesis. University of Melbourne. Australia, 1994.

(10) Wilson, G.M. Vapor Liquid Equilibrium. XI. A New Expression for the Excess Free Energy of Mixing. *J. Am. Chem. Soc.* **1964**, 86, 127.

(11) Högfeldt, E. A Three-Parameter Model for Summarizing data in Ion Exchange. *Ion Exchange and Solvent Extraction*. **1993**, 11, 109.

(12) Soldatov, V.S.; Bichkova, V.A. Quantitative Description of Ion Exchange Selectivity in Non-Ideal Systems. *Reac. Pol.* **1983**, 1, 251.

(13) Pabalan, R.T.; Bertetti, F.P. Experimental and Modelling Study of Ion Exchange Between Aqueous Solutions and The Zeolite Clinoptilolite. Journal of Solution Chemistry. **1999**, 28, 367.

(14) Shallcross, D.C.; Herman, C.C.; McCoy, B.J. Improved model for the prediction of multicomponent ion exchange equilibria. *Chem. Eng. Sci.* **1988**, 43, 279.

(15) Sandler, I.S. Chemical and Engineering Thermodynamics. John Wiley & Sons, Inc. New York, **1999**.

(16) Fletcher, P.; Townsend, R. Ternary Ion Exchange in Zeolites. *J. Chem. Soc. Faraday Trans. 2.* **1981**, 77, 955.

(17) Gaines, L.G.; Thomas, C.H. Adsorption Studies On Clay minerals II. A Formulation of the Thermodynamics of Exchange Adsorption. *J. Chem. Phys.* **1953**, 21, 714.

(18) Argersinger W.J.; Davison A.W.; Bonner O.D. Thermodynamics and Ion Exchange Phenomena. *Transaction of Kansas Academy of Sciences*. **1950**, 53, 404.

(19) Christensen, S.G.; Thomsen, K. Modeling of vapor-liquid-solid equilibria in acidic aqueous solutions. *Ind. Eng. Chem. Res.* **2003**, 42, 4260

(20) Rhee, I.H.; Dzombak, D.A. Binary and Ternary Cation Exchange on Strong Acid Cation Exchange Resin Involving Na, Mg and Zn. *Langmuir*. **1999**, 15, 6875.

(21) Shehata, F.A.; El-Kamash, A.M.; El-Sorougy, M.R.; Aly, H.F. Prediction of Multicomponent Ion-Exchange Equilirbia for Ternary Systems from data of Binary systems.

(22) Rao, H.C.S.; David, M.M. Equilibrium in the system Cu^{++} - Na^{+} - Dowex50. *AIChE J.* **1957**, 3, 187.

(23) NIST Standard Reference Database 46 Version 6.0. NIST Critically Selected Stability Constants of Metal Complexes.

7. Sorption of Solutes and Solvent in Ion Exchange Resins

This chapter is a rewriting of the article "*Experimental measurement and modeling of the distribution of solvent and ions between an aqueous phase and an ion exchange resin*" co-authored with Kaj Thomsen and accepted for publication in Fluid Phase Equilibria.

The distribution of solutes and solvent between an aqueous solution of salt and an ion exchange resin has been measured at ambient temperature. The experiments have been performed for aqueous solutions of KNO_3, KCl, $Ca(NO_3)_2$ and $CaCl_2$ in the concentration range of 0-3N. The absorption has been measured for 3 gel type and 3 macroreticular resins with a degree of crosslinking varying from 10.5 to 18.5%. The experimental results have been modeled with the Extended UNIQUAC model combined with an elastic term taking the elastic properties of the resin structure into account. The model shows very good predictions with varying degree of crosslinking, and the deviations between model results and experimental data are all within the experimental error.

7.1. Introduction

Ion exchange resins have been used commercially since the 19. century and are at present time used extensively in industry for separation and purification processes. In most cases ion exchange processes are used for recovery of ions from relatively dilute solutions. However, in some industrial ion exchange processes, e.g. in the production of fertilizer salts, high concentration solutions are involved. Apart from this, regeneration of ion exchange resins often also involve highly concentrated electrolyte solutions. When simulating e.g. wash-out curves, information about the amount of electrolyte inside the resin particle is very important. A small example of this is given in figure 7.1. The figure shows two wash-out curves for a column filled with glass beads and with a macroreticular ion exchange resin. The size distribution of the two different types of particles is the same. It is seen that the wash out curve for the resin has a longer tail due to the absorption of KCl in the resin particle and that more bed volumes of pure water therefore is needed to clean the column. To simulate this behavior, a model for the absorption of KCl in the resin particle would be very convenient.

Most thermodynamic studies of ion exchange processes have been carried out in dilute solutions, in which ion exchange is virtually equivalent; hence no absorption of co-ions are observed. In the majority of the studies of ion exchange in more concentrated solutions, the

sorption of co-ions and the changes in the solvent uptake are most often ignored. However the somewhat limited studies of ion exchange in concentrated electrolyte solutions, where both the uptake of co-ions and solvent are considered, show that these phenomena are very important when dealing with concentrated solutions.

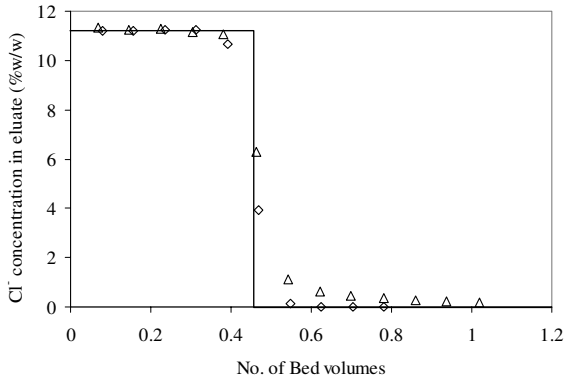

Figure 7.1. Washout curve in a 5cm^2 x 50cm column. Column loaded with 11.5% (w/w) KCl solution and washed with UP water at 3mL/min.
(–) theoretical plug flow curve. Column filled with (◇) glass beads, (△) Amberlyst 40CW.

The main purpose of this chapter is to describe the complete distribution of ions and solvent between the aqueous bulk phase and the ion exchange resin phase. The study includes the effect of different counter- and co-ions in varying concentrations (0.5 – 3 in molality) on the equilibria. Furthermore, the effect of the type of exchanger (gel vs. macroreticular) and the effect of the divinylbenzene (DVB) level (which is a measure of the degree of crosslinking) on the equilibria has been investigated.

7.2. Experimental Section

The measurement of the uptake of electrolytes by ion exchange resins is not a new study object. Most of the measurements made in the past have been carried out as batch experiments where resin and electrolyte are mixed in a bottle followed by a separation of the two phases. This method allows the measuring of the change of water and salt content in the resin phase

by a subsequent elution of salt and drying of the resin phase. However, as pointed out by e.g. Freeman et al.[1], it is very difficult to separate the two phases. Depending on the type of separation, either a portion of the external phase tends to stick to the surface of the resin or the separation has a tendency to drain the resin for a part of the internal aqueous solution.

The mentioned inaccuracies accompanying the separation of the phases have been pointed out by several authors and different methods for measuring the equilibrium without phase separation have been proposed. Pepper et al.[2] proposed a dye solution method; a solution of molecules too large to penetrate the resin is added to the mixture of the resin as well as a small amount of aqueous phase. The change of dye concentration gives a measure of the change in water content in the bulk phase and thereby the quantity of water in the resin phase. The method seems very simple; however, a very high fraction of resin to aqueous phase is needed in order to obtain a measurable change of concentration in the bulk phase. The result is a very large surface area of resin in the aqueous phase. Some dye would probably stick to the surface leading to inaccurate results. This phenomenon can be the reason why several researchers have been unable to obtain satisfactory results using this method (e.g. Scatchard and Anderson[3]).

Another method in addition to the batch experiments is to measure the volume change of the ion exchange particles in different electrolyte solutions. Assuming that the total volume of resin and bulk phase is constant, the change in volume of the resin phase could be used in calculating the complete distribution of solvent and electrolyte between the two phases (e.g. Freeman et al.[1], Freeman and Scatchard[4]). This method is relatively easy to perform and the errors related to the method are acceptable.

In this work it has been chosen to use a batch experiment method combined with a measurement of the volume change of the resin particles. The procedure used is very similar to the method of Freeman and Scatchard[4]. However, in this chapter the volume of resin and bulk phase is not assumed constant, but calculated using a simple model.

7.2.1 Preparation of Experimental Equipment

Preparation of glassware, electrolyte solutions and resin conditioning was performed as explained previously in chapter 6.

7.2.2 Measurement of the Physical/Chemical Properties of the Resin

Equilibrium water content and resin capacity were measured according to the procedures given in details in chapter 6.

7.2.2.1 Measurement of the Density and Apparent Molal Volume of the Resin

A sample of the resin was treated in the same way as for the equilibrium water content measurement. 5.00 ± 0.01g of resin was transferred to a 25mL pycnometric flask. The pycnometer was filled with UP water and the weight of water, pycnometer and resin was recorded. The pycnometer was emptied, refilled with UP water and the weight of pycnometer and water recorded. From the law of Archimedes we know that the apparent loss in weight of a body immersed in a fluid is equal to the weight of the displaced fluid:

$$w_{w,displaced} = w_R^{wet} - \left(w_{pyc+R+w} - w_{pyc+w}\right)$$

The volume of the displaced fluid can be calculated by the relation:

$$V_{w,displaced} = \frac{w_{w,displaced}}{\rho_w(T)}$$

The true wet density of the resin can then be calculated using the equation:

$$\rho_R^{wet} = \frac{w_R^{wet}}{w_{w,displaced} / \rho_w(T)} = \frac{\rho_w(T) \cdot w_R^{wet}}{w_R^{wet} - \left(w_{pyc+R+w} - w_{pyc+w}\right)} \qquad [7.1]$$

7.2.3 Measurement of Electrolyte Uptake of Ion Exchange Resins

In this work we assume that the volume of the bulk and the resin phase can be calculated by the general equation which can be applied to electrolyte solutions[5]:

$$V = V_w + \sum_i m_i \phi_{V,i} \qquad [7.2]$$

where V_w is the volume of 1kg of pure water, m_i is the molality of ion *i* and $\Phi_{V,i}$ is the apparent molal volume of ion *i* in the resin phase.

Even though the pressure inside the resin particle could be up to 1000 times the atmospheric pressure, this change in pressure would only mean a slight change in the molal volume of water and the different inorganic ions that we consider.

It is difficult to measure the volume or density of a resin particle as a function of concentration as is commonly done for inorganic ions. However, one way of proving that eq. [7.2] can be applied to an equilibrated resin particle is by considering the resin in its different forms. Gregor et al.[6] measured the volume and density of a Dowex 50 (~11%DVB) resin in its various states at 25°C when in equilibrium with pure water. From these results, the volumes of the polystyrene resin in its various forms can be calculated. If the volume of the cation in the resin phase is subtracted, this would give the apparent molal volume of the sulphonated polystyrene matrix. In the calculations, the density of pure water is assumed to be 997 kg/m^3 and the volumes of the ions are calculated by the parameters from Christensen and Thomsen[5]. The results are given in table 7.1 and show that the volume of the matrix is calculated to 130.4 cm^3/mol $\pm$ 0.7% .

Table 7.1. Apparent molal volumes calculated from experimental data of Gregor et al.[6] measured for a DOWEX 50 resin.

Cation (X)	m_{XPSS} (eqv./kg)	$\phi_{V,XPSS}$ (cm^3/eqv.)	ϕ_{V,PSS^-} (cm^3/eqv.)
H^+	5.6	131.0	131.0
Na^+	6.4	132.9	131.4
K^+	7.4	141.6	129.4
NH_4^+	7.3	150.0	130.2
Ca^{++}	6.4	124.0	130.3

Taking the experimental inaccuracies of the method used for the determination of the volumes into account, it is reasonable to conclude that the volume of the polystyrene matrix can be considered constant within a minor change in concentration.

This procedure has been repeated for the Amberjet 1200 and 1500 resins used in this study. The densities, capacities and water contents in equilibrium with pure water have been measured for the resins in their various forms and the apparent molal volumes of the polymeric segment have been calculated. The results are shown in tables 7.2 and 7.3 and

show that the variations in the apparent molal volumes of the resin lies within the experimental accuracy.

Table 7.2. Apparent molal volumes of Amberjet 1200.

Cation (X)	m_{XPSS} (eqv./kg)	$\phi_{V,XPSS}$ (cm^3/eqv.)	ϕ_{V,PSS^-} (cm^3/eqv.)
H^+	5.03	124.71	125.0
K^+	6.91	137.02	124.9
Na^+	5.92	126.28	124.9
Ca^{++}	5.93	119.03	125.0
NH_4^+	6.40	144.67	125.0

Table 7.3. Apparent molal volumes of Amberjet 1500.

Cation (X)	m_{XPSS} (eqv./kg)	$\phi_{V,XPSS}$ (cm^3/eqv.)	ϕ_{V,PSS^-} (cm^3/eqv.)
H^+	5.94	124.81	125.3
K^+	8.22	138.09	125.8
Na^+	7.13	127.40	125.7
Ca^{++}	7.90	119.27	125.3
NH_4^+	7.68	145.07	125.3

7.2.3.1 Batch Experiments

The resin was brought on the desired form, K^+ for the KCl and KNO_3 sorption and Ca^{++} for the $CaCl_2$ and $CaNO_3$ sorption experiments. A sample of the resin was treated in the same way as for the equilibrium water content measurement. Approximately 30g of resin in wet form was transferred to 100 mL closed pyrex bottles where it was mixed with 50mL of the electrolyte solution. The solutions were equilibrated under continuous shaking. Stirring would generate too high mechanical stress which could cause a rupture of the resin, therefore shaking was preferred. The concentration of salt was measured in the bulk phase after equilibration for 1, 3, 6, 12, 24, and 48 hours to identify the time required for obtaining equilibrium. For the chloride salts the amount of chloride was analyzed by potentiometric titration with 0.1N $AgNO_3$ (more information in appendix I) and for the nitrate salts the amount of NO_3^- in the bulk solution was found by UV spectrophotometry at 220nm (procedure given in appendix J). The results showed that there was no measurable difference

between 3h and 48h. 6 hour periods were therefore used for providing an ample time to reach equilibrium.

7.2.3.2 Volumetric Experiments

In the volumetric experiments, it is chosen to measure the volume change using a column method. With this method it is easier to measure small changes in volume than in the optical/microscopic methods used by other authors. In addition, the method is not very sensitive to the shape of the resin particle in comparison to optical methods that often demands very spherical particles. Furthermore, the volumetric method includes a large amount of resin in the experiment and is therefore not very sensitive to variations within a batch.

Approximately 25mL of wet resin was loaded into a 25mL column with markings for each 0.05mL. For each concentration of salt in the bulk solution the following procedure was carried out:

1. The resin was thoroughly backwashed with the solution of interest.
2. Subsequently, the solution was passed through the column at a flowrate of 5mL/min and mechanical tapping was applied until a steady level was obtained.
3. The experiment was repeated at a minimum of 4 times and the average was calculated.

All data were reported as volume change of the resin particle as function of the molality of the salt in the bulk solution. From the data it is observed that a polynomial expression can be used for describing the shrinking of the particle as a function of the molality of salt in the bulk solution:

$$V_{\text{resin}} = kV_0, \quad k = k_1 + k_2 m_{S,B} + k_3 m_{S,B}^2 \qquad [7.3]$$

Where V_0 is the volume of the resin particle in equilibrium with pure water and the k-parameters are determined from experimental data for each salt and type of resin particle.

7.3 Modeling

In the work presented here the ion exchange resin is considered as a homogeneous phase consisting of water, ions and charged polymeric segments. The presence of "inert" cross-links is assumed to change neither the chemical properties nor the nature of the functional groups[7]. The different degree of crosslinking is therefore only taken into account in the elastic term in the equilibrium conditions.

7.3.1 Equilibrium Conditions

The equilibrium conditions for the distribution of both ionic and non-ionic species between a solution phase and a phase consisting of a three-dimensional crosslinked elastic polymer have recently been derived very elegantly by Maurer and Prausnitz[8] and will shortly be presented in the following section:

The swollen resin is treated as a homogenous phase, and at equilibrium the chemical potentials of the absorbed components in the resin phase and the liquid phase are equal:

$$\sum_{i=1}^{N_{comp}} \left(\mu_i'(T, p', \underline{n}') - \mu_i''(T, p'', \underline{n}'')\right) dn_i' = 0 \qquad \Rightarrow \qquad [7.4]$$

$$\mu_i'\left(T, p', n'\right) = \mu_i''\left(T, p'', n''\right) = \mu_i''\left(T, p', n''\right) + \int_{p'}^{p''} \overline{v}_i dp \qquad [7.5]$$

Where ' refers to the bulk phase and '' refers to the resin phase.

Assuming that the pressure range of the integration is so small that partial molal volumes are independent of pressure, the following applies:

$$\mu_i'\left(T, p', n'\right) = \mu_i''\left(T, p', n''\right) + \overline{v}_i \pi \qquad [7.6]$$

Where π is the pressure difference between the two phases. The pressure difference between the two phases is caused by the elastic properties of the resin matrix; hence it can also be written in terms of the Helmholtz energy, A, of the resin membrane:

$$\pi = \left(\frac{\partial A^R}{\partial V^{''}}\right)_T \qquad [7.7]$$

If the system temperature and bulk phase pressure are chosen as the reference state for the chemical potential of the components, the phase equilibrium condition for all non-ionic components is given as:

$$ln\, a_i'(T,p',\underline{n}') = ln\, a_i''(T,p',\underline{n}'') + \frac{\overline{V}_i''}{RT}\left(\frac{\partial A^R}{\partial V''}\right)_T, i = 1,.....,N \qquad [7.8]$$

Equation [7.8] is very similar to the equilibrium condition for an osmotic equilibrium.

Due to the electro neutrality criterion, the number of phase equilibrium conditions are reduced with one when the solution contains ionic components. The electro neutrality criterion can be written as:

$$\sum_{i=1}^{N_{ions}} n_i' z_i = 0 \qquad [7.9]$$

Introducing a reference ionic species, *r,* eq. [7.9] can be written in the form:

$$n_r' = \sum_{\substack{i=1 \\ i\neq r}}^{N_{ions}} \frac{z_i}{z_r} n_i' \qquad [7.10]$$

Implementing eq. [7.10] in eq. [7.4-7.8] the equilibrium condition for an arbitrary selected ionic species, *i*, can be given as:

$$\begin{aligned} ln\, a_i'(T,p',\underline{n}') &= ln\, a_i''(T,p',\underline{n}'') + \frac{\overline{V}_i''}{RT}\left(\frac{\partial A^R}{\partial V''}\right)_T \\ &+ \left(\frac{z_i}{z_r}\right)\left(ln\, a_r'(T,p',\underline{n}') - ln\, a_r''(T,p',\underline{n}'') - \frac{\overline{V}_r''}{RT}\left(\frac{\partial A^R}{\partial V''}\right)_T \right), i = 1,...,N_{ions} \quad i \neq r \end{aligned} \qquad [7.11]$$

while all equilibrium conditions for non-ionic species is given by eq. [7.8]

7.3.2 Activity Coefficient Model

In this work the excess Gibbs energy of the aqueous phase is described using the Extended UNIQUAC model. As explained in chapter 4, the Extended UNIQUAC model is an extension of the original UNIQUAC model of Abrams and Prausnitz[9] and was first presented in the form used in this thesis by Thomsen[10]. The model has previously been applied to describe the

excess Gibbs energy of aqueous electrolytes solutions containing (K^+, Na^+, H^+, NH_4^+, Cl^-, NO_3^-, HSO_4^- ,SO_4^{--}, OH^-, CO_3^{--}, HCO_3^-, NH_2COO^-, $H_2PO_4^-$, HPO_4^{--} HSO_3^- , SO_3^{--}, $S_2O_5^{--}$)[10-13, 26].

7.3.3 The Free Energy of Elasticity

Several different authors have proposed terms for the free energy of elasticity. Some of the most well-known expressions were developed by Flory[14] and James and Guth[15]. The drawback of the two models in relation to the polymer structure of the resins used in this thesis, is however that they are based on a Gaussian assumption. This assumption is only reasonable if the chains between the crosslinks are reasonably long (>100 monomers)[16]. This is most often the case for rubbers. However in polymeric resins where the degree of crosslinking is high, the Gaussian approximation most probably will fail. In this work, the expression of Gusler and Cohen[17] has therefore been chosen to describe the free energy of elasticity. The model of Gusler and Cohen[17] is only valid for isotropic swelling and could be considered as an extension of the Flory elasticity model to non-Gaussian networks:

$$\left(\frac{\partial A^R}{\partial V^{"}}\right)_T = K_{el}\left(1-\frac{2M_c}{M}\right)\left(\frac{5}{3}\phi_R^{1/3}-\frac{7}{6}\phi_R\right) \qquad [7.12]$$

where ϕ_R is the volume fraction of the resin-polymer in the swollen network and M_c is the molecular weight of the chains between crosslinks. The term $\left(1-\frac{2M_c}{M}\right)$ takes into account the dangling chains; this means the deviation of the real network from the perfect network. In the present treatment it is assumed that $\left(\frac{2M_c}{M}\right) \ll 1$ due to the high molecular weight of the resins and only moderate degree of crosslinking[16]. Therefore eq. [7.12] can be reduced to:

$$\left(\frac{\partial A^R}{\partial V^{"}}\right)_T = K_{el}\left(\frac{5}{3}\phi_R^{1/3}-\frac{7}{6}\phi_R\right) \qquad [7.13]$$

7.3.4 Densities and Volumes of Ionic Species

Partial molal and apparent molal volumes of electrolytes can be found from density measurements or directly from measurements of apparent volumes.

If the apparent molal volumes of the ions are assumed to be additive, the volume of an aqueous solution of ions can be calculated using eq. [7.2].

It can be shown[5] that the apparent molal volume of an ion *i* can be described by the relation:

$$\phi_{V,i} = \bar{v}_i^{\nabla} + k_i\sqrt{I_m} \qquad [7.14]$$

I_m is the ionic strength given by:

$$I_m = \tfrac{1}{2}\sum_i m_i z_i^2 \qquad [7.15]$$

As shown in chapter 3, the model parameters, k_i, have been regressed for aqueous solutions of (H^+, Na^+, K^+, NH_4^+, Ca^+) (Cl^-,NO_3^-,SO_4^{--}) on the basis of more than 1800 data points of both density and apparent molal volumes.

7.4 Results and Discussion

7.4.1 Physical/chemical Properties of the Resins

All basic properties of the different resins were measured according to the methods described in section 7.2. From the experimental data, the different properties were calculated using eq. [6.1-6.2, 7.1] and are listed in table 7.4. The value of the data, e.g. water capacity, is very similar to values reported from other authors[3, 4, 6]. Pictures of the 6 different resins have been captured using a digital camera and are shown in appendix K.

Table 7.4. Physical/chemical properties of resins.

	Gel type			Macroreticular type		
	Amberjet 1200	Amberjet 1500	Amberjet 1600	Amberlyst 36W	Amberlyst 40CW	Amberlyst 35W
% DVB	10.5	12	16	12	16.5	18.5
Capacity (H-form)(eq/kg dry)	5.18	5.19	5.04	5.76	5.34	5.62
Water content (H-form) (%)	50.8	46.6	38.5	54.8	48.3	54.1
Density, wet (H-form) (g/cm^3)	1209.5	1231.1	1278.0	1239.9	1257.0	1248.3

7.4.2 Batch Experiment Results

From the batch experiments a relation between the amount of water and salt in the resin phase could be found. The amount of water $n^i_{w,R}$ in the resin transferred to the pyrex bottle can be found from the weight of the wet resin and the fraction of water in the resin. The amount of water initially in the bulk solution, $n^i_{w,B}$, and the amount of salt initially in the bulk solution, $n^i_{S,B}$, can be calculated from the concentration and the mass of the bulk solution.

We consider an absorption in the system (no reactions). Using the mole balance for the resin-bulk phase system at equilibrium the following relation can therefore be found:

$$n^{eq}_{w,R} + n^{eq}_{w,B} - n^i_{w,R} - n^i_{w,B} = 0$$

$$\begin{aligned} &n^{eq}_{S,R} + n^{eq}_{S,B} - n^i_{S,B} = 0 \quad \Leftrightarrow \\ &n^{eq}_{S,R} + m^{eq}_{S,B} \cdot \left(n^{eq}_{w,B} \cdot M_w\right) - n^i_{S,B} = 0 \quad \Leftrightarrow \\ &n^{eq}_{S,R} + \left(n^i_{w,R} + n^i_{w,B} - n^{eq}_{w,R}\right) \cdot M_w m^{eq}_{S,B} - n^i_{S,B} = 0 \end{aligned}$$

Using the above equation an expression can be found for the amount of moles of water , $\tilde{n}^{eq}_{w,R}$, and salt, $\tilde{n}^{eq}_{S,R}$, per equivalent of resin in the resin phase at equilibrium.

$$\tilde{n}^{eq}_{S,R} = \frac{n^{eq}_{S,R}}{w^w_R \cdot (1-q_w) \cdot q} = \frac{n^i_{S,B} - \left(n^i_{w,R} + n^i_{w,B}\right) M_w m^{eq}_{S,B}}{w^w_R (1-q_w) q} + \tilde{n}^{eq}_{w,R} M_w m^{eq}_{S,B} \quad \Leftrightarrow \qquad [7.15]$$

$$\tilde{n}^{eq}_{S,R} = A_1(m^{eq}_{S,B}) + A_2(m^{eq}_{S,B}) \cdot \tilde{n}^{eq}_{w,R} \qquad [7.16]$$

The results from the batch experiments could be correlated using polynomial expressions and expressions for the A_1 and A_2 parameters found as a function of salt concentration in the bulk phase. An example of this is shown in figure 7.2 where the result of the experimental data of sorption of KCl on Amberjet 1200 are shown. The reproducibility of the data for determining the A-parameters showed that the experimental error was approximately 5%. The error originates mainly from the chemical analysis methods and due to evaporations from resin and bulk phase during sampling.

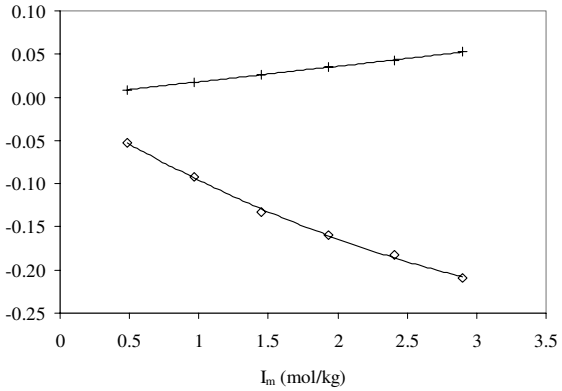

Figure 7.2. Experimental data for parameters A_1 (◇) and A_2 (+) for the sorption of KCl on Amberjet 1200. (–) polynomial fit.

7.4.3 Volumetric Results

The volume of a resin particle in equilibrium with pure water could be calculated from wet density data from pycnometric experiments using eq. [7.1]. The volume of the particle in equilibrium with a given bulk solution could be found from the volumetric experiments using the known volume of the resin in equilibrium with pure water and eq. [7.3]. An example of the volumetric experiments is shown in figure 7.3 where the shrinking of an Amberjet 1200 resin in equilibrium with $CaCl_2$ and $Ca(NO_3)_2$ solutions is shown. Error bars from the 4 successive experiments have been placed on the figure and it is seen that the volume change data could be reproduced within 0.15% accuracy.

7.4.4 Sorption of Water and Salt in the Resin Phase

The total sorption of water and salt could be calculated from the batch and volumetric experiments. The relation between number of moles of salt and moles of water in the resin particle is given by eq. [7.16]. The total volume of the particle could be found as a function of the water and salt content using eq. [7.2]. The apparent molal volumes of salt and water are found using known expressions[5] while the apparent molal volume of the resin is considered constant and is found from density experiments. By iteratively solving the two equations the

amount of salt and water in the resin is found at equilibrium. The results are shown in tables 7.5 and 7.6 (in the end of the chapter). The overall reproducibility of the data points was shown to be app. 8% which is in agreement with the error assessment from previous studies[7].

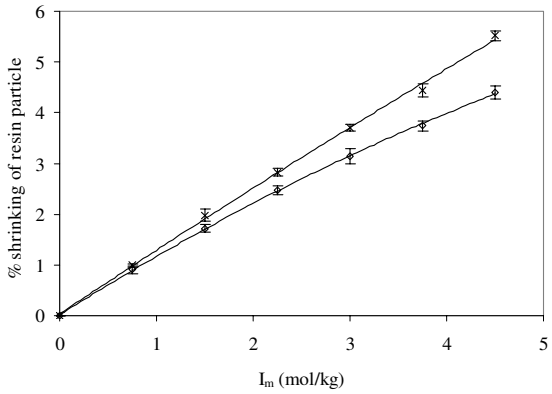

Figure 7.3. Volume change of a resin particle in contact with solutions of $CaCl_2$ (◇) and $Ca(NO_3)_2$ (×). (–) Polynomial fit.

The absorption of a strong electrolyte is mainly dependent on the Donnan potential. It has previously been shown[18-20] that the Donnan potential increases with decreasing external and increasing internal counter-ion concentration and so does the efficiency of the electrolyte exclusion. Table 7.7 shows the chloride concentration in the 3 different gel type resins when in contact with a 3N KCl solution. These results and the results in table 7.5 and 7.6 show as expected that the absorption of salt is most dominant in the resins with lowest cross-link density due to a higher degree of swelling and thereby sorption of water. However, compared with the Amberjet 1500 resin the drop in chloride concentration in the Amberjet 1600 resin is lower than expected when considering the increase in crosslinking. The reason for this is the lower capacity and thereby a proportional lower counter-ion concentration in the Amberjet 1600 resin.

Table 7.7. Chloride concentration in 3 gel type resins when in equilibrium with a 3N KCl solution.

Resin	$m_{Cl,R}$ (mol/kg)
Amberjet 1200	1.58
Amberjet 1500	1.48
Amberjet 1600	1.39

In addition to this, the results show that the calcium salts are more efficiently excluded than the potassium salts. This is not quite in agreement with the Donnan potential effect. The force with which an electric field acts on an ion is proportional to the ionic charge. This means that the Donnan potential required to balance the tendency of the counter-ions to diffuse into the surrounding solution is smaller when the valence of the counter-ions is higher. Because of the smaller Donnan potential the electrolyte exclusion is less efficient. However, the trend is in agreement with the experimental results of Gordievskii et al.[21] and Kokotov[22]. They have measured electrolyte sorption in different ion exchange membranes and resins. The higher exclusion of the calcium salts can most probably be explained due to the large size of the calcium ions which are highly solvated. For a comparison the Stokes radius is 4.7Å for K^+ and 10.4Å for Ca^{++} [23].

The chloride salts are for all resins more excluded than the nitrate salts. This behavior is also seen in the data of Ferapontov et al.[7] who measured electrolyte sorption in an anion exchanger. The phenomenon could once again be explained with the size of the ions. The Stoke radius of NO_3^- (3.3Å) is smaller than the one of Cl^- (3.9Å) and is therefore more easily absorbed.

The absorption of salt in the macroreticular resins is as expected somewhat higher than in the case of the gel type resins. This is due to the large pore structure in this type of resins.

7.4.5 Estimation of Elastic Parameter, K_{el}

The elastic coefficient could be estimated simultaneously with the activity coefficient model parameters from the experimental absorption curves. However, in order to reduce the amount of parameters it has in this work been chosen to approximate the elastic coefficient from water-vapor sorption isotherms. Boyd and Soldano[24] have measured water-vapor sorption isotherms of styrene cation exchangers on H^+ form with various crosslinking. From the water-

vapor sorption curves the osmotic pressure has been calculated for sulphonated polystyrene ion exchanger on H form in equilibrium with pure water. The results are shown in figure 7.4.

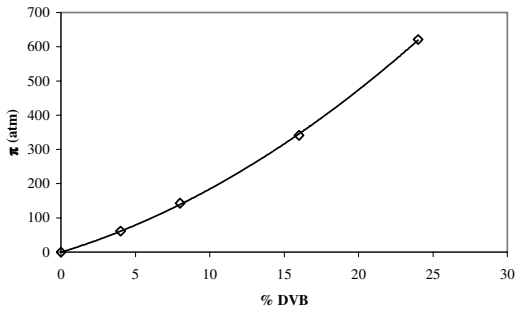

Figure 7.4. Osmotic pressure of sulphonated polystyrene ion exchanger on H-form in equilibrium with pure water. (◇) Calculated from experimental data of Boyd and Soldano[24].

Knowing the water content and osmotic pressure of the different resins on H-form used in this study, the elastic coefficient of the different resins could be calculated using eq. [7.13] with the given UNIQUAC volume parameters. The results for the different resins are shown in table 7.8.

Table 7.8. Elastic parameters

% DVB	10.5	12	16	16.5	18.5
K_{el} (atm.)	276.6	337.7	519.4	544.5	651.6

7.4.6 Regression of Model Parameters

All size, surface and interaction energy parameters for water and ionic species have been taken from previous works[10-13]. Size and surface parameters of the polymeric segment have been calculated from the r and q parameters of styrene[25] and SO_3^- [26]. The binary interaction parameters for the interaction between the polymeric segment and water, K^+, Ca^{++} have been estimated. The interaction parameters with the other anionic species have been set to 2500 in order to reduce the amount of parameters. All UNIQUAC parameters are shown in table 7.9 – 7.10.

Table 7.9:Volume and surface parameters

	r	q
H_2O	0.92	1.40
K^+	2.23	2.43
Ca^{++}	3.87	1.48
Cl^-	10.39	10.20
NO_3^-	5.40	6.21
PSS^-	14.97	13.05

Table 7.10: Parameters $u_{ij}^{(0)} = u_{ji}^{(0)}$

	H_2O	K^+	Ca^{++}	Cl^-	NO_3^-	PSS^-
H_2O	0	-	-	-	-	-
K+	535.0	0	-	-	-	-
Ca++	496.4	-275.6	0	-	-	-
Cl-	1523.4	1465.2	1805.6	2214.8	-	-
NO3-	998.9	818.6	943.3	2175.0	2753.7	-
PSS-	2302.5[2)]	2285.3[2)]	5465.8[2)]	2500[1)]	2500[1)]	2661.0[2)]

1) Parameter has been assigned to this value in order to reduce the number of adjustable parameters

2) Parameters have been estimated from absorption isotherms of Amberlyst 1200 resins

Only $u_{ij}^{(0)}$ are given due to the fact that only data at ambient temperature (24°C ±1) were treated in this work. The optimal object function used for regression of the energy parameters was found as:

$$OF = \sum\left(\frac{n_{w,R}^{Exp} - n_{w,R}^{Calc}}{n_{w,R}^{Exp}}\right)^2 + \sum\left(\frac{n_{i,R}^{Exp} - n_{i,R}^{Calc}}{n_{i,R}^{Exp}}\right)^2,\ i = K^+, Ca^{++} \qquad [7.17]$$

The average deviations of the salt absorption given in the following sections are calculated from:

$$AAD = \frac{\sum\left|\frac{n_{S,R}^{Exp} - n_{S,R}^{Calc}}{n_{S,R}^{Exp}}\right|}{N} \cdot 100\%, \qquad AAD = \frac{\sum\left|\frac{n_{w,R}^{Exp} - n_{w,R}^{Calc}}{n_{w,R}^{Exp}}\right|}{N} \cdot 100\% \qquad [7.18]$$

7.4.7 Gel type Resins

The interaction energy parameters of the Extended UNIQUAC model was estimated from the absorption isotherms of the gel type resin Amberjet 1200. The model results are shown in figure 7.5. The figure shows that there is a good agreement between the experimental data and the correlated results. However, there are some deviations in the case of KNO_3 absorption at high bulk phase concentration.

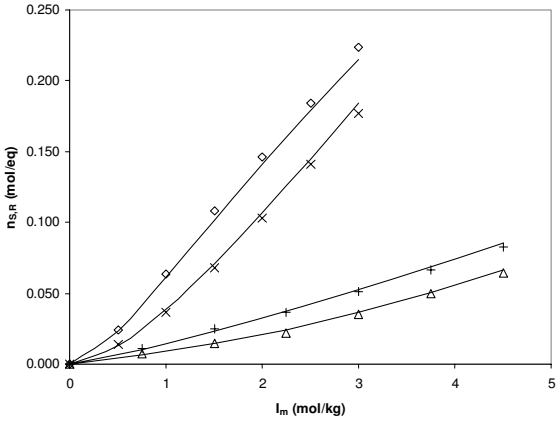

Figure 7.5. Experimental and modeling results of the salt absorption in the gel type resin Amberjet 1200. (–) Extended Uniquac model. (◇) Experimental results of the absorption of KNO_3, (×) KCl, (+) $Ca(NO_3)_2$, (△) $CaCl_2$

The salt absorption in the two gel type resins with higher degrees of cross-linking have been predicted using the energy parameters regressed from the absorption isotherms of the Amberjet 1200 resin and the elasticity parameters estimated from water-vapor sorption isotherms. The calculated results for all 3 resins are shown in table 7.5. The results are nearly all within the experimental error and the results show that the model is capable of correlating the different degrees of exclusion for the various salts.

The model predictions are compared with the experimental values for the absorption of KCl in the 3 different gel type resins in figure 7.6. The figure shows good agreement between the experimental data and the calculated results. This proves that even though some of the

physical properties, e.g. the capacity, of a sulphonated polystyrene resin varies, the elastic properties of different resins with same degree of cross-linking are with good approximation equal.

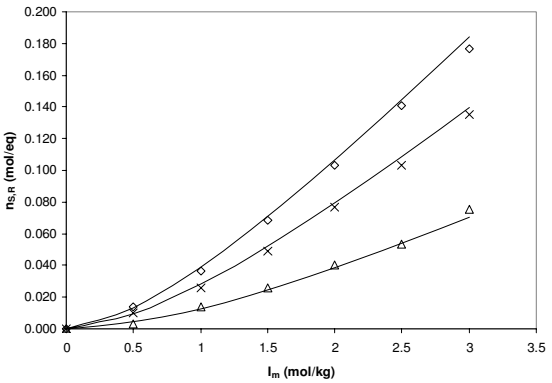

Figure 7.6. Experimental and modeling results of the KCl absorption in the gel type resins. (–) Extended UNIQUAC model. (◇) Amberjet 1200, (×) Amberjet 1500, (△) Amberjet 1600

7.4.8 Macroreticular Resins

Macroreticular resins are made of two continuous phases; a continuous pore phase and a continuous gel phase. A sketch of a macroreticular resin is shown in figure 7.7.

In this work it is assumed that the concentration of salt in the pore phase of the resin is equal to the concentration of salt in the bulk phase and that the gel phase of the resin behaves similarly as for a gel type resin with same degree of cross linking. The total amount of salt in the resin is then given as an addition of salt in the pore phase region and the bulk phase. The amount of salt in the pore phase is given by:

$$\tilde{n}^{eq}_{S,pore\ phase} = c_{S,B} \cdot \tilde{V}_{pore\ phase}$$

where $c_{S,B}$ is the concentration of salt in the bulk phase and $\tilde{V}_{porephase}$ is the volume of the pore phase per equivalent of resin (L/eq.).

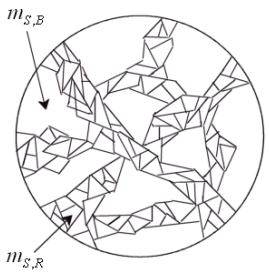

Figure 7.7. Sketch of a macroreticular resin. $m_{S,B}$ is the concentration of salt in the bulk phase and $m_{S,R}$ is the salt concentration in the gel phase.

The total salt absorption in the macroreticular resin particle can be calculated from the relation:

$$\tilde{n}^{eq}_{S,MR} = \tilde{n}^{eq}_{S,gel\ phase} + \tilde{n}^{eq}_{S,pore\ phase} = \tilde{n}^{eq}_{S,R} + c_{S,B} \cdot \tilde{V}_{pore\ phase} \qquad [7.19]$$

It is assumed that the pore volume is constant in the resin in spite of changes in equilibrium conditions and that changes in the total volume of the particle only is caused by changes in the volume of the gel phase. The volume of the pore phase has been estimated by comparison with the corresponding gel type resins. The water content of the gel type resins in equilibrium with pure water has been correlated with polynomial expressions as shown in figure 7.8.

From these expressions the water content in gel type resins with 12, 16.5 and 18.5 % DVB on H-form has been estimated. The volume of the porous phase used in the model has been found by subtracting the estimated numbers from the actual water contents of the macroreticular resins. The results are given in table 7.11. The results in the table show that the pore phase volume is constant in the 3 different forms. This holds even though the resin swells 15-25% when replacing K^+ ions with H^+. It can therefore be concluded that the assumption of a constant volume of the pore phase region is quite reasonable.

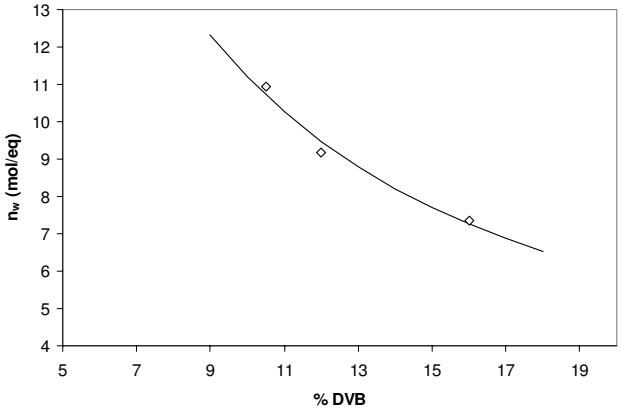

Figure 7.8. Amount of water in the resin when in equilibrium with pure water as a function of crosslinking and ionic form. (◇) Experimental results from Amberjet 1200, 1500 and 1600, (–) polynomial fit.

The total absorption in the macroreticular resins has been calculated using the model parameters estimated from the data of the gel type resins and then adding the contribution from the pore phase region corresponding to eq. [7.19]. All the results are shown in table 7.6 and it is seen that the average deviations are of the same magnitude as for the gel type resins.

Table 7.11. Pore volume of macroreticular resins

	Vpore (cm^3/eq)			
Ionic form	H-form	K-form	Ca-form	Avg.
36W	35.8	35.2	35.0	35.4
40CW	47.8	49.2	48.5	48.5
35W	92.8	92.3	91.0	92.0

The results for the 36W resin are compared with experimental values in figure 7.9. The trend of the results is similar to the one of the gel type resins; a very good prediction of the salt absorption of all 4 salts. However, a slight deviation of the absorption of KNO_3 at high bulk concentrations is noted. The results show that absorption of salt in macroreticular resins can be calculated using the assumption that the absorbed phase consists of a gel region and a

porous region. In addition, it is shown that the properties of a gel phase region in the macroreticular resins can be compared to the properties of a gel type resin with the same degree of cross-linking. This implies that relevant parameters could be regressed from data of gel type resins and then be applied for predictions of absorptions in macroreticular resins. This means that the amount of data material could be reduced drastically when screening different resins for the sorption properties.

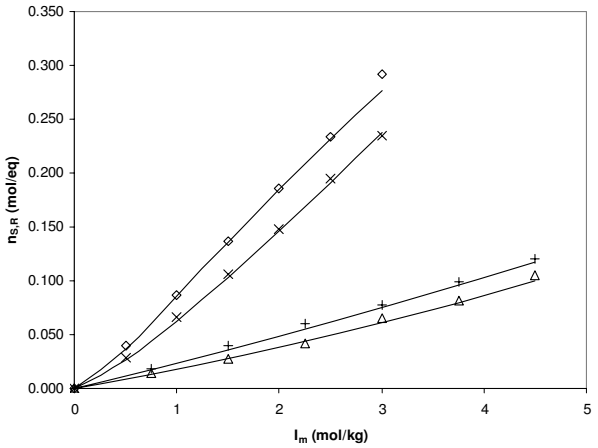

Figure 7.9. Experimental and modeling results of the salt absorption in the macroreticular resin Amberlyst 36W. Extended UNIQUAC model (–). Experimental results of the absorption of KNO_3 (◇), KCl (×), $Ca(NO_3)_2$ (+), $CaCl_2$ (△)

7.5 Conclusion

The absorption of water and salt at ambient temperature has been measured for 3 gel type and 3 macroreticular resins with varying degrees of crosslinking. The experiments were performed for aqueous solutions of KNO_3, KCl, $Ca(NO_3)_2$ and $CaCl_2$ in the concentration range of 0-3N. The absorption has been calculated on the basis of batch experiments combined with measurements of the volume change of the resin when in equilibrium with the electrolyte solutions. The experimental results have an experimental error of approximately 8% which is acceptable for this kind of studies.

The experimental data have been modeled with the Extended UNIQUAC model combined with an elastic term taking the elastic properties of the resin structure into account. The model shows very good predictions with varying degree of crosslinking, and the deviations between model results and experimental data are all within the experimental error.

Table 7.5. Results for gel type resins

Resin/salt	I_m (mol/kg)	$100\times n_{S,R}$, calc. (mol/eq.)	$100\times n_{S,R}$, exp. (mol/eq.)	% AAD	n_w, calc. (mol/eq.)	n_w, exp. (mol/eq.)	% AAD
Amberjet 1200							
KCl	0	0.00	0.00		8.50	8.28	
	0.5	1.34	1.38		7.85	7.69	
	1	3.90	3.66		7.39	7.34	
	1.5	7.08	6.83		7.00	7.04	
	2	10.65	10.30		6.66	6.78	
	2.5	14.47	14.10		6.35	6.30	
	3	18.42	17.40	4.198	6.06	6.12	1.331
KNO_3	0	0.00	0.00		8.50	8.28	
	0.5	2.34	2.41		7.86	7.75	
	1	6.16	6.35		7.43	7.50	
	1.5	10.18	10.80		7.09	7.10	
	2	14.11	14.60		6.80	6.89	
	2.5	17.89	18.80		6.54	6.65	
	3	21.50	22.70	4.185	6.31	6.42	1.393
$CaCl_2$	0	0.00	0.00		8.25	8.35	
	0.75	0.64	0.70		8.09	8.11	
	1.5	1.44	1.44		7.94	7.88	
	2.25	2.43	2.19		7.78	7.75	
	3	3.63	3.48		7.61	7.61	
	3.75	5.05	4.96		7.43	7.49	
	4.5	6.65	6.44	4.682	7.26	7.32	0.614
$Ca(NO_3)_2$	0	0.00	0.00		8.25	8.35	
	0.75	1.05	1.12		8.09	8.13	
	1.5	2.33	2.48		7.96	7.91	
	2.25	3.73	3.66		7.84	7.79	
	3	5.24	5.09		7.72	7.68	
	3.75	6.85	6.68		7.60	7.58	
	4.5	8.56	8.29	3.773	7.49	7.47	0.539

Amberjet 1500							
KCl	0	0.00	0.00		7.10	6.89	
	0.5	0.95	1.01		6.59	6.54	
	1	2.82	2.59		6.20	6.22	
	1.5	5.20	4.92		5.86	6.01	
	2	7.93	7.68		5.54	5.62	
	2.5	10.89	10.30		5.26	5.37	
	3	13.99	13.50	5.443	4.99	5.04	1.600
KNO_3	0	0.00	0.00		7.10	6.89	
	0.5	1.94	2.27		6.60	6.57	
	1	5.14	5.04		6.24	6.34	
	1.5	8.52	8.86		5.95	6.08	
	2	11.85	11.53		5.69	5.81	
	2.5	15.07	14.20		5.46	5.58	
	3	18.15	17.50	5.479	5.25	5.34	1.842
$CaCl_2$	0	0.00	0.00		7.46	7.34	
	0.75	0.45	0.52		7.31	7.21	
	1.5	1.01	1.12		7.16	7.11	
	2.25	1.73	1.67		7.00	6.94	
	3	2.62	2.71		6.82	6.78	
	3.75	3.68	3.91		6.64	6.58	
	4.5	4.91	4.97	6.233	6.46	6.42	0.962
$Ca(NO_3)_2$	0	0.00	0.00		7.46	7.34	
	0.75	0.82	0.85		7.31	7.23	
	1.5	1.82	1.76		7.19	7.12	
	2.25	2.93	2.71		7.07	7.01	
	3	4.13	4.05		6.96	6.87	
	3.75	5.42	5.21		6.84	6.79	
	4.5	6.80	6.46	4.353	6.72	6.67	1.053
Amberjet 1600							
KCl	0	0.00	0.00		4.52	4.61	
	0.5	0.42	0.35		4.21	4.35	
	1	1.29	1.40		3.93	4.03	

	1.5	2.45	2.61		3.67	3.82	
	2	3.84	4.05		3.42	3.57	
	2.5	5.40	5.32		3.18	3.22	
	3	7.07	7.52	7.784	2.94	3.01	2.744
KNO_3	0	0.00	0.00		4.52	4.61	
	0.5	1.32	1.18		4.21	4.13	
	1	3.55	3.25		3.95	4.06	
	1.5	5.95	5.74		3.73	3.87	
	2	8.35	8.15		3.53	3.65	
	2.5	10.70	9.54		3.34	3.49	
	3	12.99	12.20	7.370	3.16	3.30	2.536
$CaCl_2$	0	0.00	0.00		5.85	5.68	
	0.75	0.18	0.21		5.73	5.56	
	1.5	0.42	0.46		5.61	5.48	
	2.25	0.74	0.78		5.47	5.37	
	3	1.15	1.21		5.32	5.24	
	3.75	1.67	1.84		5.15	5.09	
	4.5	2.29	2.41	7.906	4.99	5.05	2.036
$Ca(NO_3)_2$	0	0.00	0.00		5.85	5.68	
	0.75	0.44	0.48		5.74	5.64	
	1.5	0.99	1.04		5.64	5.55	
	2.25	1.60	1.76		5.54	5.47	
	3	2.29	2.42		5.44	5.31	
	3.75	3.04	3.08		5.34	5.24	
	4.5	3.86	3.65	5.715	5.23	5.16	1.896

Table 7.6. Results for macroreticular type resins

Resin/salt	I_m (mol/kg)	$100\times n_{S,R}$, calc. (mol/eq.)	$100\times n_{S,R}$, exp. (mol/eq.)	% AAD	n_w, calc. (mol/eq.)	n_w, exp. (mol/eq.)	% AAD
Amberlyst 36W							
KCl	0	0.00	0.00		9.06	9.05	
	0.5	2.69	2.81		8.52	8.61	
	1	6.26	6.63		8.10	8.20	
	1.5	10.29	10.60		7.73	8.00	
	2	14.62	14.80		7.40	7.64	
	2.5	19.13	19.50		7.08	7.11	
	3	23.73	23.30	2.97	6.78	6.89	1.52
KNO_3	0	0.00	0.00		9.06	9.05	
	0.5	3.68	3.98		8.52	8.66	
	1	8.55	8.70		8.12	8.31	
	1.5	13.55	13.70		7.79	7.89	
	2	18.43	18.60		7.50	7.60	
	2.5	23.12	23.40		7.24	7.40	
	3	27.62	29.20	2.97	7.00	7.08	1.39
$CaCl_2$	0	0.00	0.00		9.42	9.40	
	0.75	1.33	1.42		9.26	9.10	
	1.5	2.77	2.71		9.10	9.01	
	2.25	4.34	4.21		8.92	8.77	
	3	6.08	6.57		8.74	8.70	
	3.75	7.99	8.21		8.55	8.63	
	4.5	10.04	10.50	4.36	8.36	8.57	1.21
$Ca(NO_3)_2$	0	0.00	0.00		9.42	9.40	
	0.75	1.70	1.79		9.25	9.08	
	1.5	3.56	3.95		9.11	8.87	
	2.25	5.50	6.03		8.97	8.82	
	3	7.52	7.75		8.83	8.77	
	3.75	9.61	9.86		8.69	8.72	
	4.5	11.77	12.00	5.22	8.55	8.68	1.26

Amberlyst 40W							
KCl	0	0.00	0.00		7.00	7.09	
	0.5	2.82	2.99		6.67	6.88	
	1	5.99	5.63		6.36	6.48	
	1.5	9.36	10.06		6.07	6.02	
	2	12.87	13.10		5.79	5.90	
	2.5	16.48	16.00		5.51	5.60	
	3	20.11	19.60	4.39	5.24	5.38	1.89
KNO_3	0	0.00	0.00		7.00	7.09	
	0.5	3.71	4.11		6.65	6.74	
	1	8.21	8.00		6.35	6.46	
	1.5	12.80	13.00		6.08	6.11	
	2	17.30	18.00		5.83	6.04	
	2.5	21.68	22.70		5.59	5.70	
	3	25.93	26.40	4.01	5.36	5.46	1.72
$CaCl_2$	0	0.00	0.00		8.42	8.16	
	0.75	1.39	1.26		8.29	8.08	
	1.5	2.82	2.66		8.16	7.92	
	2.25	4.31	4.22		8.01	7.86	
	3	5.88	5.93		7.84	7.77	
	3.75	7.52	7.81		7.67	7.41	
	4.5	9.25	9.67	4.70	7.48	7.34	2.45
$Ca(NO_3)_2$	0	0.00	0.00		8.42	8.16	
	0.75	1.63	1.72		8.28	8.01	
	1.5	3.35	3.43		8.16	7.95	
	2.25	5.10	5.15		8.03	7.84	
	3	6.89	6.89		7.90	7.74	
	3.75	8.71	8.66		7.77	7.61	
	4.5	10.57	10.44	1.69	7.64	7.49	2.55
Amberlyst 35W							
KCl	0	0.00	0.00		8.40	8.60	
	0.5	4.78	4.89		8.08	8.21	
	1	9.72	10.01		7.77	7.93	

	1.5	14.72	15.31		7.47	7.76	
	2	19.75	20.82		7.16	7.32	
	2.5	24.75	26.52		6.84	7.05	
	3	27.81	28.80	4.05	6.31	6.52	2.59
KNO_3	0	0.00	0.00		8.40	8.60	
	0.5	5.61	5.29		8.05	8.24	
	1	11.85	9.99		7.72	7.86	
	1.5	18.10	17.70		7.41	7.54	
	2	24.24	22.30		7.11	7.30	
	2.5	30.23	29.42		6.80	7.07	
	3	36.14	36.63	6.63	6.49	6.77	2.67
$CaCl_2$	0	0.00	0.00		10.15	9.98	
	0.75	2.39	2.20		10.02	9.76	
	1.5	4.78	4.43		9.89	9.56	
	2.25	7.20	7.12		9.74	9.39	
	3	9.65	9.09		9.57	9.35	
	3.75	12.15	12.49		9.40	9.30	
	4.5	14.69	14.80	4.53	9.21	9.24	2.17
$Ca(NO_3)_2$	0	0.00	0.00		10.15	9.98	
	0.75	2.57	2.32		10.00	9.75	
	1.5	5.17	4.91		9.86	9.62	
	2.25	7.78	7.63		9.71	9.46	
	3	10.38	10.14		9.57	9.33	
	3.75	12.99	13.40		9.42	9.27	
	4.5	15.60	16.10	4.44	9.27	9.21	2.03

7.6 References

(1) Freeman, D.H.; Patel, V.C.; Buchanan T.M., Electrolyte Uptake Equilibria with Low Cross-Linked Ion-Exchange Resins. *J. Phys. Chem.* **1965**, 69, 1477.

(2) Pepper, K.W.; Reichenberg, D.; Hale, D.K. Properties of Ion-exchange Resins in Relation to Their Structure. Part IV. Swelling and Shrinkage of Sulphonated Polystyrenes of Different Crosslinking. *J. Chem. Soc.* **1952**, 8, 3129.

(3) Scatchard, G.; Anderson, N.J. The Determination of the Equilibrium Water Content of Ion Exchange Resins. *J. Phys. Chem.* **1961**, 65, 1536.

(4) Freeman, D.H.; Scatchard G. Volumetric Studies of Ion Exchange Resin Particles Using Microscopy. J. Phys. Chem. **1965**, 1, 70.

(5) Christensen, S.G.; Thomsen,K. Representation of volumetric data of electrolyte solutions at varying concentrations and temperatures. Submitted to *Ind. Eng. Chem. Res.*

(6) Gregor, H.P.; Gutoff, F; Bregman, J.I. Studies on ion-exchange resins. II. Volumes of varios cation-eschange resin particles. J. Coll. Sci. **1951**, 6, 245

(7) Ferapontov, N.B.; Gorshkov V.I.; Parbuzina L.R.; Trobov H.T.; Strusovskaya N.L. Heterophase Model of Swollen Cross-Linked Polyelectrolyte. Reac. Func. Pol. **1999**, 41, 213.

(8) Maurer, G.; Prausnitz, J.M. Thermodynamics of phase equilibrium for systems containing gels. Fluid Phase Equilibria. **1996**, 115, 113

(9) Abrams, D.S.; Prausnitz, J.M. Statistical Thermodynamics of Liquid Mixtures: A new Expression for the Excess Gibbs Energy of Partly or Completely Miscible Systems. *AIChE J.* **1975**, 21, 116.

(10) Thomsen, K. Aqueous Electrolytes: Model Parameters and Process Simulation. Ph.D. Thesis. *Technical University of Denmark,* Lyngby, **1997**.

(11) Thomsen, K.; Rasmussen, P.; Gani, R. Correlation and Prediction of thermal properties and phase behaviour for a class of aqueous electrolyte system. *Chem. Eng. Sci*. **1996**, 51, 3675.

(12) Thomsen, K.; Rasmussen P. Modeling of vapor-liquid-solid equilibrium in gas-aqueous electrolyte systems. *Chem. Eng. Sci.* **1999**, 54, 1787.

(13) Christensen, S.G.; Thomsen, K. Modeling of vapor-liquid-solid equilibria in acidic aqueous solutions. *Ind. Eng. Chem. Res.* **2003**, 42, 4260

(14) Flory, P.J. Principles of Polymer Chemistry. *Cornell University Press*, Ithaca, NY, **1953**.

(15) James, H.M.; Guth, E. Theory of the elastic properties of rubber. *J. Chem. Phys.* **1943**, 11, 455.

(16) Flory P.J. Statistical thermodynamics of random networks. *Proc. R. Soc. London. Ser. A.* **1976**, 65, 351

(17) Gusler G. M. and Cohen Y. Equilibrium Swelling of Highly Cross-linked Polymeric Resins. *Ind. Eng. Chem. Res.* **1994**, 33, 2345.

(18) Bauman, W.C.; Eichhorn, J. Fundamental properties of a synthetic cation-exchange resin. *J. Am. Chem. Soc.* **1947**, 69, 2830.

(19) Boyd, G. E.; Schubert, J.; Adamson, A.W. The exchange adsorption of ions from aqueous solutions by organic zeolites. I. Ion-exchange equilibria. *J. Am. Chem. Soc.* **1947**, 69 2818.

(20) Gregor, H.P.. A general thermodynamic theory of ion-exchange processes. *J. Am. Chem. Soc.* **1948**, 70 1293.

(21) Gordievskii, A.V.; Filippov, E.L.; Shterman, V.S. Ion-exchange membranes. II. Sorption of electrolytes. *Zhurnal Fizicheskoi Khimii.* **1966**, 40, 2421.

(22) Kokotov, Y.A. Generalized Thermodynamics Theory of Ion Exchange Isotherm. *Solvent Extraction and Ion Exchange.* **1999**, 17, 1001.

(23) Marcus, Y. Ion Properties. Marcel Dekker, New York, **1997**.

(24) Boyd, G.E.; Soldano, B.A., *Z. Elektrochem.*, **1953**, 57, 162

(25) Magnussen, T.; Rasmussen, P.; Fredenslund, Aa., "UNIFAC Parameter Table for Prediction of Liquid-Liquid Equilibria," *Ind. Eng. Chem. Process Des. Dev.* **1981**, 20, 331

(26) Pereda, S.; Thomsen, K.; Rasmussen, P. Vapor-liquid-solid equilibria of sulfur dioxide in aqueous electrolyte solutions. *Chem. Eng. Sci*. **2000**, 55, 2663.

8. Conclusions

The thesis has addressed the thermodynamics involved when describing the properties of aqueous solutions of electrolytes and of mixtures with ion exchanging materials. The main conclusions are summarized in this chapter.

The first part of the thesis has addressed the thermodynamic properties of aqueous electrolyte solutions. The volumetric properties for aqueous solutions of (H^+, Na^+, K^+, NH_4^+, Ca^{++}, Mg^{++}) (Cl^-,NO_3^-,SO_4^{--}) have been modeled using a modification of the Masson equation combined with Young's rule based on ion specific parameters. The model only requires 5 parameters per ion in the entire range of concentration and temperature which is much less than seen in previous works. In addition, due to the ion specific parameters, it is shown that using this model, the parameters can be regressed on the basis of data from only a few selected salts. This can be done without influencing the overall accuracy of the model and is a huge advantage as reliable volumetric properties do not exist for all salts. The model has been applied to multicomponent mixtures, and it has been shown that the relative errors of the predicted results in both ternary and quaternary systems are well within the experimental accuracy of the data. Due to the simplicity and good predictivity in multicomponent systems the model could easily be implemented in industrial process calculations. The drawback of the model is, that it does not give perfect correlations in systems where a high degree of speciation exists. This problem has been solved for the H_3PO_4 system by including speciation data, but these kinds of data are not always available. More investigations of extending the model to highly non-ideal systems would therefore be important.

In the second part of the thesis, the Extended UNIQUAC model has successfully been applied to describe the phase behavior and thermal properties of various acidic aqueous solutions of electrolytes. The model is capable of describing the dissociation of both H_3PO_4 and HNO_3 in aqueous solutions and of describing the solubility of several different salts in aqueous solutions of these two acids. In addition, the model reproduces the thermal properties of these solutions with high accuracy. The Extended UNIQUAC model is very useful for industrial relevant calculations. One of the reasons for this is that the model only includes binary interaction parameters and thereby is relatively simple to use. Another advantage is the

flexibility of the model, and the fact that the model usually gives good predictions in multicomponent solutions. With the parameters given in this thesis, the model could easily be applied to both optimization and design purposes in the fertilizer and related industries. However, as mentioned in chapter 4 the model does not give perfect correlation for all the investigated systems. These inaccuracies are partly due to parameters found in previous works and the overall accuracy of the model could still be improved.

The latter part of the thesis has addressed the thermodynamics of ion exchange equilibria. New experimental isotherms for a macroreticular ion exchange resin have been measured for the H^+ - (Na^+, K^+, Ca^{++}) systems with (Cl^-, NO_3^-, SO_4^{--}, $H_2PO_4^-$) as co-ions at 1N and 25°C. The experiments have been performed using a column method and the accuracy of the data is very reasonable. These new experiments illustrate the impact of speciation on ion exchange equilibria isotherms.

Ion exchange isotherms have been modeled using an approach in which the ion exchanger is considered a solid phase. The aqueous phase has been modeled using the Extended UNIQUAC model, while the ion exchanger phase has been modeled using the Margules 1 coefficient model. The thermodynamic equilibrium constant has been calculated individually from the experimental data. The method has been applied to a large amount of ion exchange systems, and the results show that using the simple Margules model gives very similar results as when using the more complex Wilson model.

The work shows that excellent predictions can be obtained at varying concentrations with parameters regressed at one concentration. The new experimental data have been modeled by regressing parameters from the chloride data and the predictions for the isotherms with other co-ions are very reasonable. The conclusions from these calculations are that speciation implicit is included in the aqueous phase activity coefficients. This means, that the conventions used when the parameters of the aqueous thermodynamic model originally were regressed should always be used when activities later on are calculated using the same model parameters. However, due to the limited amount of data for ion exchange isotherms in systems with high speciation, most of the results should mainly be taken as indications. More comprehensive experiments should be performed to cover a larger system of ions and thereby be used for validating the model.

The approach for calculating binary ion exchange isotherms could easily be extended to multicomponent systems and has in this work been successfully applied on a ternary system. The method gives good predictions in the ternary system from the binary parameters, and the results show that the three thermodynamic equilibrium constants calculated from the binary systems obey the Triangle rule within 3%. This result is better than previously reported results and indicates that the simple method for obtaining the thermodynamic equilibrium constant used in this work gives consistent values. However, the method should be applied to more ternary systems before any final conclusions can be made.

In the last part of the thesis, the absorption of water and salt at ambient temperature has been measured for 3 gel type and 3 macroreticular resins with varying degrees of crosslinking. The experiments were performed for aqueous solutions of KNO_3, KCl, $Ca(NO_3)_2$ and $CaCl_2$ in the concentration range of 0-3N. The absorption has been calculated using a method consisting of batch experiments combined with measurements of the volume change of the resin when in equilibrium with the electrolyte solutions. The experimental results have an experimental reproducibility of 8% which is acceptable for this kind of studies. The conclusion of this is, that the new procedures proposed in this thesis for these kinds of experiments are valid. The experimental data have been modeled with the Extended UNIQUAC model combined with an elastic term taking the elastic properties of the resin structure into account. Volumetric properties of both the two phases are modeled using the method developed in this thesis and it is shown that the volume of the resin phase could be considered as constant within small variation in concentrations. The absorption in the macroreticular resins has been modeled under the assumption that this type of resins consists of a gel type region and a discrete porous region. The model shows very good predictions with varying degree of crosslinking for both types of resins, and the deviations between model results and experimental data are all within the experimental error. This means that the model is capable of predicting the salt and water absorption in various polystyrene ion exchange resins from absorption isotherms of one type of resin as long as the capacity, swelling in pure water and pure water density of the various resins are known. This could be a huge help in screening different resins for special properties. However, the models capabilities are not fully utilized in this study. First of all more experiments should be performed in order to fully validate the obtained results. Furthermore, it would be interesting to observe the models capabilities in systems with two or

more competing counter-ions. These types of experiments are very time consuming and were unfortunately not performed in this study due to a limited time in the laboratory facilities.

Notation

a_i	Activity of component *i*
a	Distance of closest approach (m)
A	Helmholz energy (J)
A_{ij}	Wilson parameter
A_{DH}	Debye-Hückel parameter ($kg^{½}mol^{-½}$)
b	Extended Debye-Hückel parameter ($kg^{½}mol^{-½}$)
c	concentration (mol/L)
C	Heat capacity (J/mol/K)
EP	Equivalence point
F	Faradays constant (C/mol)
g	Molar Gibbs energy (J/mol)
G	Gibbs energy (J)
H	Enthalpy (J)
I_m	Ionic strength based on the molality scale (mol/kg)
K	Solubility product
K_C	Apparent equilibrium constant
K_{eq}	Thermodynamic equilibrium constant
L	Relative enthalpy (J/mol)
m	Molality (mol/kg)
M	Molecular mass (kg/mol)
MR	Resin in M-form
n	Mole number (mol)
$\underline{n}$	Vector of n

N_A	Avogadros number
P	Pressure (Pa)
q	Capacity of resin (meq/g dry)
q_w	Fraction of water content of resin when equilibrated with pure water
R	Gas constant (J/mol/K)
S	Entropy (J/K)
t	Temperature (°C)
T	Absolute temperature (K)
U	Internal energy (J)
v	Molar volume (cm^3/mol)
V	Volume (cm^3)
$\bar{V}$	Partial molal volume (cm^3/mol)
w	Weight (g)
x	Mole fraction
y	Equivalent fraction
z	Ionic charge

Greek letters

ε_r	Relative permittivity of water (C^2/J/m)
ε_0	Vacuum permittivity
μ	Chemical potential (J/mol)
ρ	Density (kg/m^3)
π	Pi (3.1416)
γ	Activity coefficient

ϕ	Volume fraction
ϕ_V	Apparent molal volume (cm^3/mol)
Λ_{ij}	Margules parameter

Superscript

dry	Dry state property
i	Initial
E	Excess Property
eq	At equilibrium
m	Property based on molality scale
wet	Property when in equilibrium with pure water
¯	Partial molar property
~	Property per equivalent of resin
´	Bulk phase property
´´	Resin phase property
0	Standard state – symmetrical convention
∇	Standard state – unsymmetrical convention

Subscript

B	Bulk solution
i	Component *i*
MR	Resin in M-form
pyc	Pycnometer
R	Resin
s	Salt

Appendix A

The non-ideality in a dilute electrolyte solution according to the limiting law of Debye and Hückel theory could be described by:

$$G^E = -\frac{4}{3} RTn_w M_w A^*_{DH} \sqrt{\rho_w} I_m^{3/2}$$

Where $A^*_{DH}\sqrt{\rho_w} = A_{DH}$

$$\left(\frac{\partial\sqrt{\rho_w}}{\partial P}\right)_{T,\underline{n}} = \frac{1}{2}\frac{1}{\sqrt{\rho_w}}\left(\frac{\partial\rho_w}{\partial P}\right)_{T,\underline{n}}$$

$$\left(\frac{\partial A^*_{DH}}{\partial P}\right)_{T,\underline{n}} = \frac{F^3}{4\pi N_A}\sqrt{\frac{1}{2(RT\varepsilon_0)^3}}\frac{\partial}{\partial P}\left(\sqrt{\frac{1}{\varepsilon_r^3}}\right)_{T,\underline{n}}$$

$$= \frac{F^3}{4\pi N_A}\sqrt{\frac{1}{2(RT\varepsilon_0)^3}}\cdot -\frac{3}{2}\varepsilon_r^{-5/2}\left(\frac{\partial\varepsilon_r}{\partial P}\right)_{T,\underline{n}}$$

$$= -\frac{3}{2}A^*_{DH}\frac{1}{\varepsilon_r}\left(\frac{\partial\varepsilon_r}{\partial P}\right)_{T,\underline{n}}$$

$$\left(\frac{\partial G^E}{\partial P}\right)_{T,\underline{n}} = -\frac{4}{3}RTn_w M_w I_m^{3/2}\left(\sqrt{\rho_w}\left(\frac{\partial A^*_{DH}}{\partial P}\right)_{T,\underline{n}} + A^*_{DH}\left(\frac{\partial\sqrt{\rho_w}}{\partial P}\right)_{T,\underline{n}}\right)$$

$$\left(\frac{\partial G^E}{\partial P}\right)_{T,\underline{n}} = -\frac{4}{3}RTn_w M_w I_m^{3/2}\left(-\frac{3}{2}A^*_{DH}\sqrt{\rho_w}\frac{1}{\varepsilon_r}\left(\frac{\partial\varepsilon_r}{\partial P}\right)_{T,\underline{n}} + \frac{1}{2}A^*_{DH}\frac{1}{\sqrt{\rho_w}}\left(\frac{\partial\rho_w}{\partial P}\right)_{T,\underline{n}}\right)$$

$$\left(\frac{\partial G^E}{\partial P}\right)_{T,\underline{n}} = \frac{2}{3}RTn_w M_w A_{DH} I_m^{3/2}\left(\frac{3}{\varepsilon_r}\left(\frac{\partial\varepsilon_r}{\partial P}\right)_{T,\underline{n}} + \frac{1}{\rho_w}\left(\frac{\partial\rho_w}{\partial P}\right)_{T,\underline{n}}\right)$$

Appendix B

The non-ideality in a dilute electrolyte solution according to the so-called extended Debye and Hückel theory could be described by:

$$G^{elec} = -4RT\frac{A^*_{DH}\sqrt{\rho_w}}{b_m^3}n_w M_w\left[\ln(1+b_m\sqrt{I_m}) - b_m\sqrt{I_m} + \frac{b_m^2 I_m}{2}\right]$$

Where b_m is given by:

$$b_m = a\sqrt{\frac{2\rho_w F^2}{\varepsilon_0\varepsilon_r RT}}$$

$$\left(\frac{\partial\sqrt{\rho_w}}{\partial P}\right)_{T,\underline{n}} = \frac{1}{2}\frac{1}{\sqrt{\rho_w}}\left(\frac{\partial\rho_w}{\partial P}\right)_{T,\underline{n}} = \kappa$$

$$\left(\frac{\partial A^*_{DH}}{\partial P}\right)_{T,\underline{n}} = -\frac{3}{2}A^*_{DH}\frac{1}{\varepsilon}\left(\frac{\partial\varepsilon}{\partial P}\right)_{T,\underline{n}} = \lambda$$

$$\left(\frac{\partial b_m}{\partial P}\right)_{T,\underline{n}} = \sqrt{\frac{2F^2}{\varepsilon_0 RT}}\frac{\partial}{\partial P}\left(a\sqrt{\frac{\rho_w}{\varepsilon_r}}\right)_{T,\underline{n}}$$

$$= \sqrt{\frac{2F^2}{\varepsilon_0 RT}}\sqrt{\frac{\rho_w}{\varepsilon_r}}\left(\frac{\partial a}{\partial P}\right)_{T,\underline{n}} + \frac{1}{2}a\sqrt{\frac{2F^2}{\varepsilon_0 RT}}\sqrt{\frac{\varepsilon_r}{\rho_w}}\frac{\partial}{\partial P}\left(\frac{\rho_w}{\varepsilon_r}\right)_{T,\underline{n}}$$

$$= \sqrt{\frac{2F^2}{\varepsilon_0 RT}}\sqrt{\frac{\rho_w}{\varepsilon_r}}\left(\frac{\partial a}{\partial P}\right)_{T,\underline{n}} + \frac{1}{2}a\frac{1}{\varepsilon_r^2}\sqrt{\frac{2F^2}{\varepsilon_0 RT}}\sqrt{\frac{\varepsilon_r}{\rho_w}}\left(\varepsilon_r\frac{\partial\rho_w}{\partial P} - \rho_w\frac{\partial\varepsilon_r}{\partial P}\right)_{T,\underline{n}}$$

$$= \sqrt{\frac{2F^2}{\varepsilon_0 RT}}\sqrt{\frac{\rho_w}{\varepsilon_r}}\left(\frac{\partial a}{\partial P}\right)_{T,\underline{n}} + \frac{1}{2}a\frac{1}{\varepsilon_r}\sqrt{\frac{2F^2}{\varepsilon_0 RT}}\sqrt{\frac{\rho_w}{\varepsilon_r}}\left(\frac{\varepsilon_r}{\rho_w}\frac{\partial\rho_w}{\partial P} - \frac{\partial\varepsilon_r}{\partial P}\right)_{T,\underline{n}}$$

$$= \frac{1}{2}b_m\left(\frac{2}{a}\frac{\partial a}{\partial P} + \frac{1}{\rho_w}\frac{\partial\rho_w}{\partial P} - \frac{1}{\varepsilon_r}\frac{\partial\varepsilon_r}{\partial P}\right)_{T,\underline{n}} = \frac{1}{2}b_m\omega$$

$$\left(\frac{\partial\ln(1+b_m\sqrt{I_m})}{\partial P}\right)_{T,\underline{n}} = \frac{1}{1+b_m\sqrt{I_m}}\frac{\partial(1+b_m\sqrt{I_m})}{\partial P} = \frac{\sqrt{I_m}}{1+b_m\sqrt{I_m}}\frac{\partial b_m}{\partial P} = \frac{1}{2}\frac{b_m\sqrt{I_m}}{1+b_m\sqrt{I_m}}$$

$$\frac{\partial}{\partial P}\left(A^*_{DH}\sqrt{\rho_w}\right)_{T,\underline{n}} = \left[-\frac{3}{2}\sqrt{\rho_w}A^*_{DH}\frac{1}{\varepsilon_r}\left(\frac{\partial \varepsilon_r}{\partial P}\right)_{T,\underline{n}} + \frac{1}{2}A^*_{DH}\frac{1}{\sqrt{\rho_w}}\left(\frac{\partial \rho_w}{\partial P}\right)_{T,\underline{n}}\right]$$

$$= \frac{1}{2}A^*_{DH}\sqrt{\rho_w}\left[\frac{1}{\rho_w}\left(\frac{\partial \rho_w}{\partial P}\right)_{T,\underline{n}} - \frac{3}{\varepsilon_r}\left(\frac{\partial \varepsilon_r}{\partial P}\right)_{T,\underline{n}}\right] = \frac{1}{2}A^*_{DH}\sqrt{\rho_w}\kappa$$

$$G^{elec} = -4RT\frac{A^*_{DH}\sqrt{\rho_w}}{b_m^3}n_w M_w\left[\ln(1+b_m\sqrt{I_m}) - b_m\sqrt{I_m} + \frac{b_m^2 I_m}{2}\right]$$

$$G^{elec} = -4RTn_w M_w A^*_{DH}\sqrt{\rho_w}\left[b_m^{-3}\ln(1+b_m\sqrt{I_m}) - b_m^{-2}\sqrt{I_m} + \frac{I_m}{b_m 2}\right]$$

$$\frac{\partial G^{elec}}{\partial P} = -4RTn_w M_w\left[\begin{array}{l} A^*_{DH}\sqrt{\rho_w}\dfrac{\partial}{\partial P}\left(b_m^{-3}\ln(1+b_m\sqrt{I_m}) - b_m^{-2}\sqrt{I_m} + \dfrac{I_m}{b_m 2}\right) \\ +\left(\dfrac{\ln(1+b_m\sqrt{I_m})}{b_m^3} - \dfrac{\sqrt{I_m}}{b_m^2} + \dfrac{I_m}{b_m 2}\right)\dfrac{\partial}{\partial P}\left(A^*_{DH}\sqrt{\rho_w}\right) \end{array}\right]$$

$$\frac{\partial G^{elec}}{\partial P} = -4RTn_w M_w\left[\begin{array}{l} A^*_{DH}\sqrt{\rho_w}\dfrac{1}{2}\omega\left(\dfrac{\sqrt{I_m}}{b_m^2(1+b_m\sqrt{I_m})} - \dfrac{3\ln(1+b_m\sqrt{I_m})}{b_m^3} + \dfrac{2\sqrt{I_m}}{b_m^2} - \dfrac{I_m}{2b_m}\right) \\ +\left(\dfrac{\ln(1+b_m\sqrt{I_m})}{b_m^3} - \dfrac{\sqrt{I_m}}{b_m^2} + \dfrac{I_m}{2b_m}\right)\left(\dfrac{1}{2}A^*_{DH}\sqrt{\rho_w}\kappa\right) \end{array}\right]$$

$$\frac{\partial G^{elec}}{\partial P} = -2RTn_w M_w A_{DH}\left[\begin{array}{l} \omega\left(\dfrac{\sqrt{I_m}}{b_m^2(1+b_m\sqrt{I_m})} - \dfrac{3\ln(1+b_m\sqrt{I_m})}{b_m^3} + \dfrac{2\sqrt{I_m}}{b_m^2} - \dfrac{I_m}{2b_m}\right) \\ +\kappa\left(\dfrac{\ln(1+b_m\sqrt{I_m})}{b_m^3} - \dfrac{\sqrt{I_m}}{b_m^2} + \dfrac{I_m}{2b_m}\right) \end{array}\right]$$

$$\omega = \left(\frac{2}{a}\frac{\partial a}{\partial P} + \frac{1}{\rho_w}\frac{\partial \rho_w}{\partial P} - \frac{1}{\varepsilon_r}\frac{\partial \varepsilon_r}{\partial P}\right)_{T,\underline{n}}$$

$$\kappa = \left(\frac{1}{\rho_w}\left(\frac{\partial \rho_w}{\partial P}\right)_{T,\underline{n}} - \frac{3}{\varepsilon_r}\left(\frac{\partial \varepsilon_r}{\partial P}\right)_{T,\underline{n}}\right)$$

Appendix C

Database of volumetric properties.

During the Ph.D. project density and other volumetric data have been collected for a large amount of salts. At present time, data have been systematically collected from nearly 100 different articles.

All experimental data have been included in the data file dens.dat. The index system of the data file is as follows:

First line in data series:

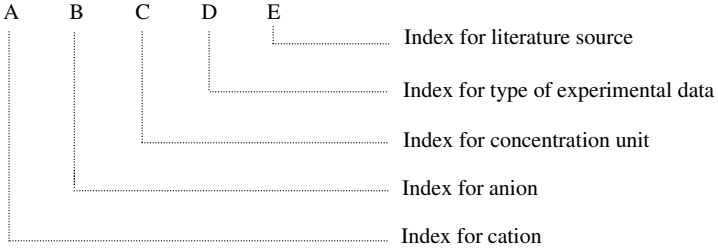

Data series:

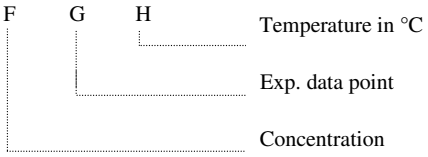

Index for cation and anions follow the system of Thomsen.

Type of concentrations is indexed as follows:

1. Molality (mol/kg)
2. Molarity (mol/L)
3. Ionic strength of solution (mol/L)
4. Weight percent of salt

The index for types of exp. data is:

1. Apparent molal volume of salt (cm^3/mol)
2. Density of solution (g/cm^3)

3. Density of solution (kg/m^3)
4. 1000(d-d_0) (g/cm^3)
5. Specific gravity (cm^3/g)

The index for the literature source corresponds with the numbering given in the file vol_lit.dat where all references are given.

A computer program has been created for retrieving selected data from the data file. The input parameters are:

- Number of ions
- Index of ions
- Temperature interval of interest
- Concentration interval of interest

The program then creates a file vol_dat.out with the relevant data converted into the form:

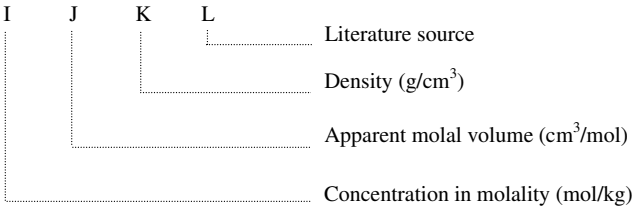

Appendix D

Representation of volumetric data in aqueous systems with phosphoric salts.

In the original work presented in chapter 3 the species $H_2PO_4^-$ was not included. The reason for this is that only very few data points exist for the volumetric properties of these type of salts. In addition to this, phosphoric acid does not fully dissociate and could therefore not directly be represented by the general equations used in the chapter. In spite of the limited data, parameters are given in this appendix for the calculation of fully dissociated $H_2PO_4^-$ salts. Furthermore, an alternative procedure is suggested for the calculation of the volumetric properties of phosphoric acid. All parameters are only valid at 25°C.

Parameters for $H_2PO_4^-$

The parameters in eq. [3.26] is found from regression of apparent molal volume data of NaH_2PO_4 and KH_2PO_4 measured by Surdo et al.[1] The parameters are given in the table D.1 and the results are shown in figure D.1.

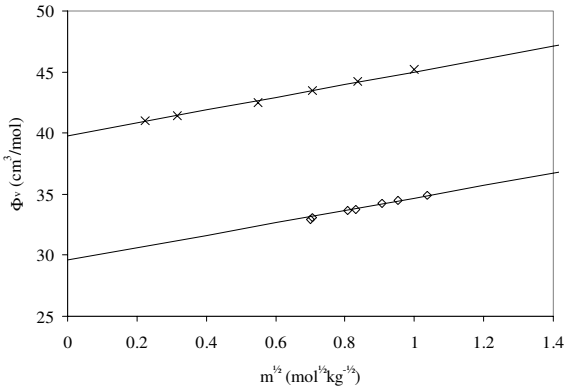

Figure D.1. Representation of apparent molal volume of aqueous solutions of phosphoric salts. (×) KH_2PO_4, (◇) NaH_2PO_4, (–) correlation calculated with eq. [3.26].

The figure shows a good correlation of the two phosphoric salts and the deviation is within the experimental accuracy. The results also show that it is fairly easy to implement a new species to the system given in chapter 3.

Parameters for H_3PO_4:

As mentioned in chapter 4, H_3PO_4 is not a strong acid and is therefore not fully dissociated in aqueous solutions:

$$H_3PO_4(s) \rightleftarrows H^+(aq) + H_2PO_4^-(aq)$$
$$H^+(aq) + H_2PO_4^-(aq) \rightleftarrows H_3PO_4(aq)$$

Eq. [3.26] can therefore not be directly applied to this species. Due to speciation the apperent molal volume of H_3PO_4 is not a function of the square root of molality. To take this into consideration the apparent molal volume of H_3PO_4 is calculated as a contribution from dissociated H_3PO_4 and undissociated H_3PO_4:

$$\phi_{V,H_3PO_4} = \frac{n_{H^+}\phi_{V,H^+} + n_{H_2PO_4^-}\phi_{V,H_2PO_4^-} + n_{H_3PO_4}\phi_{V,H_3PO_4}}{n_{H^+} + n_{H_2PO_4^-} + n_{H_3PO_4}}$$

The speciation is calculated using the dissociation data of Preson and Adams[2]. The data have been correlated using a power expression as shown in figure D.2.

Table D.1: Parameters for eq. [3.26]

I	$\bar{v}_i^{(1)}$	$k_i^{(1)}$
$H_2PO_4^-$	30.8	4.1
H_3PO_4	47.852	0.3039

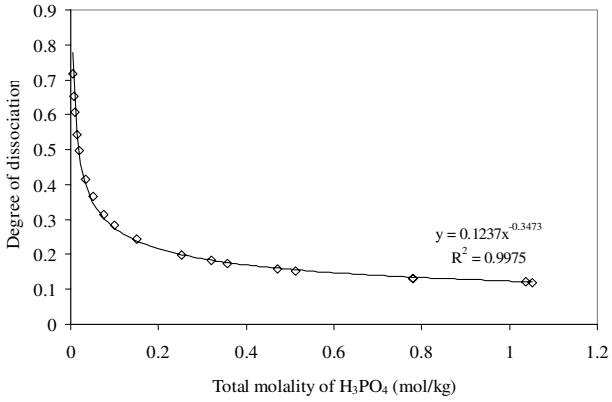

Figure D.2. Degree of dissociation of H_3PO_4 in water. (◇) data of Preston and Adams[2], (–) power correlation with parameters given in the figure.

The parameter for H_3PO_4 (aq) has been regressed from experimental data of Surdo et al.[1] and the result is shown in figure D.3.

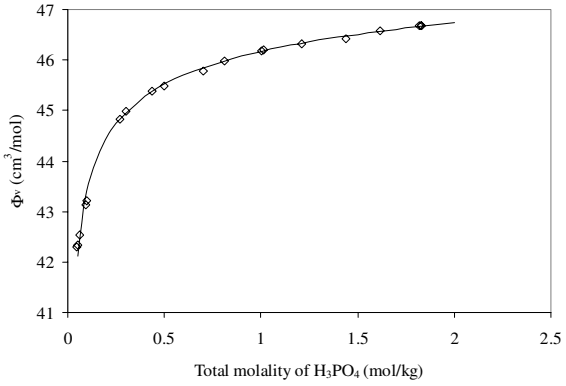

Figure D.3. Apparent molal volume of H_3PO_4 in aqueous solutions at 25°C. (◇) Experimental data of Surdal et al.[1], (–) calculated using eq. [3.26] and parameters in table D.1.

The figure shows excellent agreement and proves that eq. [3.26] could be extended to apply to highly speciated systems by applying dissociation data. It has not been possible to validate these parameters in multicomponent mixtures due to lack of experimental data. However, this would be very important in future works if relevant data shows up in literature.

References:

(1) Surdo, A.L.; Bernstrom, K.; Jonsson, C.-A.; Millero, F. Molal Volumes and Adiabatic Compressibility of Aqueous Phosphate Solutions at 25°C. *Am. Chem. Soc*. **1979**, 83, 1255.

(2) Preston, C. M.; Adams, W. A. A Laser Raman Spectroscopic Study of Aqueous Phosphoric Acid. *Can. J. Spectroscopy*. **1977**, 22, 125.

Appendix E

Determination of H+ in aqueous solutions.

Theory.
The amount of H^+ (H_3O^+) in a solution could be found by titration of the solution with a basic solution:

$$H_3O^+ + OH^- \rightarrow 2H_2O$$

If a glass electrode is in contact with the acid solution then according to the Nernst equation the potential of the glass electrode corresponds to the hydrogen ion activity:

$$E_{glass} = E^0_{glass} + k \log a_{H^+} = E^0_{glass} + k \cdot pH$$

If the electrode also contains a reference electrode then the overall cell voltage is:

$$E_{cell} = E_{glass} - E_{ref} = \left(E^0_{glass} - E_{ref}\right) - k \cdot pH$$

Titrating the acid solution with a basic titrant and monitoring the pH as a function of the volume titrant, the amount of H^+ in the initial solution can be found. The equivalence point will show as a steep rise in pH as shown in figure E.1.

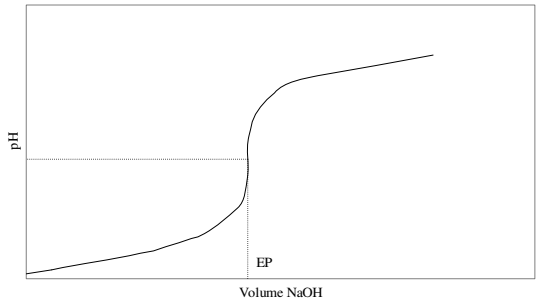

Figure E.1

Experimental procedure.

The chloride content of the solution was determined with a potentiometric method using a Metrohm 799 GPT Titrino titrator with a silver chloride reference electrode. Merck NaOH standard solutions at 0.1±0.001N were used as titrant.

100±0.1mL of eluent was transferred to a 50mL tritration beaker using a pipette. The solutions were titrated using the Metrohm device and the equilibrium point found numerically by the device. The experiment was repeated several times and the average experimental reproducibility was found to be approximately 2%.

Appendix F

Including the co-ion in reaction [6.1] gives:

$$|z_B|A^{z_A} + \left|\frac{z_A z_B}{z_X}\right| X^{z_X} + |z_A| BR_{z_B} \rightleftarrows |z_B| AR_{z_A} + \left|\frac{z_A z_B}{z_X}\right| X^{z_X} + |z_A| B^{z_B}$$

The thermodynamic equilibrium constant for the reaction is:

$$K_A^B = \frac{(a_{BX})^{z_A/z_X}}{(a_{AX})^{z_B/z_X}} \frac{\left(a_{AR_{z_A}}\right)^{z_B}}{\left(a_{AR_{z_B}}\right)^{z_A}}$$

Where the activity of the salt $A_{z_x} X_{z_A}$ in the solution is defined as:

$$a_{A_{z_X} X_{z_A}} = (m_A \gamma_A)^{z_X} (m_X \gamma_X)^{z_A}$$

Written in terms of activity coefficients equation [2.A] gives:

$$K_A^B = \frac{\left((m_B \gamma_B)^{z_X} (m_X \gamma_X)^{z_B}\right)^{z_A/z_X} \left(x_{AR_{z_A}} f_{AR_{z_A}}\right)^{z_B}}{\left((m_A \gamma_A)^{z_X} (m_X \gamma_X)^{z_A}\right)^{z_B/z_X} \left(x_{AR_{z_B}} f_{AR_{z_B}}\right)^{z_A}}$$

$$= \frac{(m_B \gamma_B)^{z_A} (m_X \gamma_X)^{\frac{z_A z_B}{z_X}}}{(m_A \gamma_A)^{z_B} (m_X \gamma_X)^{\frac{z_A z_B}{z_X}}} \frac{\left(x_{AR_{z_A}} f_{AR_{z_A}}\right)^{z_B}}{\left(x_{AR_{z_B}} f_{AR_{z_B}}\right)^{z_A}} = \frac{(m_B \gamma_B)^{z_A}}{(m_A \gamma_A)^{z_B}} \frac{\left(x_{AR_{z_A}} f_{AR_{z_A}}\right)^{z_B}}{\left(x_{AR_{z_B}} f_{AR_{z_B}}\right)^{z_A}}$$

Appendix G

Calculation of the thermodynamic equilibrium constant of ion exchange isotherms.

The thermodynamic equilibrium constant is defined as:

$$ln\,K_A^B = ln\,K_C + ln\left(\gamma_{AR_{z_A}}\right)^{z_B} - ln\left(\gamma_{BR_{z_B}}\right)^{z_A} \qquad [G.1]$$

From the definition of the equilibrium constant following therefore applies:

$$d\,ln\,K_C + d\,ln(\,\gamma_{AR_{z_A}})^{z_B} - d\,ln(\,\gamma_{BR_{z_B}})^{z_A} = 0 \qquad [G.2]$$

The Gibbs-Duhem equation for the ion exchanger phase gives:

$$n_{AR_{z_A}} d\mu_{AR_{z_A}} + n_{BR_{z_B}} d\mu_{BR_{z_B}} = 0 \qquad [G.3]$$

When considering a unit of resin carrying one equivalent of exchange sites and introducing the expression for the chemical potential, equation [G.3] gives:

$$y_{AR_{z_A}} d\,ln(\,\gamma_{AR_{z_A}} x_{AR_{z_A}})^{z_B} + y_{BR_{z_B}} d\,ln(\,\gamma_{BR_{z_B}} x_{BR_{z_B}})^{z_A} = 0 \qquad [G.4]$$

where $y_{BR_{z_B}}$ is the equivalent molefraction of BR_{z_B} defined as:

$$y_{BR_{z_B}} = \frac{z_B n_{BR_{z_B}}}{z_B n_{BR_{z_B}} + z_A n_{AR_{z_A}}}$$

Combination of equation [G.2] and [G.4] could be used for decoupling the equilibrium constant from the resin phase activity coefficients:

Solving for $\gamma_{AR_{z_A}}$:

$$d\,ln\,K_C + d\,ln(\,\gamma_{AR_{z_A}})^{z_B} - d\,ln(\,\gamma_{BR_{z_B}})^{z_A} = 0 \Leftrightarrow \qquad [G.5]$$

$$d\,ln(\,\gamma_{BR_{z_B}})^{z_A} = d\,ln\,K_C + d\,ln(\,\gamma_{AR_{z_A}})^{z_B} \qquad [G.6]$$

Inserting this in [G.3] gives:

$$y_{AR_{z_A}} d\,ln(\,\gamma_{AR_{z_A}} x_{AR_{z_A}})^{z_B} + y_{BR_{z_B}} d\,ln(\,\gamma_{BR_{z_B}} x_{BR_{z_B}})^{z_A} = 0 \Leftrightarrow \qquad [G.7]$$

$$y_{BR_{z_B}} d\,ln(\,\gamma_{BR_{z_B}})^{z_A} = -y_{AR_{z_A}} d\,ln(\,\gamma_{AR_{z_A}} x_{AR_{z_A}})^{z_B} - y_{BR_{z_B}} d\,ln(\,x_{BR_{z_B}})^{z_A}$$

$$y_{BR_{z_B}} d\,ln\,K_C + y_{BR_{z_B}} d\,ln(\,\gamma_{AR_{z_A}})^{z_B} = -y_{AR_{z_A}} d\,ln(\,x_{AR_{z_A}} \gamma_{AR_{z_A}})^{z_B} - y_{BR_{z_B}} d\,ln(\,x_{BR_{z_B}})^{z_A}$$

$$(y_{BR_{z_B}} + y_{AR_{z_A}}) d\, ln(\gamma_{AR_{z_A}})^{z_B} = -y_{BR_{z_B}} d\, ln\, K_C - y_{AR_{z_A}} d\, ln(x_{AR_{z_A}})^{z_B} - y_{BR_{z_B}} d\, ln(x_{BR_{z_B}})^{z_A}$$

$$d\, ln(\gamma_{AR_{z_A}})^{z_B} = -y_{BR_{z_B}} d\, ln\, K_C - y_{AR_{z_A}} d\, ln(x_{AR_{z_A}})^{z_B} - y_{BR_{z_B}} d\, ln(x_{BR_{z_B}})^{z_A} \quad [G.8]$$

Similarly for $\gamma_{BR_{z_B}}$:

$$d\, ln(\gamma_{BR_{z_B}})^{z_B} = y_{AR_{z_A}} d\, ln\, K_C - y_{BR_{z_B}} d\, ln(x_{BR_{z_B}})^{z_A} - y_{AR_{z_A}} d\, ln(x_{AR_{z_A}})^{z_B} \quad [G.9]$$

Integration of equation [G.8] between a point Q on the ion exchange equilibrium isotherm and the point, a, where the ion exchanger is on pure AR_{z_A} form gives:

$$\int_a^Q d\, ln(\gamma_{AR_{z_A}})^{z_B} = -\int_a^Q y_{BR_{z_B}} d\, ln\, K_C - \int_a^Q y_{AR_{z_A}} d\, ln(x_{AR_{z_A}})^{z_B} - \int_a^Q y_{BR_{z_B}} d\, ln(x_{BR_{z_B}})^{z_A} \quad [G.10]$$

$$\int_a^Q y_{BR_{z_B}} d \ln K_C = \Big[y_{BR_{z_B}} \ln K_C \Big]_a^Q - \int_a^Q \ln K_C dy_{BR_{z_B}} \quad [G.11]$$

$$\int_a^Q y_{AR_{z_A}} d \ln(x_{AR_{z_A}})^{z_B} = \int_a^Q \frac{z_B z_A x_{AR_{z_A}}}{z_A x_{AR_{z_A}} + z_B x_{BR_{z_B}}} \frac{1}{x_{AR_{z_A}}} dx_{AR_{z_A}} = \int_a^b \frac{1}{x_{AR_{z_A}} \left(\frac{\perp}{z_B} - \frac{\perp}{z_A} \right) + \frac{\perp}{z_A}} dx_{AR_{z_A}}$$

$$= \left[\frac{1}{\frac{\perp}{z_B} - \frac{\perp}{z_B}} \ln \left(\frac{x_{AR_{z_A}}}{z_B} + \frac{x_{BR_{z_B}}}{z_A} \right) \right]_a^Q$$

$$\int_a^Q y_{BR_{z_B}} d \ln(x_{BR_{z_B}})^{z_A} = \left[\frac{1}{\frac{\perp}{z_A} - \frac{\perp}{z_B}} \ln \left(\frac{x_{AR_{z_A}}}{z_B} + \frac{x_{BR_{z_B}}}{z_A} \right) \right]_a^Q = -\int_a^Q y_{AR_{z_A}} d \ln(x_{AR_{z_A}})^{z_B} \quad [G.12]$$

$$\int_a^Q d \ln(\gamma_{AR_{z_A}})^{z_B} = -\Big[y_{BR_{z_B}} \ln K_C \Big]_a^Q + \int_a^Q \ln K_C dy_{BR_{z_B}} \quad [G.13]$$

$$\ln \frac{\gamma_{AR_{z_A}}(Q)^{z_B}}{\gamma_{AR_{z_A}}(a)^{z_B}} = -\Big[y_{BR_{z_B}} \ln K_C \Big]_a^Q + \int_a^Q \ln K_C dy_{BR_{z_B}}$$

$$\ln \gamma_{AR_{z_A}}(Q)^{z_B} = \ln f_{AR_{z_A}}(a)^{z_B} - \Big[y_{BR_{z_B}} \ln K_C \Big]_a^Q + \int_a^Q \ln K_C dy_{BR_{z_B}} \quad [G.14]$$

Simarly for $\gamma_{BR_{z_B}}$:

$$\int_b^Q d \ln(\gamma_{BR_{z_B}})^{z_A} = -\Big[y_{AR_{z_A}} \ln K_C \Big]_b^Q - \int_b^Q \ln K_C dy_{AR_{z_A}}$$

$$\ln \frac{\gamma_{BR_{z_B}}(Q)^{z_A}}{\gamma_{BR_{z_B}}(b)^{z_A}} = -\Big[y_{AR_{z_A}} \ln K_C \Big]_b^Q - \int_b^Q \ln K_C dy_{AR_{z_A}}$$

$$\ln \gamma_{BR_{z_B}}(Q)^{z_A} = \ln \gamma_{BR_{z_B}}(b)^{z_A} - \left[y_{AR_{z_A}} \ln K_C \right]_b^Q - \int_b^Q \ln K_C dy_{AR_{z_A}} \quad [G.15]$$

Inserting eq. [G.14] and [G.15] in eq. [G.1] gives:

$$\ln K = \ln \frac{(\gamma_{AR_{z_A}}(a))^{z_B}}{(\gamma_{BR_{z_B}}(b))^{z_A}} + \int_a^b \ln K_C dy_{BR_{z_B}} \quad [G.16]$$

The activity coefficients in the two pure states are per definition 1. Eq. [G.16] is therefore reduced to:

$$ln\, K = \int_0^1 ln\, K_C d\bar{y}_B \quad [G.17]$$

Appendix H

Isotherm data for H^+ - K^+, H^+ - Ca^{++} and H^+ - Na^+ ion exchange on Amberlyst 40CW in 1N solutions.

Type of Exchange	Type of anion							
H^+ and	Cl^-		NO_3^-		SO_4^{--}		$H_2PO_4^-$	
	x_{H^+}	x_{HR}	x_{H^+}	x_{HR}	x_{H^+}	x_{HR}	x_{H^+}	x_{HR}
K^+	0.097	0.094	0.100	0.100	0.100	0.046	0.100	0.010
	0.101	0.096	0.200	0.165	0.200	0.070	0.200	0.038
	0.185	0.149	0.300	0.234	0.300	0.092	0.300	0.072
	0.186	0.148	0.400	0.294	0.400	0.135	0.400	0.101
	0.295	0.209	0.500	0.356	0.500	0.183	0.500	0.132
	0.394	0.269	0.600	0.410	0.600	0.260	0.579	0.168
	0.479	0.328	0.700	0.506	0.700	0.335	0.700	0.255
	0.492	0.329	0.800	0.613	0.800	0.443	0.800	0.378
	0.492	0.331	0.900	0.762	0.900	0.654	0.900	0.550
	0.583	0.401						
	0.600	0.417						
	0.696	0.492						
	0.700	0.493						
	0.786	0.584						
	0.800	0.611						
	0.885	0.737						
	0.900	0.769						
Ca^{++}	0.100	0.031	0.100	0.037			0.100	0.005
	0.200	0.058	0.200	0.065			0.200	0.011
	0.300	0.091	0.300	0.098			0.300	0.021
	0.400	0.115	0.400	0.108			0.400	0.025
	0.500	0.142	0.500	0.141			0.500	0.038
	0.600	0.198	0.600	0.182			0.600	0.051
	0.700	0.301	0.700	0.294			0.700	0.075
	0.800	0.434	0.800	0.419			0.800	0.124
	0.900	0.653	0.900	0.648			0.900	0.349

Na^+	0.100	0.100	0.100	0.100	0.100	0.053	0.100	0.013
	0.200	0.184	0.200	0.183	0.200	0.078	0.200	0.042
	0.300	0.264	0.300	0.259	0.300	0.103	0.300	0.086
	0.400	0.332	0.400	0.317	0.400	0.150	0.400	0.121
	0.500	0.408	0.500	0.416	0.500	0.205	0.500	0.162
	0.600	0.492	0.600	0.487	0.600	0.289	0.600	0.223
	0.700	0.582	0.700	0.578	0.700	0.373	0.700	0.307
	0.800	0.682	0.800	0.692	0.800	0.495	0.800	0.459
	0.900	0.827	0.900	0.861	0.900	0.784	0.900	0.644

Appendix I

Determination of Cl^- in aqueous solutions.

Theory.

The amount of chloride ion contained in a sample can be evaluated by titrating the chloride ion with a standard $AgNO_3$ solution:

$$Ag^+(aq) + Cl^-(aq) \leftrightarrow AgCl(s)$$

The equivalence point can be determined by monitoring the change in potential between an indicating electrode and a reference electrode. The observed potential difference between the two electrodes is given by:

$$E_{obs} = E_{ref,anode} + E_{AgCl/Ag,Cathode}$$

The Nernst equation for the AgCl/Ag electrode at 25°C could be expressed as:

$$E_{AgCl/Ag} = 0.222V - 0.05916\log\left(a_{Cl^-}\right)$$

Combining these two equations gives:

$$E_{Obs} = E_{ref} + 0.222V - 0.05916\log\left(a_{Cl^-}\right)$$

As standard AgNO3 titrant is added to the solution, the change in the chloride ion activity produces a change in the observed potential. The equivalence point of the titration is found when the change in the observed potential per aliquot of titrant added is at maximum. A graphical output from a titration is shown schematically in the figure below.

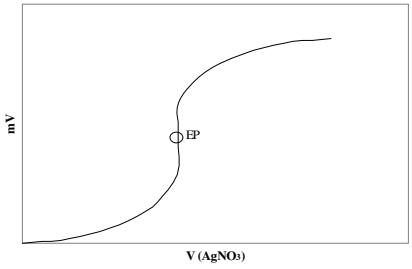

Using a graphical analysis one can in this way accurately determine the titrant volume needed to reach the equivalence point.

Experimental procedure.

The chloride content of the solution was determined with a potentiometric method using a Metrohm 799 GPT Titrino titrator. An Ag/AgCl electrode with saturated KCl as reference was used. A standard solution of app. 0.1N $AgNO_3$ was produced using analytical grade $AgNO_3$ from Merck and ultrapure water. The solution was calibrated by 3 successive titrations of 0.500g dried KCl.

1mL of the solution of interest was transferred to a 50mL glass beaker using a 500-1000µL micropipette. The pipette was calibrated using a weighing method and it was found that the average error when dosing 1mL was 0.7%. A small amount of HNO_3 was added to the beaker to prevent $AgNO_3$ from oxidizing during the titration. The solution was titrated with the calibrated $AgNO_3$ solution and the equivalence point was found by calculating the slope of the curve. By carrying out the experiment 20 times, the average standard deviation of the analysis method was found to be 3%.

Appendix J

Determination of NO_3^- in aqueous solutions.

Theory.

The UV absorbance in dilute solutions varies linearly with both the cell path length and the analyte concentration. These two relationships can be combined to yield a general equation called Beer's Law:

$A = \varepsilon L c$

A is the absorbance, L is the the path length of the cuvette in which the sample is contained and the quantity ε is the molar absorptivity. The molar absorptivity varies with the wavelength of light used in the measurement. Nitrate absorbs ultraviolet light at 220nm. By measuring the absorbance in solutions of a known amount of nitrate at 220nm, it is possible to produce a calibration curve which could be used for rapidly determining the nitrate content in solutions which lies within the concentration range of the calibration curve.

Experimental procedure:

The nitrate content was analyzed using an Agilent UV spectrophotometer with a matched pair of silica cells. Acid-washed, ashless hard-finish filter paper was used for cleaning the cells before measurements. Standard solutions of KNO_3 were prepared using dried KNO_3. A calibration curve was created each time the spectrophotometer was started. An example of a calibration cure is given in the figure below.

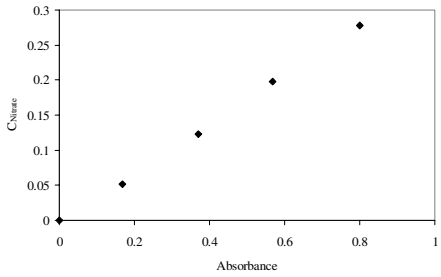

From the figure it is seen that Beers law holds in the concentration range used for the calibration curve.

The analysis was performed by transferring 10mL (±0.02ml) of solution to a 100mL volumetric flask to ensure that the concentration was within the range of Beers law. From the volumetric flask a sample was transferred to one of the silica cells while the other silica cell contained ultra pure water. The procedure (including dilution step) was repeated 20 times and the average error of the measured concentration was found to be 4%.

Appendix K

Photos of the different resins used in the experiments are presented in this appendix. The harmonic mean size for the macroreticular resins is app. 0.6 – 0.8 mm and slightly lower for the gel type resins.

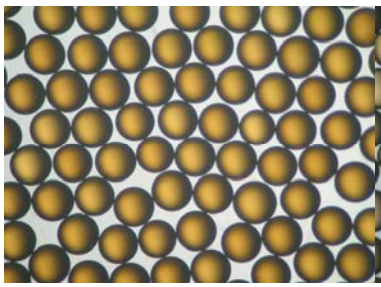

Amberjet 1200

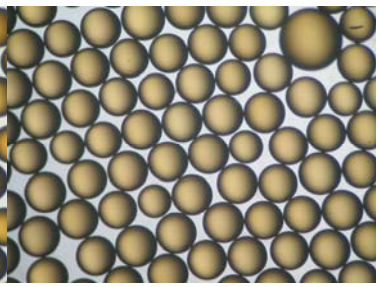

Amberjet 1500

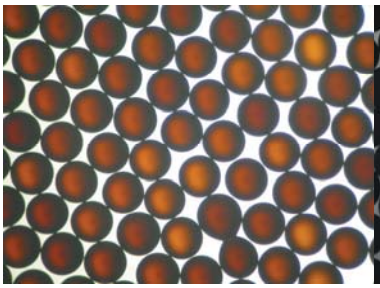

Amberjet 1600

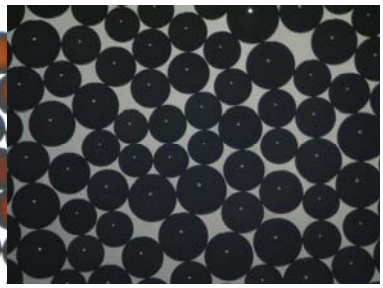

Amberlyst 40CW

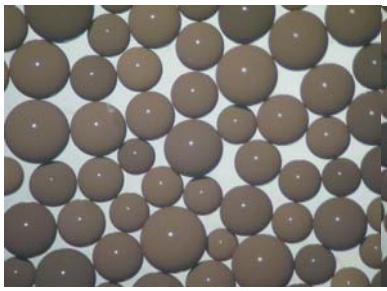

Amberlyst 35W

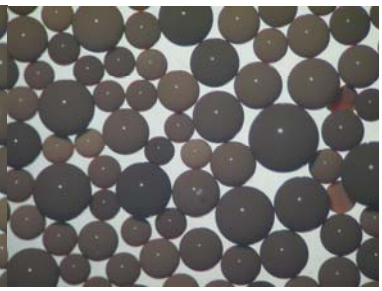

Amberlyst 36W

Søren Gregers Christensen

Thermodynamics of Aqueous Electrolyte Solutions - Application to Ion Exchange Systems

ISBN: 87-91435-18-8